UNIVERSITÀ DI PARMA

Università degli Studi di Parma
Dipartimento di Ingegneria dei Sistemi e delle Tecnologie Industriali

Dottorato di Ricerca in Ingegneria Industriale
Ciclo XXXVII

Sustainable methane synthesis enhancement in power-to-gas systems using adsorption technologies

Coordinatore:
Chiar.mo Prof. Dr. Gianni Royer Carfagni
Tutore:
Chiar.mo Prof. Dr. Mirko Morini
Co-tutore:
Chiar.mo Dr. Panayotis Dimopoulos Eggenschwiler

Dottorando:
Andrea Barbaresi

Anni Accademici 2021/2022 - 2023/2024

Sustainable methane synthesis enhancement in power-to-gas systems using adsorption technologies

Andrea Barbaresi

Abstract

Making industrial activities sustainable is necessary in order to curb current climate alterations. In this regard, the energy sector is among the most critical ones, hence its defossilization is crucial. One possibility for enabling the energy transition in the immediate term is the production of sustainable alternatives to fossil fuels to be used as their replacement. This would allow machines and infrastructures currently in use to remain unaltered. Synthetic methane, in particular, could be extremely attractive as a natural gas substitute. Natural gas is widely used in multiple sectors and has an extremely widespread network that can be easily used for the transmission and distribution of a sustainable energy carrier such as synthetic methane.

By exploiting renewable electricity to produce hydrogen from water and by using captured carbon dioxide, power-to-gas systems combine the two species through catalytic methanation processes, enabling the production of synthetic methane in a sustainable manner. In particular, the efficient implementation of the carbon dioxide capture process and the methanation process is crucial. In fact, on the one hand, efficient carbon dioxide capture allows minimizing climate-altering emissions while, on the other hand, efficient methane synthesis allows obtaining a gas of adequate purity to be distributed in the natural gas network. Since both processes deal with gas mixtures of various types, both carbon dioxide capture and catalytic methane synthesis could benefit from the use of adsorbent materials. Such materials, in fact, are capable of selectively trapping a specific gas by adsorbing it onto the surface pores and then separating it from the rest of the mixture that does not interact with the solid. The trapped gas can, subsequently, be released by desorption.

However, for the effective application of adsorption technologies in power-to-gas plants, there is the need to analyze in detail the behavior of the system in its entirety and the interaction between the various components, in dynamic conditions. This is necessary because the alternation between adsorption and desorption phases sets the system in a permanent transient state. Accordingly, the purpose of this thesis is to investigate aspects related to the dynamics of power-to-gas systems that include adsorption technologies. In particular, this research will deal with aspects related to adsorptive carbon dioxide capture and sorption-enhanced catalytic methanation, in each case the process is considered in the perspective of power-to-gas systems.

The methodologies adopted for investigation include both the development of dynamic mathematical models for simulation and experimental tests. Specifically, with reference to carbon dioxide capture, the behavior of an adsorption bed with different sources of carbon dioxide from post-combustion will be evaluated. In addition, the use of hydrogen as a purge agent to assist desorption will be examined. The conversion of the captured carbon dioxide and purge hydrogen into methane will be analyzed by additionally including a catalytic methanation reactor in the system. Reference will be made to the cyclic behavior of the system once the regime condition is reached. With reference to sorption-enhnaced methanation, the response of the system will be examined in response to transient partial load conditions. In addition, by analyzing the operation two sorption-enhanced methanation reactors alternating between the methane production and the bed regeneration phases, the importance of proper drying of the catalytic bed to ensure adequate purity of the synthesized gas will be evaluated.

Supervisors:

Prof. Dr. Mirko Morini

Dr. Panayotis Dimopoulos Eggenschwiler

Dedicated to those who never stop to be curious.

Contents

List of Figures

List of Tables

Nomenclature

Symbols

A Surface area [m^2]

a Polynomial coefficient

a_p Specific adsorbent area [$\frac{m^2}{m^3}$]

$C_{\mathbf{v}}$ Valve mass flow rate coefficient

c Specific heat [$\frac{J}{kg\,K}$]

c_p Specific heat at constant pressure [$\frac{J}{kg\,K}$]

D Diameter [m]

d Pellet diameter [m]

d_p Particle equivalent diameter [m]

$\Delta H_{\mathbf{ads}}$ Isosteric heat of adsorption [$\frac{J}{mol}$]

ΔH_r^0 Standard reaction enthalpy [$\frac{kJ}{mol}$]

E Adsorbent characteristic energy [$\frac{J}{mol}$]

f Friction factor

h Specific enthalpy [$\frac{J}{kg}$]

i Gas species in mixture

j Gas species in mixture

K Reaction equilibrium constant

k Reaction rate coefficient $[\frac{\text{kmol}}{\text{kg}_{\text{cat}}\,\text{s}\,\text{bar}}]$

L Length [m]

l Control volume thickness [m]

M Molar mass $[\frac{\text{g}}{\text{mol}}]$

m Mass [kg]

$\dot{m}$ Mass flow rate $[\frac{\text{kg}}{\text{s}}]$

M Rotational speed [rpm]

Nu Nusselt number

n Number of moles

$\dot{n}$ Mole flow rate

$n_{\text{D-A}}$ Dubinin-Astakhov isotherm exponent

n_{s} Sutherland constant

Pr Prandtl number

p Pressure [bar]

p_α Partial pressure of species α [bar]

$\dot{Q}$ Thermal power [W]

Q_{v} Volumetric flow rate $[\frac{\text{m}^3}{\text{s}}]$

q Adsorbed phase concentration

R Universal gas constant $[\frac{\text{J}}{\text{K}\,\text{mol}}]$

Re Reynolds number

r Reaction rate $[\frac{\text{kmol}}{\text{kg}_{\text{cat}}\,\text{s}}]$

S Cross section area [m^2]

T Temperature [°C]

t Time [s]

U Global heat transfer coefficient $[\frac{\mathrm{W}}{\mathrm{m^2\,K}}]$

u Velocity $[\frac{\mathrm{m}}{\mathrm{s}}]$

V Volume $[\mathrm{m}^3]$

X Mole fraction [-]

Y Valve expansion factor

y Angular momentum fraction

Z Concentrated pressure drop factor

Greek symbols

α Chemical species

β Kinetics adsorption constant

γ Heat transfer coefficient $[\frac{\mathrm{W}}{\mathrm{m^2\,K}}]$

δ Duration [min]

ε Void fraction [-]

ζ Reaction rate multiplicative factor

Λ Load percentage [%]

λ Thermal conductivity $[\frac{\mathrm{W}}{\mathrm{m\,K}}]$

μ Dynamic viscosity [Pa s]

ξ Conversion

ρ Density $[\frac{\mathrm{kg}}{\mathrm{m}^3}]$

ϱ Mass diffusion resistance parameter [s]

σ Degree of saturation [%]

τ Time variable

Φ Mole flux $[\frac{\mathrm{mol}}{\mathrm{m^2\,s}}]$

ϕ Fluidity

ψ Form factor

χ Discretization multiplicative factor

Subscripts and superscripts

ads Adsorption

avg Average

bed Adsorption bed

c Corrected

cat Catalyst bed

cdm Carbon dioxide methanation

cmm Carbon monoxide methanation

conv Convective

cool Coolant

cum Cumulative

des Desorption

eff Effective

ext External

g Gas phase

gen Generated

in Inlet

int Internal

j Reaction index

max Maximum

oil Thermal oil

out Outlet

rad Radial

reg Regeneration

rwgs Reverse water gas shift

s Solid phase

sat Saturation

start Beginning of the production phase

surf Solid surface

w Wall

$'$ Modified

$*$ Equilibrium

0 Reference quantity

$-$ Mixture average

Acronyms

AEC Alkaline Electrolyzer Cell

CCCM Combined Carbon Capture and Methanation

CCS Carbon Capture and Storage

CCU Carbon Capture and Utilization

CFD Computational Fluid Dynamics

CHP Combined Heat and Power

CV Control Volume

DAC Direct Air Capture

DME DiMethyl Ether

IGCC Integrated Gasification Combined Cycle

IPCC Intergovernmental Panel on Climate Change

LCA Life Cycle Assessment

MEA MonoEthanolAmine

MFC Mass Flow Controller

PEM Proton Exchange Membrane

PID Proportional Integral Derivative

PSA Pressure Swing Adsorption

PtG Power-to-Gas

PTSA Pressure and Temperature Swing Adsorption

PtX Power-to-X

RMS Root Mean Square

SOEC Solid Oxide Electrolyzer Cell

TRL Technology Readiness Level

TSA Temperature Swing Adsorption

Chapter 1

Introduction

In the perspective of a sustainable development, the current structure of the energy system can no longer be regarded as acceptable. To effectively address and mitigate the impacts of the ongoing climate change, it is essential to develop and deploy technologies that enable a rapid transition to a clean energy use. However, an immediate replacement of infrastructures and value chains supporting fossil fuels is not viable. An alternative approach is the production of climate-neutral substitutes for fossil sources.

In this framework, as a substitute for natural gas, Power-to-Gas (PtG) systems allow methane to be synthesized by combining captured carbon dioxide and hydrogen from renewable-powered electrolysis. Two key processes in PtG systems are the carbon dioxide capture and the methanation. The former can be done following combustion processes, anaerobic digestion processes for biogas production, or directly from the air. The latter is the chemical process whereby hydrogen and carbon dioxide are converted into methane. It can be conducted catalytically or biologically.

These processes handle in a number of ways both single gases and gas mixtures. For this reason, being able to address the selective separation of gases from mixtures, adsorption technologies will be evaluated for their potential to enhance production processes. Adsorption is the ability of some materials to retain specific gas molecules on their surface, with the effect of separating the adsorbed gas from the mixture in which it was previously contained. By shifting the thermodynamic conditions, the retained (adsorbed) molecules can be released (desorbed) and utilized as needed.

This dissertation aims to contribute to the development of the state of the art of green synthetic methane as a substitute for natural gas. In particular, the challenge is to investigate the role that adsorption could play in improving carbon dioxide capture and catalytic methanation with special reference to the dynamic operation of the system. Hereafter, the motivation will be explained and the objective of the thesis will be stated.

1.1 Motivation

The technological advancements shaping global societies over the past century are closely associated with a massive use of energy. To date, energy generation in all of its forms is heavily dependent on the exploitation of fossil sources, making it challenging to transition away from them. As a result, the infrastructure supporting industrial growth has been designed specifically around fossil fuels use.

However, coal, oil, and natural gas reserves are far from infinite. According to a recent report by the Energy Institute [1] examining the reserves-to-production ratio, which estimates the remaining years based on known reserves and current extraction rates, coal reserves are projected to last 139 years, oil 56 years, and natural gas 49 years. Given the increasing rate of fossil fuels consumption, there is a significant risk of depleting these resources, potentially making it difficult to sustain even essential activities.

More importantly, it has to be considered that the emission of greenhouse gases from the use of fossil fuels is the main cause of climate changes currently taking place on planet Earth. In this regard, the Intergovernmental Panel on Climate Change (IPCC) reports that the average global surface temperature reached values 1.1 °C higher in the second decade of the 21st century than in the pre-industrial era, and that in the third decade of the 21st century, anthropogenic emissions further increased [2]. Therefore, in order to achieve the energy transition to clean energy sources it is fundamental to replace fossil-based infrastructures and technologies.

For all the above reasons, the immediate replacement of fossil energy sources results to be crucial. The use of renewable energy sources and the electrification of industry and transportation is significantly contributing in moving towards this direction. Fortunately, investments in renewables are increasing greatly. In particular, annual investments on clean energy in 2016 surpassed those on fossil fuels, and the trend seems to indicate that this difference is increasing [3]. However, nowadays technologies using renewable sources mainly produce electricity. Of these, the most prevalent are wind and solar, which have unprogrammable availability that makes it hard to balance the moments of production with those of demand. Accordingly, as the penetration of renewables increases, it becomes necessary to improve energy storage technologies in both the short and the long term. This, in fact, makes it possible to decouple the periods of energy generation from those of its use.

From this perspective, the PtG technology is particularly noteworthy as it enables the production of synthetic methane from renewable electricity. In this way, electrical energy is converted into chemical energy and stored in the chemical bonds of an energy carrier. Specifically, this technology involves firstly the use of electricity to produce hydrogen from

water through electrolysis. The hydrogen is then converted to methane by combination with captured carbon dioxide by means of the Sabatier process [4]. Consequently, the emissions resulting from the combustion of the produced methane are counterbalanced by those avoided through carbon capture, thereby leading to significant reductions in carbon dioxide emissions per generated unit of useful energy. The methane obtained from this system can also be stored over a long period and used when needed for a variety of energy uses, from heating to power generation.

Moreover, synthesized methane can be used as a substitute for natural gas by making use of currently existing transportation networks and all the technologies currently powered by natural gas. Among the various fossil fuels, natural gas is distinguished by its versatility of use. Although it is used extensively in the industrial sector, the ability to be easily transported and distributed makes it widely used in residential contexts as well, as evidenced by Figure 1.1 [5].

A significant issue to consider is the uneven geographical distribution of gas reserves. Indeed, Figure 1.2 [6] shows that there are states that benefit from reservoirs with large amounts of natural gas while others where it is not present at all.

Given the extensive use of natural gas across various sectors, as previously discussed, the bargaining power of the few states with large reserves is enormous. In addition, a limited market competition causes the price of gas to be extremely volatile. Geopolitical

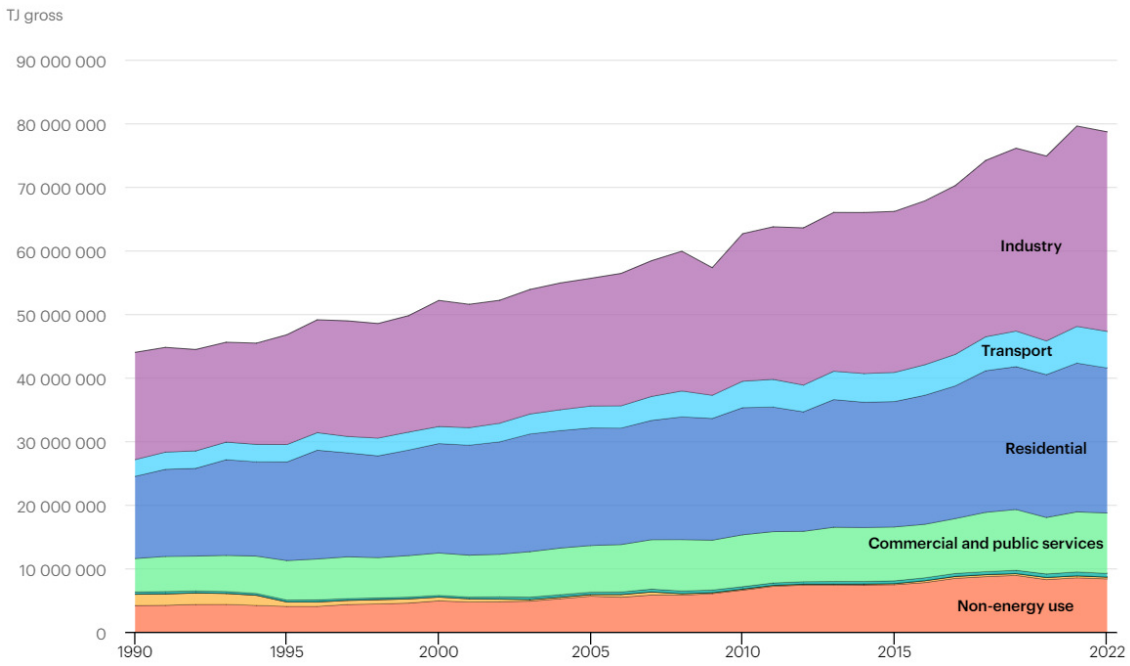

Figure 1.1: Worldwide natural gas final consumption by sector.

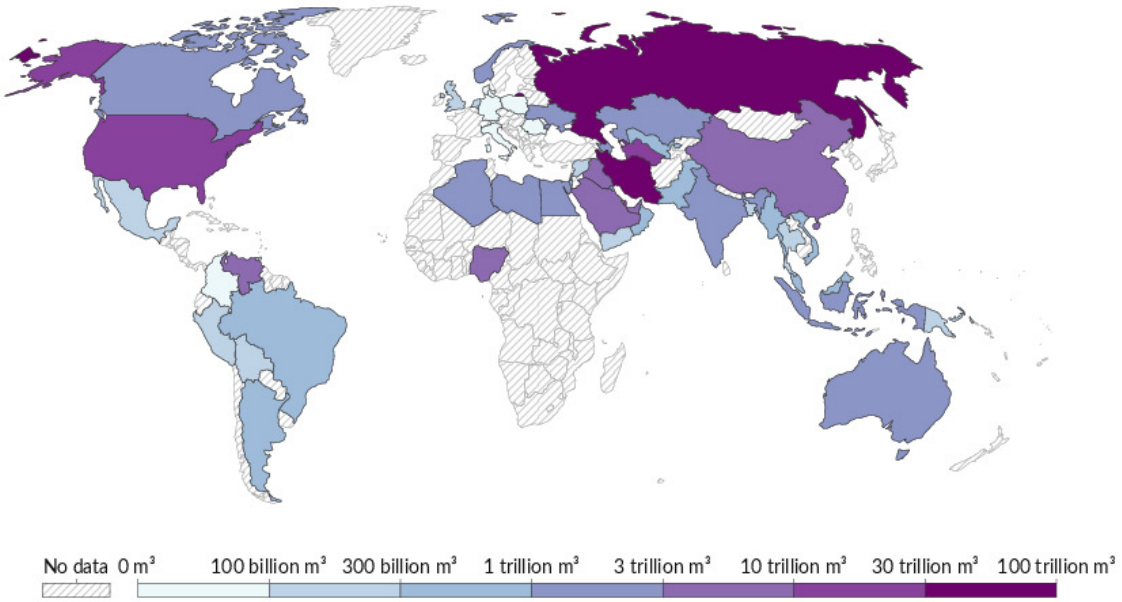

Figure 1.2: Geographical distribution of natural gas reserves.

instabilities, for instance, can lead to uncontrolled changes in gas prices. A recent example is the price spike that occurred as a result of the conflict between Russia and Ukraine in 2022. As can be seen from Figure 1.3 [7], gas prices have reached peaks one order of magnitude higher than in the years before 2022. The on-site synthesis of green gas as a substitute for natural gas, therefore, is also extremely attractive from this perspective.

Among the advantages, it is noteworthy that the diffusion of PtG facilities would act

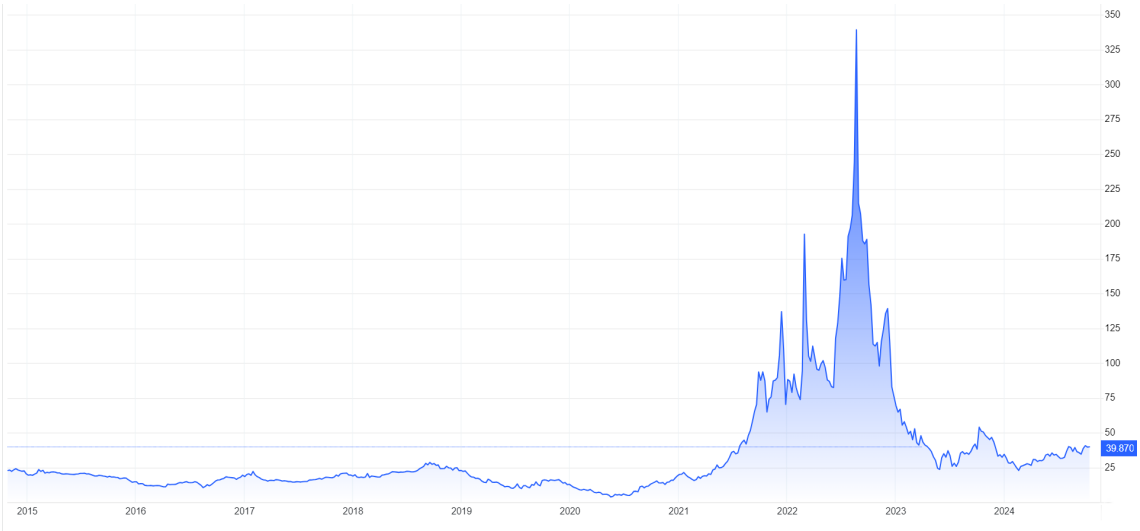

Figure 1.3: Natural gas price trend at the EU Dutch Title Transfer Facility [EUR/MWh].

as an accelerator for the advancement of the Technology Readiness Level (TRL) for two critical innovative areas for energy transition technologies: the use of hydrogen as an energy carrier and the carbon dioxide capture, storage, and utilization.

As introduced earlier, the challenge of this thesis is to contribute to the development of power-to-gas systems by comprehensively evaluating the exploitation of adsorption in the involved processes. Adsorption is a phenomenon through which particular types of materials can attract specific gaseous molecules onto their surface. In cases where these molecules belong to a mixture, the effect is to separate them from other gases. In systems where there are a variety of types of gases in mixture, the impact of using such technologies could be extremely important. It is noted that, in order to exploit adsorption, the process needs to switch between a phase in which the relevant gas is trapped by adsorption and a phase in which it is released by desorption.

Therefore, it is underlined that the study of systems of this kind cannot be separated from the use of a dynamic approach, driven by two key factors. First, renewable energy sources, often non-programmable in nature, lead to intermittent hydrogen generation, and subsequently the methane production. Second, the inclusion of adsorbent materials necessitates cyclic operational conditions with alternating phases.

1.2 Scope and structure of the thesis

As a technology that can be used immediately in the early stages of the energy transition, and for all the reasons stated above, it is believed that power-to-gas needs to be thoroughly studied and consequently improved to achieve effective implementation.

The purpose of this dissertation is to explore potential developments and improvements for systems of this type using technologies capable of getting the most out of the components of this system. Specifically it is intended to examine the impact that adsorption technologies may have when integrated into power-to-gas systems.

The question that is to be addressed by the research illustrated throughout this work concerns the actual applicability of adsorption technologies and the extent of their potential contribution in the context of power-to-gas, considering both the overall system as well as the individual components. In particular, it is intended to research limitations and opportunities of using adsorption both in carbon dioxide capture and in methanation processes, particularly from the perspective of dynamic operation.

In order to provide an answer as clearly as possible, the thesis is structured as follows.

- Chapter 2 will present the technical-theoretical background of the topics that will be covered. This will provide the reader with solid tools to understand the actual

scientific contribution of the dissertation.

- In Chapter 3, a literature review will be presented to highlight the state of the art of scientific research on these topics and the research gaps to be filled.
- The mathematical modeling approch adopted will be illustrated in Chapter 4 presentig the general equations utilized for the develpment of the specific models used in the analyses of the thesis.
- Chapters 5 and 6 will delve into detail on the contribution of the thesis. This will be accomplished by presenting, respectively, the potential of adsorption in improving carbon dioxide capture and in improving methanation, in power-to-gas contexts.
- Chapter 7 will draw the overall conclusions of the thesis and will indicate a possible path that can be followed in order to further develop these issues.

Chapter 2

Background

2.1 Power-to-gas systems overview

As anticipated in the introduction, power-to-gas systems allow a gaseous energy carrier to be produced from renewable electricity. Essentially, hydrogen produced from renewable sources is combined with captured carbon dioxide to synthesize methane. There are mainly three constituent components of PtG systems: an electrolysis unit, a carbon capture unit and a methanation unit. The first two are needed to supply hydrogen and carbon dioxide, while the third is used to implement their conversion to methane.

The first PtG plant dates back to 1995 with a demonstrator built at Tohoku University, Japan [8]. However, it is only after 2010 that the concept gained significant traction and began to develop [9]. In the following, the main features of the technologies constituting such plants will be described.

2.1.1 Electrolysis

Electrolysis is an electrochemical process in which liquid water molecules are dissociated to obtain gaseous hydrogen and oxygen. The device used to conduct electrolysis is called electrolyzer. It consists of a number of constituent elements, the electrolytic cells. The electrolytic cell consists itself of two electrodes, one positively charged (i.e., anode) and the other negatively charged (i.e., cathode).

The oxidation reactions take place in the cathode while the reduction reactions take place in the anode. The electrolyte is the element that allows the transfer of electrical charges. The overall reaction that takes place is the following [10]:

$$H_2O_{(l)} \rightarrow H_{2_{(g)}} + \frac{1}{2}O_{2_{(g)}}, \qquad \Delta H_r^0 = +285.8 \ \text{kJ/mol} \tag{2.1}$$

Although the overall reaction is always the same, the half-reactions of oxidation and reduction, change depending on the electrolysis technology employed. The technologies that can be adopted for electrolysis are generally classified according to the temperature. Specifically, low-temperature electrolyzers, such as Alkaline Electrolyzer Cell (AEC) and Proton Exchange Membrane (PEM) are distinguished from high-temperature electrolyzers, with Solid Oxide Electrolyzer Cell (SOEC) being the most established. The operating conditions differ significantly between these typologies. Low-temperature electrolyzers operate at a maximum of 80 °C to 90 °C, whereas high-temperature electrolyzers within a range of 700 °C to 900 °C [11].

Because of the coupling of electrolysis with renewable sources, a key feature to consider in PtG contexts is flexibility. This aspect was thoroughly investigated in the work of Lange et al. [12] in which flexibility was analyzed in terms of load changes and load change gradients. Although heating and pressurization are limiting factors, various electrolysis technologies already demonstrate good flexibility. Among the proposed technologies, PEM electrolysis appears to be the best one by being able to operate with a load between 0 % and 100 % of rated power with ability to follow rapid load changes, a cold start that can be achieved in less than 15 minutes and a hot start in less than 10 seconds.

Since the electrolysis technology has already achieved a TRL suitable for commercialization, its detailed investigation falls outside the scope of this thesis.

2.1.2 Carbon capture

The carbon dioxide is one of the key ingredients for hydrocarbon synthesis as it acts as the carbonaceous source. Capture methodologies are categorized into post-combustion, pre-combustion and oxy-fuel combustion [13]. In the first case, carbon dioxide is removed after the combustion, in the second case before actuating combustion, and in the third case, combustion with only oxygen is implemented.

In the case of post-combustion, carbon dioxide is taken from smokestacks in industrial processes or in other contexts where combustion takes place. In pre-combustion, the separation technique strongly depends on the fuel utilized. In general, through gasification or steam reforming processes, it is possible to obtain syngases from which it is easier to remove the carbonaceous constituent. In the case of oxy-fuel combustion, only oxygen is used as oxidizer instead of using air. This avoids the presence of significant amounts of nitrogen in the flue gas. Once the particulate matter (fly ash) has been removed, a mixture containing only carbon dioxide, water vapor and small amounts of other species is obtained. From this mixture the carbon dioxide can be separated from the vapor by condensation.

Carbon dioxide can also be taken from the air, this procedure is known as Direct Air Capture (DAC). The carbon dioxide is present in the air in concentrations around 415 ppm, values that are not negligible. However, this concentration is very low when compared with other sources. Therefore, the energy expenditure of DAC is relatively very high in that, compared with post-combustion sources, much larger streams must be vented and processed to obtain the same amount of carbon dioxide [14].

With reference to post-combustion capture, the main capture technologies are absorption, adsorption and membrane systems. In addition, methods such as cryogenics and algae-based methods are also mentioned [13]. The most widely adopted solution is chemical absorption of gaseous carbon dioxide in a liquid matrix. Many studies, in fact, point out that this technology suffers from significant energy consumption for the production of steam to be sent to the stripper [15, 16, 17]. Although there are promising new solvents in terms of energy saving, their TRL is still quite low to draw conclusions [18].

Adsorption of gaseous carbon dioxide onto solid matrixes is a viable alternative considering the significant energy savings it would entail [19]. In fact, as will be explained later, the bonds that the adsorbed molecules form are weak and the energy required for desorption is less than what would be required if a liquid mixture were to be heated. Despite this, other issues such as physical friction of particles, thermal stability of materials and space occupation have not yet allowed the commercialization of this type of technology [20]. Currently, carbon dioxide separation is a costly practice from both economic and energy perspectives. In general, the higher the concentration of carbon dioxide in the mixture from which it is taken, the lower the cost of separation.

2.1.3 Methanation

The methanation reaction allows hydrogen and carbon dioxide to be combined in order to produce methane and water. Methanation can be carried out thermochemically in catalytic reactors or biologically. In the second case, the reaction is catalyzed by microorganisms such as autotrophic hydrogenotrophic methanogens (archaeal bacteria) already used in the anaerobic digestion for biogas production. Although there are several attempts to implement biological methanation, in the following there will be only reference to thermochemical methanation as it has more possibilities for industrialization and scale-up.

Catalytic reactors that can be used to implement thermochemical methanation can be of several types. The most common are undoubtedly fixed-bed reactors, in which the catalyst is arranged on a fixed solid support. However, there are also examples of fluidized bed reactors and three-phase reactors. Depending on the catalyst (generally nickel, ruthenium or iron [21]) the thermodynamic conditions of reaction can change.

They range in temperature between 300 °C and 550 °C and pressures between 1 bar and 100 bar [22]. The overall reaction that takes place is the following Equation 2.2:

$$CO_{2_{(g)}} + 4H_{2_{(g)}} \leftrightarrows CH_{4_{(g)}} + 2H_2O_{(g)}, \qquad \Delta H_r^0 = -165 \ \text{kJ/mol} \tag{2.2}$$

The process in question, known as Sabatier process, is composed of the following sub-reactions:

$$CO_{2_{(g)}} + H_{2_{(g)}} \leftrightarrows CO_{(g)} + H_2O_{(g)}, \qquad \Delta H_r^0 = +41.2 \ \text{kJ/mol} \tag{2.3}$$

$$CO_{(g)} + 3H_{2_{(g)}} \leftrightarrows CH_{4_{(g)}} + H_2O_{(g)}, \qquad \Delta H_r^0 = -206.3 \ \text{kJ/mol} \tag{2.4}$$

Respectively, reverse water gas shift (Equation 2.3, endothermic) and carbon monoxide hydrogenation (Equation 2.4, exothermic). If thermodynamic conditions favor it, the formation of solid carbon can also take place according to the Boudouard reaction (Equation 2.5). This should be avoided in order to not compromise catalysis.

$$2CO_{(g)} \leftrightarrows C_{(s)} + CO_{2_{(g)}}, \qquad \Delta H_r^0 = -172.5 \ \text{kJ/mol} \tag{2.5}$$

As mentioned, overall, the methanation reaction is exothermic, which implies that, according to Le Chatelier's principle, it is favored at low temperature. Conversely, however, the operating temperature cannot be too low otherwise the chemical kinetics would be disfavored and the reaction would be very slow in igniting. Therefore, the most suitable temperature level depends on the type and amount of catalyst.

2.2 Mechanism and characteristics of adsorption

The phenomenon of adsorption has been known for a long time, the fundamental theory of pure component equilibria was developed by Langmuir in 1918 [23]. Adsorption phenomena involve a porous solid medium and a gas (or, in some cases, liquid) phase interacting with each other. The porosity of the solid is necessary to maximize the contact surface area. The ability of certain materials to selectively adsorb a specific gas from a mixture has led to the exploitation of this phenomenon in industrial separation processes [24]. Solid materials that can be used for adsorption, the so-called adsorbents (or sorbents), are several. The most common are, activated carbon, alumina, zeolite and silica gel. Adsorbents are often classified according to pore size.

Two fundamental characteristics of adsorption are equilibria and kinetics [25]. Through the former, it is possible to define the concept of adsorption capacity, which is the amount of gas phase that the solid is able to adsorb, given the thermodynamic conditions. Through kinetic studies, on the other hand, it is possible to assess the aspect of diffusional resistance that the gas encounters on its way through the porous surface. The behavior of gaseous flows in porous media can be described by the following transport mechanisms [25].

- Poiseuille flow
- Knudsen diffusion
- Continuum diffusion
- Surface diffusion

The first is determined by the pressure gradient while the second is induced by the collision of the gaseous molecules on the pores walls. In both Poiseuille flow and Knudsen diffusion the driving force is indipendent of the type of gas molecules flowing. The third is the result of the collisions among different type of molecules. The continuum diffusion is more pronounced the smaller the mean free path with respect to the diameter of the capillary. Lastly, the surface diffusion happens because different gas molecules have different mobility on the pore surface due to the difference in the interaction with the solid sorbent.

From a thermodynamic point of view, it is also important to consider that when a particle is adsorbed, it releases heat. This is referred to as the isosteric heat of adsorption. This released energy, given by the difference in enthalpy of the molecule between before and after its adsorption, affects both kinetics and adsorption capacity.

The reverse of adsorption is known as desorption. In this case the previously adsorbed molecules are released. Adsorption is favored at high pressures and low temperatures while desorption, in contrast, is favored at low pressures and high temperatures. Therefore, in order to switch from one phase to the other, it is necessary to change the thermodynamic conditions by implementing a so-called swing. Swing procedures can have various approaches. The most widely adopted are: pressure (and vacuum) swing adsorption (i.e., pressure decrease during desorption), temperature swing adsorption (i.e., temperature increase during desorption), concentration swing adsorption (i.e., sorbent bed purged with another gas flow during desorption) and electrothermal swing adsorption (i.e., electrical heating provided during desorption) [20].

As long as the adsorption bed is not saturated, the concentration of the adsorbed species at the reactor exit is very low in comparison with the inlet. When saturation is reached (at give thermodynamic conditions), the bed is no longer able to hold additional

molecules and consequently the concentration at the outlet equals the one at the inlet. This aspect can be represented in the so-called breakthrough curves.

The interaction of the solid and gas phases occurs either through chemical bonds or through weak electrostatic interactions. In the former case, it is referred to as chemisorption while in the latter as physisorption. In the case of chemisorption, covalent bonds between solid (adsorbent) and gas (adsorbate) are established. Electrostatic interactions that are established in physisorption include London, dipole-dipole and van der Waals forces [26]. Generally, the chimisorption interactions are two orders of magnitude stronger than those occurring in the physisorption. This affects the applicable operating conditions (physisorption cannot take place at high temperatures) and the energy required for desorption.

2.3 Adsorption in power-to-gas systems

Generally, adsorbent materials have been used for gas separation in various industrial processes. In PtG plants, it is necessary to deal with different types of gases. These need to be mixed, converted, compressed but also separated. Therefore, the application of adsorbent materials in this context could be advantageous. In the following, brief hints will be given about the possibilities of exploiting adsorption for the improvement of carbon dioxide capture and methane synthesis.

2.3.1 Adsorption in carbon capture

Adsorptive separation of carbon dioxide for capture purposes is gaining interest [15]. The biggest advantage, as mentioned earlier, is the lower energy (energy penalty) required for desorption when compared to the regeneration of conventional methods based on a liquid solvent. When dealing with the capture of carbon dioxide it is important to distinguish between the concepts of Carbon Capture and Storage (CCS) and Carbon Capture and Utilization (CCU). The carbon capture perfomed in PtG plants is included in the framework of CCU as the capture of carbon dioxide has the aim of its subsequent use [27]. In the case of adsorptive carbon capture, often, the carbon dioxide is collected in dilute form (e.g., mixed with an inert gas that is used during desorption [15]). The effective desorption carried out involving a purge gas can be exploited in the CCU if the diluent is easily removable (i.e., water steam by condesation) or if the diluent takes part of the subsequent process (i.e., hydrogen in case of methanation) and is in the correct amount.

2.3.2 Combined carbon capture and methanation

An additional benefit that could be derived from adsorbent systems in the PtG context is that of Combined Carbon Capture and Methanation (CCCM). In this case, in the same plant adsorptive carbon dioxide and methanation are performed. This can be done in different ways as shown by Fig 2.1 [28]. In particular capture and methanation can be made in different vessels, in the same vessels using two different materials or using a bi-functional material capable of adsorbing and converting carbon dioxide in the same site.

Despite the idea of using a single vessel for a double aim, the challenges for the effective implementation of such a technology are many. The biggest problem lies in the need to establish quite different thermodynamic conditions between the capture and methanation phases [28]. In addition, such a technology presents many difficulties in scaling-up and implementing effective industrialization.

2.3.3 Adsorption in methanation

Adsorption can assist methanation in a completely different way than in the case of carbon dioxide capture. In fact, in this case, it may be advantageous to adsorb water vapor. With reference to Equation 2.2, in fact, it can be seen that water is a reaction product along with methane. For the purposes of synthesizing methane as an energy carrier, water has no utility and therefore can be considered a reaction by-product whose removal does not

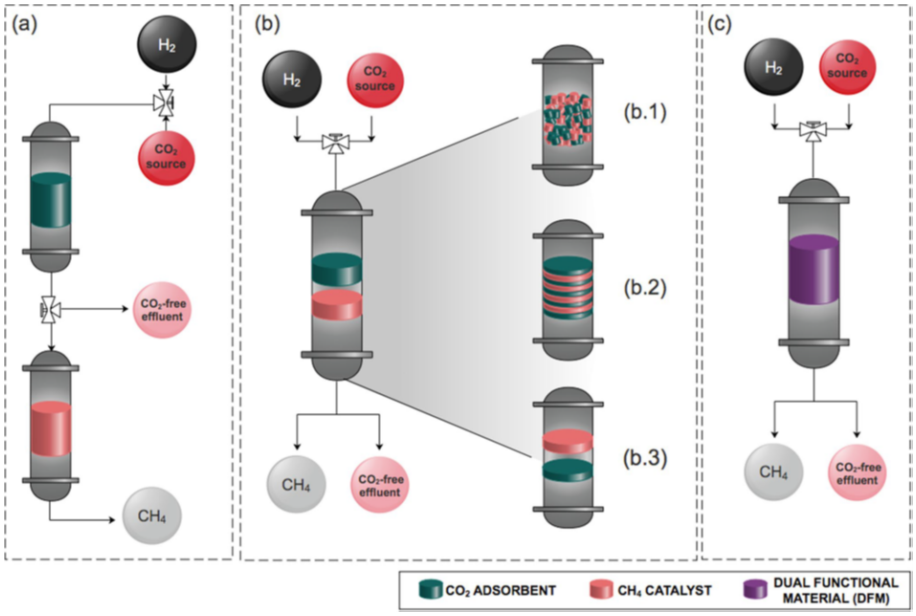

Figure 2.1: Combined carbon dioxide capture and methanation configurations.

pose problems for the intended purposes. Conversely, on the other hand, in-situ water vapor removal in the methanation chemical reactor can be beneficial. In fact, by removing a reaction product, the equilibrium is shifted to the products side. It occurs because the partial pressure of the reactants is increased with respect to the total.

What can be implemented, then, is the replacement of the catalyst support with a water-selective adsorbent material. Usually, the catalyst support does not play a role in the chemical process but only serves as a structural support in the packed bed. With this substitution, the support acquires an active role in the production process. In this way, it is possible to intensificate the process. In these cases, it is referred to as sorption enhancement [29].

Chapter 3

Literature review

3.1 Experimental and modeling research on power-to-gas systems

In order to provide a comprehensive overview of the state of the art of the research on PtG systems, in this chapter it was decided to illustrate both experimental and simulation works. With regard to the experimental ones, they range from laboratory activities to large demonstration plants. In order to highlight the novelties, emphasis will be placed on the purposes that distinguish these investigations. Alongside with experimental and demonstration activities, in the scientific literature there are many works concerning the mathematical modeling of the technologies of PtG. Distinction will be made between models related to individual components as well as models capable of reproducing the behavior of the system. The level of detail of mathematical modeling will also be stressed. There will be a reference to "algebraic models" by subintending that algebraic equations cannot keep track of the evolution of the calculated variables while to "dynamic models" in which differential equations capable of having memory of past trends are included. In the following, the most noteworthy investigations involving the modeling of carbon dioxide capture and of methanation will be outlined. The characteristics of the models used and the conclusions drawn from their application will be highlighted.

3.1.1 Experimental activities

Although the PtG technology is not yet commercialized, there are several examples of experimental work regarding these plants [9]. Many include both the carbon capture and the methanation technologies. The size varies greatly as there are examples of bench-scale, laboratory-scale, and industrial-scale works. The first proof-of-concept came in 1995 at Tohoku University in which through a photovoltaic-powered seawater electrolyzer hydro-

gen was produced and combined with carbon dioxide originating from flue gas through catalytic methanation for methane synthesis [8].

Among the most important projects figures Store&Go, which, through a consortium of companies and universities, in several european cities, evaluated the applicability of the PtG concept in different ways. Some of the most noteworthy activities include the evaluation of a honeycomb-type catalytic structure for better heat dissipation during the methanation process [30] and the attempt of the use of a DAC unit for carbon dioxide capture [31]. The use of direct capture of carbon dioxide from the air in the PtG context has also been evaluated in other works, among which the investigation of Friedl et al. [32] is mentioned.

In the work of Castellani et al. [33] the recycling of carbon dioxide by membrane separation from flue gas and its conversion to methane is evaluated in a context where ammonia is also being produced. The carbon footprint of the PtG process is evaluated and it is concluded that this system is effective in achieving the emission reduction targets. The ongoing Lübesse Energie project aims to make the small german village of Lübesse entirely renewable [34]. The synthesis gas is supposed to complement the energy supply of an existing wind power plant. The aim is to recover heat from the methane production for district heating.

The Jupiter 1000 project is among the largest demonstrators of PtG [35]. It includes hydrogen production by a PEM electrolyzer and an AEC electrolyzer, both of the size of 500 kWe [36]. Carbon dioxide is taken from the flue gases of a nearby power plant, and methane is synthesized in order to be injected into the natural gas grid [37]. In the Exytron project, in contrast, the electrolysis and methanation units are integrated with a Combined Heat and Power (CHP) plant that is fed by the synthetic methane produced [38]. The emitted carbon dioxide is re-utilized within the system. The capture of carbon dioxide from the flue gases of a CHP is also implemented in the Methfuel project [39]. In this case, carbon capture is realized by absorption through gas scrubbing with ionic liquids while methanation is conducted in a bubble column reactor.

Another noteworthy demonstration plant is the one at the Łaziska power station [40], in Poland. Figure 3.1 [40] shows its principal units. The system can separate the carbon dioxide by absorption through amine scrubbing while for the methane is produced by a two-stage catalytic reactor. Indications on the operating conditions to be implemented in order to improve the conversion into methane are provided.

The focus on methanation is also placed on the work conducted by Bailera et al. [41]. In this case, a methanation reactor with ruthenium catalyst is experimentally characterized in the perspective of the integration of PtG and oxy-fuel combustion with oxygen resulting from electrolysis. The authors used experimental reactor data to validate a mathematical

Figure 3.1: Power-to-gas demonstrator at the Łaziska power plant.

model. From the above-illustrated works it is concluded that although many aspects are being under experimentation, lot of work needs to be done to define a PtG system that can be considered as the state of the art.

3.1.2 Carbon capture modeling

The research on mathematical modeling of carbon dioxide capture processes has been reviewed by various authors. Miller et al. [42] focused specifically on the modeling research on carbon capture. Different routes that can be taken for mathematical modeling were analyzed, emphasizing the possibility of implementing multi-scale modeling. The extent to which simulating can drastically reduce cost and development time, especially in a field such as carbon capture, is highlighted. Research hotspots related to carbon capture and storage are identified by Li et al. [43]. From a modeling point of view, various methods for the study of CCS are analyzed, dwelling also on Life Cycle Assessment (LCA), on optimization, and economic aspects. The possibility of mathematically analyzing capture and storage processes from post-combustion was also analyzed by Asgharian et al. [44] with particular focus on cryogenic separation.

Several studies focus on mathematical modeling by going into the details of the individual components. Ryan et al. [45] evaluated through a Computational Fluid Dynamics (CFD) simulation the operation of a fluidized bed with an amine-functionalized solid phase, discussing which modeling approach may be the most suitable. Im et al. [46] modeled a rotating packed bed reactor for carbon dioxide absorption with monoethanolamine (MEA) and dynamically simulated absorber and stripper. Yuan et al. [47] simulated the separation of carbon dioxide by membrane for a post-combustion CCS by evaluating the most efficient configuration. Seo et al. [48] modeled a post-combustion adsorption capture unit based on a thin film with optimization purposes. Mahapatra et al. [49] delved deeper into modeling in the CCS domain, looking for a way to streamline the computationally

onerous dynamic models while maintaining good physical fidelity.

In order to simulate the process in its entirety, carbon dioxide capture is greatly analyzed also using mathematical models of the whole system. Ramasubramanian et al. [50] simulated an air-sweep process that included membrane separation. Following techno-economic considerations, it is concluded that the technology needs refinement. Khalilpour et al. [51] algebraically modeled a hollow fiber memabrane system for the separation of carbon dioxide from a multicomponent gas. Various features of the technology are evaluated. Li et al. [52] studied a system that included DAC and wind power for the purpose of operation optimization. The capture technology considered was calcium looping, that was concluded to be suitable to be powered by fluctuating renewable electricity. Furst et al. [53], in the power-to-methane context, compared different system layouts for carbon dioxide capture by simulation with an algebraic model. The importance of thermal integration to increase system efficiency is emphasized.

Bassano et al. [54] considered coal gasification with carbon dioxide capture and sequestration. Two different processes are compared. In both of them the capture is entrusted to an acid gas removal unit. It is argued that the CCS only relatively affects the efficiency of this system. Ma et al. [55] considered a very large system that included CHP, PtG and CCS and developed a model with the aim of system optimization. Güler et al. [56] evaluated CCS by means of absorption in the naval sector. The algebraic model also included economic aspects. Drechsler and Agar [57] exploited a mathematical algebraic system model to analyze a very interesting concept. Indeed, in the context of integrating DAC and PtG, the joined capture of carbon dioxide and water vapor by adsorption on a solid bed is evaluated. The collected water can be thus electrolyzed for hydrogen production. García-Luna and Ortiz [58] in the framework of CCU evaluated a waste-to-methane system with adsorption capture on amines. In this case, the mathematical model had the utility of being able to facilitate the design of an innovative plant of this type. Wu et al. [59] analyzed a large system including both PtG and wind energy. Taking into account carbon trading a model useful to implement optimization from an economic point of view is developed. A similar approach was implemented by He et al. [60] considering electricity dispatch.

Fewer studies deal with dynamic simulations of such systems. Zhang et al. [61], for instance, dynamically analyzed the characteristics of a complex system that included capture by absorption on a liquid matrix. Lima et al. [62] considered an Integrated Gasification Combined Cycle (IGCC) with membrane-based carbon capture. The dynamic modeling of the two components is also exploited for optimization purposes. Lastly, Mostafa et al. [63] developed a dynamic model of an adsorption capture process in the context of Power-to-X (PtX) systems. The dynamics of various components is evaluated by calculating their

time constants and the slowest components are identified.

3.1.3 Methanation modeling

In the literature, there are many examples of methanation investigations that approach the study on the subject through mathematical modeling. Also in this case, it is possible to differentiate between methanation reactor modeling as a separate component with respect to the entire methane synthesis process modeling [64].

Considering the multiple ways in which the methanation reactor can be configured, many authors addressed its analysis dealing with it as a single component. The first study to develop a mathematical model of the methanation reactor was conducted by Lunde in 1974 [65]. The model was based on previously obtained experimental data and was able to capture the dynamics of a ruthenium-catalyzed reactor. Fischer et al. [66] analyzed the mathematical modeling of wall-cooled fixed bed reactors by comparing various types models, ranging from one-dimensional to two-dimensional and considering both homogeneous and heterogeneous reactor beds. The limitations of using models that are too approximate are highlighted. Barbaresi et al. [67] analyzed and simulated different modeling scales guiding for the more suitable modeling approach in the PtG context.

There are numerous instances of detailed models. As an example, Sun et al. [68] studied a circulating fluidized bed reactor by means of a three-dimensional dynamic model. Schlereth and Hinrichsen [69] developed on a small scale a catalytic bed model. The importance of studying intraparticle mass transport to evaluate the limitations on heat transfer that occurs in fixed catalytic beds is emphasized. Gruber et al. [70] modeled a boiling water-cooled fixed-bed reactor in considerable detail. Being a three-dimensional model, it is considered by the authors themselves to be too complex to be applied extensively. Among the various results it appears that, based on their model, there is not much difference between the gas temperature and the surface temperature of the catalytic bed, for this reason the authors stated that using homogeneous models instead of heterogeneous ones do not lead to excessive approximation.

Moioli et al. [71] focused on small ruthenium-catalyzed reactors as they have the advantage of being able to achieve good conversions at relatively low temperatures. Various zones at different temperatures within the bed, useful for analyzing the spatial evolution of conversion rates, are distinguished. The authors also compared, in application to the Sabatier process, catalysis with ruthenium with that implemented via nickel [72]. Higher conversion is achieved with ruthenium but it has a significantly higher cost than nickel. For this reason it is concluded that ruthenium is good for small applications while for larger applications nickel is more suitable.

Bremer et al. [73] through a two-dimensional dynamic model defined the best control strategies for the start-up of fixed-bed reactors. Transient operation is also analyzed by Güttel et al. [74]. Through a dynamic model the steady state operation is compared with the periodic operation and the step response. The intent is to guide the design during unsteady operation. It is concluded that methanation reactors manage to self-stabilize during cyclic operation.

In addition to above-analyzed models, more approximate models can also be found in the literature. These models are used for other purposes with respect to the more complex ones. An example is the algebraic model used by Koytsoumpa and Karellas [75] to analyze the possibility of an effective injection of synthetic methane into the natural gas grid. Algebraic models, however, are often used when there is a need to analyze the entire methane production process. Considering the injection of synthesized gas into the natural gas grid, Fambri et al. [76] evaluated various modeling approaches. The authors underlined the fact that models that are too approximated could lead to non-negligible overestimates or underestimates.

In a system perspective Kezibri and Bouallou [77] algebraically considered mass and energy fluxes during the steady state to analyze the oxy-combustion of the produced gas. Solomon et al. [78] considered other components in addition to the methanation reactor, including renewable energy generation. The calculations were made based on the efficiencies of the various components, and this allowed also for techno-economic evaluations. It is concluded that the hydrogen production and the hydrogen storage are the most economically expensive technologies in the whole system. A techno-economic assessment was also performed by Iaquaniello et al. [79]. In this case, a staged reactor model with intermediate water condensation is used for direct methanation of flue gases.

Considerable emphasis is also placed on the thermal management of the reactor. For these purposes Sun and Simakov [80] evaluated the use of molten salts for reactor temperature control by simulating the internal cooling. The authors underlined that the thermal management of the Sabatier process is critical since a lot of energy is released. Kao et al. [81] defined the best control strategies to avoid temperature spikes in fixed-bed reactors. Considering the methods evaluated, effluent recycling is the most effective in containing the formation of hot-spots.

As a result of the above, however, it is pointed out that only in a few cases the literature investigations dynamically consider the behavior of the entire system. Among these it is possible to find the analysis conducted by Giglio et al. [82]. In that case the off-design operation is examined, considering both partial load and hot start-up in a system involving three cooled reactors in series.

3.2 Research on adsorption in carbon capture and methane synthesis plants

The research on adsorbent materials and adsorption processes is extensive. In the following a selection of works in which adsorption is applied in technologies included in PtG systems is presented.

3.2.1 Adsorption for carbon dioxide capture

As mentioned in the Section 2.1.2, there are multiple capture methods. Among them, adsorption capture has great potential for development because of the significant energy savings it could bring compared to classical liquid-based absorption technologies [20]. In addition, there are several ways in which the adsorbent bed can be designed. As stated by Dhoke et al. [83], there is not a configuration that is clearly superior to the others, each has its own advantages and disadvantages. For these reasons, the adsorptive carbon capture technology needs to be improved on several fronts with appropriate research.

Research on capture by physical adsorption has been reviewed by more than one study. Mention is made of the work of Ben-Mansour et al. [84] in which both experimental work on suitable materials and mathematical models developed for their study are outlined. It is reported that, for the regeneration procedure, Pressure Swing Adsorption (PSA) is preferred to Temperature Swing Adsorption (TSA) as it consumes less energy. However, the best performance is obtained by combining the two techniques and then implementing Pressure and Temperature Swing Adsorption (PTSA). Akpasi and Isa [27], on the other hand, reviewed carbon dioxide capture research by considering PtG plants and focusing on adsorption capture. The materials that can be used for these purposes and their characteristics are explained. It is concluded that in order to solve the capture problem, it is not possible to rely on a single method but it is necessary to evaluate the most suitable one on a case-by-case basis.

The aspect of the materials choice was experimentally investigated by Veselovskaya et al. [85]. Specifically, a composite sorbent (potassium carbonate and alumina) was used to capture carbon dioxide from air and demonstrated its cyclic operability. Razaei and Grahn [86], on the other hand, focused on the thermal management of adsorbent materials. The thermodynamic study is implemented based on a dynamic model of the physics involved in adsorbent solids. It is stated that materials of this type can handle well both temperature variations and non-isothermal conditions.

3.2.2 Combined carbon capture and methanation

As illustrated in Section 2.3.2, the combined capture of carbon dioxide and methanation on a solid sorbent can be configured in several ways. It is possible to make use of two separate vessels, a single vessel that includes both adsorbent and catalytic material, or a single vessel that contains a bi-functional material. All of these configurations have been, some more than others, investigated in the literature of this field. The paper by Melo et al. [28] reviewed the topic by presenting studies that have dealt with each of these configurations.

Duyar et al. [87] experimentally made use of a bi-functional material to capture carbon dioxide from flue gases and implemented methanation in the same site. The adsorbent material was calcium oxide while the catalyst was ruthenium, both were placed on an alumina support. The authors demonstrated the feasibility of the concept by operating multiple cycles. Jeong-Potter and Farrauto [88] continued the above-presented work. Here, again using a bi-functional material, the authors experimentally evaluated DAC by also analyzing the effects that air humidity can have. The feasibility of methane synthesis from hydrogen and air by using this technology is stated. The CCCM in the same site was considered also by Chai et al. [89] and by Martins et al. [90]. In the former, various materials were analyzed and the more suitable indicated. In the latter two identical vessels that alternated between the adsorption and methanation phases were tested. The authors performed analyses regarding the operating conditions. The advantage of this configuration is that there is no need to transport carbon dioxide.

Capture and methanation in two separate sites were analyzed by the group of Veselovskaya et al. in multiple papers. In the study [91] two separate vessels were considered. Through an approach more devoted to the study of the component materials than the whole process, chemical kinetics were analyzed demonstrating high conversion rates. In addition, in the investigation [92], capture and methanation were implemented in two different locations of the same vessel. The capture of carbon dioxide from the air is evaluated. It is underlined that using two separate vessels facilitates the operation as different thermodynamic conditions can be maintained. An experimental demonstration of this technology with a process perspective was realized by Yamamoto et al. [93]. In this case, four adsorbent beds were used for carbon dioxide capture, alternating between the various process phases. Furthermore, from the methanation reactors, heat was collected and used for the preheating and the regeneration of the adsorbent beds.

3.2.3 Sorption-enhanced methanation

The utilization of adsorbent materials for process intensification is highly investigated in the literature. Focusing on the field of energy carrier synthesis, the following is reported. Iliuta et al. [94] dynamically modeled the sorption-enhanced production of dimethyl ether (DME) by simulating different operating conditions and analyzing the influence they might have on conversion. It is highlighted that it is essential to evaluate the dynamics of these processes since, operating cyclically, they never reach a lasting steady state condition. For this very reason, the modeling approach adopted by Dehghani et al. [95] was dynamic. In this case, the sorption-enhanced production of methanol was evaluated and via an evolutionary algorithm a dynamic optimization was implemented taking into account the long-term catalyst deactivation. The methanol synthesis is also evaluated in the work of Moioli and Schildhauer [96]. Here the focus was on the configuration of the catalytic adsorptive reactor. The authors compared, in this regard, the performance of a fixed bed reactor with an entrained flow reactor and propose a third configuration where the sorbent is recirculated by bubbling.

The sorption-enhanced approach applied to methanation was initially evaluated by Borgschulte et al. in 2013 [97]. In this study, the preparation of the bi-functional material consisting of catalyst particles (nickel) on sorbent support (zeolite) is reported. The path of the chemical reaction taking place was analyzed. It is underlined an intermediate step for the carbon monoxide formation and successively its conversion in methane. The same group produced several other investigations on this subject. In the study [98] the authors focused on the bi-functional material by evaluating the effect of sorbent pore size. It is concluded that the structure of catalyst and sorbent is crucial in improving material selectivity and process kinetics. In the investigation [99] the long-term stability of the materials was tested. It is found that, compared to the conventional variant, sorption-enhanced catalysis leads to greater carbon deposition. This, however, does not lead to problems of catalyst deactivation but rather of diffusion of the adsorbed water. In the work [100], the progressive diffusion of water in the solid sorbent by the neutron radiography method was evaluated. A front moving along the reactor is shown. This front affects both adsorption and reaction as this phenomena are strictly related since where adsorption occurs there is a great conversion due to Le Chatelier's principle.

Walspurger et al. [101] demonstrated experimentally the very high conversions that can be achieved at relatively low pressures. The authors stated that with conventional reactors high conversions can be achieved only by highly increasing the pressure, however, this affects the cost of components and the compressor consumption. Wei et al. [102] tested different bi-functional materials suitable for sorption-enhanced methanation with different catalyst content by evaluating and comparing their performance. In addition,

these materials were tested for various cycles to evaluate their decrease in performance over time. Agirre et al. [103] and Coppola et al. [104] also tested various sorbents. The former with the purpose to optimize the operating conditions while the latter evaluating them for cyclic operation in fluidized beds.

Gomez et al. [105] considered both carbon monoxide and carbon dioxide methanation with sorption enhancement. Once again, it is shown experimentally that this technology allows high product purity to be obtained. Furthermore, the optimal operating conditions were studied. It is concluded that higher purities of methane can be obtained when carbon monoxide and carbon dioxide are converted separately because the two reaction paths need different optimal operating conditions. Kiefer et al. [106] investigated both the water adsorption alone and the sorption-enhanced reaction. From an up-scaling perspective the authors confirmed that heat dissipation is the major issue and must be at the basis of reactor design considerations. The experimental characterization is complemented with a simple mathematical model.

Few other papers on this topic make use of a mathematical approach. Massa et al. [107] used the Gibbs free energy minimization method to study the sorption-enhanced reaction from a thermodynamic point of view, focusing on low pressures. The limits leading to carbon deposition are analyzed. Bareschino et al. [108] studied numerically the reactor behavior by means of a two-dimensional model. The focus was on the evaluation of breakthrough times. This was performed by sensitivity analyses on the variation of flow rate and other operating parameters.

Considering what was presented, it is highlighted that mathematical models developed for the simulation of the whole sorption-enhanced methanation process are lacking in the literature.

3.3 Research gaps and thesis contribution

Based on the literature review presented above, considering the important research efforts regarding the development of PtG plants, it is clear that systems of this type have the potential to make a fundamental impact on the energy transition. In addition, it emerges that the use of adsorption technologies can be highly efficient when there is a need to implement gas separation or in the intensification of synthesis processes.

It is noted, however, that there is a general lack of detailed investigations concerning the dynamics of the entire process from both a modeling and experimental point of view. Based on the highlighted research gaps, the contribution that the thesis at hand provides can be summarized by the following main aspects.

- Comprehensive analysis of the role that adsorptive materials can play in improving power-to-gas systems.
- Development of a dynamic model of adsorptive carbon dioxide capture. Assessment of the role that hydrogen can have as a purge agent for the subsequent use of the desorbed mixture as a feedstock for methane production.
- Experimental characterization of the operation of a sorption-enhanced catalytic methanation system in transient operation.
- Development of a sorption-enhanced methanation process model validated on the experimentally obtained data. Evaluation of the alternating operation of two reactors in parallel for continuous methane synthesis.

These novelties will be explained in detail in the next chapters of the dissertation. Specifics of the mathematical models developed, of the experimental procedures employed, and of the applications will be illustrated.

Chapter 4

Mathematical modeling approach

This chapter discusses the general approach used for the mathematical modeling of the investigations carried out within the thesis. Based on the general models presented here, further details of the model developed for the specific application will then be given in the next chapters. Since packed beds received special attention during mathematical models developments, Section 4.1 will cover the methodology used for modeling these elements. These include both adsorption beds and fixed-bed chemical reactors. In Section 4.2, the other components used in the various systems studied will be presented.

4.1 Packed beds

Packed beds, or fixed beds, are configured as vessels filled with solid beads (pellets) that compose the bed. In contrast to fluidized beds, the pellets are static. They can be either monotubular or multitubular and can exchange heat with a heat transfer fluid on either the outer or inner surface. They are often used in the chemical industry for heterogeneous catalysis but they can also be used for other purposes. In the case of fixed-bed chemical reactors, the pellets support the catalyst. Generally, a gaseous flow passes through the packed beds and interacts with the surface of the pellets.

This section will illustrate the modus operandi for packed beds modeling. The general rationale behind it will first be presented, and then a declination of it in application to fixed-bed chemical reactors will be presented.

4.1.1 Rationale

The mathematical models of packed beds that were used for the thesis analyses involve a one-dimensional discrete finite volume approach. Considering cylindrical monotubular packed beds, a spatial discretization was implemented along the axis of the cylinder as

shown in Figure 4.1. The Control Volume (CV) is the fundamental unit of this axial discetization. The number of CVs can be extended as desired based on the level of detail desired for a given simulation.

Regarding specifically the simulations of this thesis, the number of CVs adopted is always moderate due to the need to preserve computational time. As stated in [109], for approaches similar to the one adopted in this thesis, with a low number of control volumes, the error is higher but of the same order of magnitude as more sophisticated models. Significant benefits in terms of error reduction are only seen at high numbers of control volumes, which comes at the expense of computational times orders of magnitude greater.

Each CV was characterized using a lumped parameter approach, assuming homogeneous properties of gases present inside the control volume. In this configuration, axial diffusion phenomena were considered negligible. In fact, based on estimations of thermal and species Péclet numbers, it can be concluded that diffusive transport is negligible compared to advective transport. This assumption is commonly employed in the modeling of similar components [110].

It was decided to include the possibility of modeling the heat exchange with the external environment by considering a possible coolant flowing in the cylindrical jacket of the packed bed. As will be seen in the following, while the gas flow was modeled as one-dimensional in the axis direction, heat exchange with the coolant was evaluated as radially, considering the cylindrical lateral surface of each CV. The solid phase within the CV is considered to be porous through a bulk and a particle density, leading to the void fraction, and a tortuosity factor. As will be seen below, the interaction between the gas and solid phase is modeled both from a transport point of view, considering the velocity in porous media, and from a thermal point of view. In the second case, thermal capacity and conductivity of the solid take effect when the radially exchanged heat is calculated.

In each control volume, the conservation equations of mass and energy were written in differential form. This choice was made in order to dynamically simulate the variation of the desnsity ρ of each species. The mass conservation was expressed by Equation 4.1.

$$(Sl)\,\varepsilon\frac{\partial \rho_\alpha}{\partial t} = Q_{\mathrm{v,in}}\,\rho_{\alpha,\mathrm{in}} - Q_{\mathrm{v}}\,\rho_\alpha \tag{4.1}$$

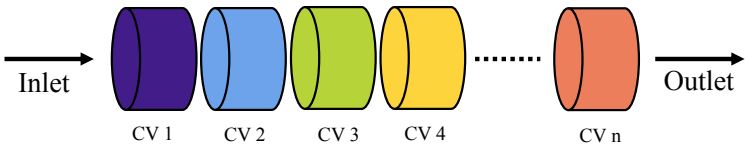

Figure 4.1: Schematic representation of packed beds models discretization.

Where the product of S and l represents the volume of the CV. In the right side of the equation is it possible to see inlet and outlet mass flow rates The subscript "in" refers to the inlet of the CV, which corresponds to the outlet of the preceding one. The subtracted term refer to the mass flow rate calculated in the specific control volume. That mass flow rate is the one leaving the CV and entering in the following one. The volumetric flow rate Q_{v} was calculated by considering the bed porosity ε as follows.

$$Q_{\mathrm{v}} = S\varepsilon u \tag{4.2}$$

The gas flow velocity through each control volume was determined based on the pressure drop between that CV and the subsequent one, considering that the control volumes are arranged in series.

$$u = \sqrt{\frac{\Delta p\, \psi\, d_{\mathrm{p}}}{f\, l\, \rho}} \tag{4.3}$$

By calculating the pressure in an outlet volume downstream of the bed, the flow velocity in the final control volume could also be determined. The friction factor for the pressure drops calculation was evaluated using the Ergun correlation [111] as can be seen in Equation 4.4.

$$f = \frac{1-\varepsilon}{\varepsilon^3}\left(1.75 + 150\frac{1-\varepsilon}{\psi\, d_{\mathrm{p}}\, \rho\, u/\mu}\right) \tag{4.4}$$

The energy conservation equation considered the contribution reported in Equation 4.5.

$$(\rho c)_{\mathrm{eff}}\,(Sl)\,\frac{\partial T}{\partial t} = \sum_{\alpha}\left(\dot{m}_{\alpha,\mathrm{in}} h_{\alpha,\mathrm{in}} - \dot{m}_{\alpha} h_{\alpha}\right) - \dot{Q}_{\mathrm{rad}} \tag{4.5}$$

Where the terms $h_{\alpha,\mathrm{in}}$ and h_{α} refers, respectively, to the specific enthalpy of the inlet gas and the specific enthalpy of the species α contained in the specific control volume. The speciftic enthalpies are calculated as follows.

$$h = c_{\mathrm{p}} T \tag{4.6}$$

Where c_{p} depends on the temperature and on the gas mixture composition, as will be detailed in Equation 4.29 [112] . The subscript "eff" indicates the effective thermal capacity of both the solid bed and the gaseous flow. For each control volume, the radial heat $\dot{Q}_{\mathrm{rad}}$ exchanged with the external environment (the coolant fluid circulating in the cylindrical

jacket) was estimated by assuming a constant global heat transfer coefficient, denoted with U in Equation 4.7.

$$\dot{Q}_{\mathrm{rad}} = \pi\,(Dl)\,U\,(T - T_{\mathrm{cool}}) \tag{4.7}$$

The value of the global heat transfer coefficient U was estimated a priori considering heat and mass transfers in packed beds with fluid flow, as outlined by Tsotsas in [113]. One of the contributions of U, the heat transfer coefficient γ at the reactor inner wall (subscript w), was evaluated using the following equation.

$$\gamma_{\mathrm{w}} = \mathrm{Nu}_{\mathrm{w}} \frac{\lambda_{\mathrm{g}}}{d} \tag{4.8}$$

With the Nussult number at the wall evaluated with Equation 4.9.

$$\mathrm{Nu}_{\mathrm{w}} = \left(1.3 + \frac{5}{\frac{D}{d}}\right) \frac{\lambda_{\mathrm{bed}}}{\lambda_{\mathrm{g}}} + 0.19\,\mathrm{Re}^{\frac{3}{4}}\,\mathrm{Pr}^{\frac{1}{3}} \tag{4.9}$$

In this case, the characteristic length for the Reynolds number was the pellet diameter. Fluid properties were determined according to the methodology outlined in [114]. Specifically, the viscosity was determined using the Wilke correlation, while the thermal conductivity was calculated using the correlation provided by Mason and Saxena.

The boundary conditions of the fixed bed are mass flow rate, mole fraction and temperature of the inlet gas, outlet pressure, and coolant temperature. The inital conditions are the pressure and composition of the fill gas.

4.1.2 Fixed-bed reactors

The model described above can be used as a basis for modeling heterogeneous fixed-bed chemical reactors. In that case it is necessary to additionally consider the fact that the conversion of reactants into products is implemented. In particular, mass flow rate terms related to the generation and disappearance of the species have to be included in the mass conservation equation.

$$(Sl)\,\varepsilon \frac{\partial \rho_{\alpha}}{\partial t} = (Q_{\mathrm{v,in}}\,\rho_{\alpha,\mathrm{in}} - Q_{\mathrm{v}}\,\rho_{\alpha}) + \dot{m}_{\alpha,\mathrm{gen}} \tag{4.10}$$

Where the generation term (subscript gen) can be positive or negative depending on whether there is formation or disappearance of a given chemical species α. For the purpose of this calculation, it is essential to take into account the chemical kinetics of the reactions considered, as evidenced by Equation 4.11.

$$\dot{m}_{\alpha,\text{gen}} = (Sl)\,\rho_{\text{cat}}(1-\varepsilon)M_\alpha \sum_j v_{\alpha j} r_j \tag{4.11}$$

In addition, an internal heat generation term must be included in the energy conservation equation. This will make it possible to take into account the heat release of exothermic reactions and, if the generation term is negative, the heat absorption of endothermic reactions.

$$(\rho c)_{\text{eff}}\,(Sl)\,\frac{\partial T}{\partial t} = \sum_\alpha (\dot{m}_{\alpha,\text{in}} h_{\alpha,\text{in}} - \dot{m}_\alpha h_\alpha) + \dot{Q}_{\text{gen}} - \dot{Q}_{\text{rad}} \tag{4.12}$$

Based on these concepts, the approach developed here could be applied to a wide variety of fixed-bed reactors. In what follows, details of the application of these concepts to a methanation reactor will be presented.

In this case, the reactions included in the kinetic model considered the carbon dioxide methanation (cdm, Equation 4.13), the carbon monoxide methanation (cmm, Equation 4.14), and the reverse water gas shift (rwgs, Equation 4.15) [10] as reported below.

$$CO_{2_{(\text{g})}} + 4H_{2_{(\text{g})}} \leftrightarrows CH_{4_{(\text{g})}} + 2H_2O_{(\text{g})}, \qquad \Delta H_r^0 = -165.1 \ \text{kJ/mol} \tag{4.13}$$

$$CO_{(\text{g})} + 3H_{2_{(\text{g})}} \leftrightarrows CH_{4_{(\text{g})}} + H_2O_{(\text{g})}, \qquad \Delta H_r^0 = -206.2 \ \text{kJ/mol} \tag{4.14}$$

$$CO_{2_{(\text{g})}} + H_{2_{(\text{g})}} \leftrightarrows CO_{(\text{g})} + H_2O_{(\text{g})}, \qquad \Delta H_r^0 = +41.3 \ \text{kJ/mol} \tag{4.15}$$

The reaction rates were modeled according to the approach proposed by Xu and Froment in [115], using the following equations.

$$r_{\text{cdm}} = \frac{\frac{k_{\text{cdm}}}{p_{H_2}^{3.5}}\left(p_{CH_4}\,p_{H_2O}^2 - \frac{p_{H_2}^4\,p_{CO_2}}{K_{\text{cdm}}}\right)}{\left(1+\beta_{CO}\,p_{CO}+\beta_{H_2}\,p_{H_2}+\beta_{CH_4}\,p_{CH_4}+\frac{\beta_{H_2O}\,p_{H_2O}}{p_{H_2}}\right)^2} \tag{4.16}$$

$$r_{\text{cmm}} = \frac{\frac{k_{\text{cmm}}}{p_{H_2}^{2.5}}\left(p_{CH_4}\,p_{H_2O} - \frac{p_{H_2}^3\,p_{CO}}{K_{\text{cmm}}}\right)}{\left(1+\beta_{CO}\,p_{CO}+\beta_{H_2}\,p_{H_2}+\beta_{CH_4}\,p_{CH_4}+\frac{\beta_{H_2O}\,p_{H_2O}}{p_{H_2}}\right)^2} \tag{4.17}$$

$$r_{\text{rwgs}} = \frac{\frac{k_{\text{rwgs}}}{p_{H_2}}\left(p_{CO}\,p_{H_2O} - \frac{p_{H_2}\,p_{CO_2}}{K_{\text{rwgs}}}\right)}{\left(1+\beta_{CO}\,p_{CO}+\beta_{H_2}\,p_{H_2}+\beta_{CH_4}\,p_{CH_4}+\frac{\beta_{H_2O}\,p_{H_2O}}{p_{H_2}}\right)^2} \tag{4.18}$$

Where k, K, and β represent temperature-dependent functions. These three equations are based on the partial pressure (p_α) of the chemical species involved.

4.2 Other elements

The analyses performed included in each case system simulations. The components that were involved in the various analyses are listed below. Depending on the system considered, some or all of these elements could be present.

- Tanks
- Pipes
- Heat exhangers
- Valves
- Fans
- Compressors

These elements were modeled through a zero-dimensional lumped-parameter approach. The equations used for the mathematical model of these components are provided in the following.

The modeling approach for the tanks was based on the mass dynamics of gases inside confined volumes. The gas flows entered and exited the tanks at a specified temperature and composition, causing the pressure to vary dynamically [116]. The gas pressure variations in the tanks were determined, thus, using the mass conservation equation and the ideal gas law, as described in [112].

$$p = \frac{M_\alpha(t)}{V} \sum_\alpha X_\alpha R_\alpha T \tag{4.19}$$

With X representing the gas mole fraction and M the molar mass of the species α.

With regard to pipes models, the mass flow rates of the gases passing through the pipes were modeled considering the diffrence between upstream and downstream pressures by means of Equation 4.20.

$$p_{\text{in}} - p_{\text{out}} = \frac{\dot{m}^2}{\rho S}\left(\frac{fL}{D_{\text{int}}} + Z\right) \tag{4.20}$$

Where f is the friction factor and Z representes the concentrated pressure losses. The heat exchanger model was treated as a pipe, where the mass flow rate was determined based on the pressure drop. In addition, heat exchange occurred radially through the walls of the heat exchanger duct, assuming a constant global heat transfer coefficient. The temperature change of the gas flow was thus calculated as follows.

$$\frac{\partial T}{\partial t} = \pi \left(Dl\right) U \left(T - T_{\text{ext}}\right) \tag{4.21}$$

The valve model was based on the principles of flow dynamics within restrictions, as outlined in [112] and expressed by Equation 4.22.

$$\dot{m} = C_{\text{v}} Y \sqrt{\rho_{\text{in}} \Delta p} \tag{4.22}$$

The flow compressibility was accounted for by the valve expansion factor Y, which depends on the upstream and downstream pressures. The valve openings were regulated using Proportional Integral Derivative (PID) controllers to manage the outlet mass flow rates.

Fans and compressors were modeled using performance maps, which were scaled according to similarity laws. The performance maps were accessed through the terms of corrected rotational speed, the corrected mass flow rate and the pressure ratio.

$$N_{\text{c}} = \frac{N}{\sqrt{R_\alpha T_{\text{in}}}} \tag{4.23}$$

$$\dot{m}_{\text{c}} = \frac{\dot{m}\sqrt{R_\alpha T_{\text{in}}}}{p_{\text{in}}} \tag{4.24}$$

The temperature rise of the gas due to compression was calculated by means of a polytropic equation. In it, the compressibility coefficient was calculated by means of the Amgat approximation.

4.3 Gas mixture physical properties

Lastly, the more relavant equations for the calculation of the gas propeties are reported below. The gas mixture viscosity was calculated by means of the Davidson equation (Equation 4.25) while the viscosity of each species was calculated using the Sutherland model (Euation 4.28). For the sake of clarity, in this section, the average properties of the mixtures are overlined.

$$\overline{\mu}\left(T,X\right)=\frac{1}{\sum_{ij}y_iy_j\left(\overline{\phi}_{ij}\right)^{\frac{1}{3}}\left(\mu_i\mu_j\right)^{-\frac{1}{2}}} \tag{4.25}$$

$$\overline{\phi}_{ij}=\frac{y_i\phi_{ij}+y_j\phi_{ij}}{y_i+y_j} \tag{4.26}$$

$$\phi_{ij}=\frac{2M_j}{M_i+M_j} \tag{4.27}$$

$$\mu_i\left(T\right)=\mu_i^0\frac{T_i^0+n_{S,i}}{T+n_{S,i}}\left(\frac{T}{T_i^0}\right)^{\frac{3}{2}} \tag{4.28}$$

Where the mixture viscosity is calculated considering the viscosities of the single species, the fluidity ϕ and the angular momentum fraction y.

The specific heat at constant pressure of the single gases was calculated by means of a cubic interpolation [117]. The specific heat of the gas mixture was calculated considering the mole fractions.

$$\overline{c_p}(T,X)=\frac{1}{M_{avg}}\sum_i X_ic_{p,i}(T) \tag{4.29}$$

$$c_{p,i}=\frac{R\left(a_{1,i}+\frac{a_{2,i}}{2}\ T+\frac{a_{3,i}}{3}T^2+\frac{a_{4,i}}{4}T^3\right)}{M_i} \tag{4.30}$$

The density was calculated using the perfect gas law. The gas mixture was considered perfect due to the relatively low pressure levels investigated and the fact that the gas molecules considered contain a small number of atoms.

$$\overline{\rho}\left(p,T,X\right)=\frac{pM_{avg}}{R_{avg}T} \tag{4.31}$$

Chapter 5

Adsorption-based carbon capture in power-to-gas plants

In the framwork of CCU, where the utilization of carbon dioxide is expressed in its conversion to methane, this chapter investigates the use of adsorption for carbon dioxide capture. Specifically, Section 5.1 will examine in detail how adsorption-based carbon capture can be carried out [118] while Section 5.2 will expand the system under investigation to include the catalytic conversion process of captured carbon dioxide into methane.

5.1 Adsorptive capture of carbon dioxide in the power-to-gas context

This section will outline the methods adopted for the analysis by first presenting the system analyzed and then the mathematical model used for its simulation. The results will illustrate both the behavior of carbon dioxide adsorption and of a cycle with both adsorption and desorption. Furthermore, considerations related to hydrogen-aided bed regeneration will be outlined.

5.1.1 Methods

5.1.1.1 System layout

The layout of the studied system is depicted in Figure 5.1. The process involves two cyclically alternating phases. In the first phase carbon dioxide is captured inside the adsorption bed through adsorption. In the second phase the bed is regenerated via desorption.

The two phases (adsorption and desorption, indicated respectively in blue and red) were alternated and conducted cyclically. The adsorption unit consisted of a packed bed

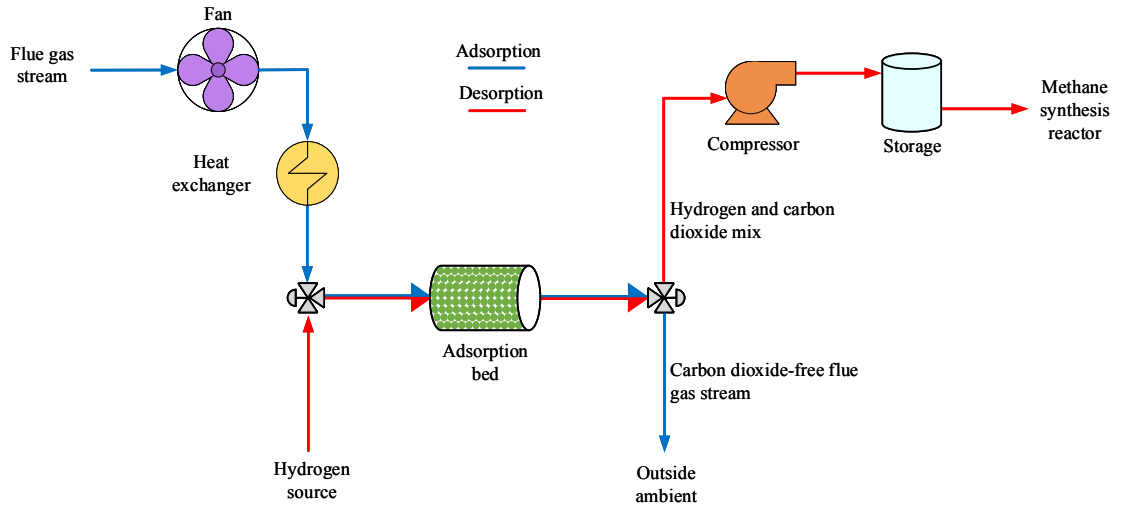

Figure 5.1: Layout of the carbon capture system.

with a radius of 35 cm and a length of 5 m. The bed void fraction was equal to 0.52 and the sorbent material selected was a commercial activated carbon (NORIT R2030).

During the adsorption phase, a fan directed the gas stream, containing carbon dioxide to be removed, towards the adsorption bed. The exhaust gas stream was considered to be pre-dried. Before the entrance of the bed, the gas stream was cooled to approximately room temperature using a heat exchanger. This cooling step was necessary because the adsorption capacity of the bed increases with lower temperatures. After passing through the adsorption bed, the gas stream, now depleted of its carbon dioxide content, was discharged into the external environment.

During the desorption phase, hydrogen was introduced to purge the adsorption bed, enabling carbon dioxide desorption. The model assumed a hydrogen source at a specified pressure, representing a potential supply from an electrolysis system. To facilitate desorption, the adsorption bed was heated to 250 °C, and the hydrogen flow entering the adsorption unit was preheated to the same temperature.

At the conclusion of the desorption phase, the adsorption bed released the carbon dioxide that had been adsorbed in the previous phase. Subsequently, the bed conditions were set for the next cycle. At the outlet of the bed, the mixture of desorbed carbon dioxide and hydrogen was directed to a storage system using a compressor. The compressor speed was regulated to maintain suction conditions that ensured a constant depressurization within the bed. The regeneration process, achieved through a combination of temperature increase and depressurization, was categorized as pressure and temperature swing adsorption (PTSA).

It was assumed that the adsorption bed was 100 % selective to carbon dioxide and so

that there was no adsorption of other chemical species. This assumption was made by considering the fact that the chosen sorbent material presents much better affinity with carbon dioxide with respect to other species. This aspect can be seen graphically in Figure 5.2 according to the data of [119]. The figure presents isotherms for nitrogen and carbon dioxide (the two species taht will be analyzed later on) at three different temperatures and a relevant pressure range. It can be seen that the equilibrium uptake quantity for the carbon dioxide is more than one order of magnitude higher thant that of nitrogen.

5.1.1.2 Mathematical model

The study was conducted using a dynamic model that represented the entire system described earlier. The model was implemented within a MATLAB®/Simulink® environment and solved using a variable-step solver designed for stiff differential equations (ode15s). The system, shown in Figure 5.1, was modeled in its entirety.

The adsorption bed model was designed in more details and included also the dynamics of adsorption. Specifically, the model of this component was developed on the basis of the model of packed beds described in Chapter 4. In this case the bed was spatially discretized into 10 control volumes. This choice was undertaken to achieve results that were deemed acceptable without burdening the computational costs of the calculation, considering that the model contained other components that needed to interact with each other.

The mass balance for a generic species α was calculated in each CV using Equation 4.1. In the case of carbon dioxide, a sink term was additionally included to account for the adsorbed (ore desorbed, if negative) flow rate [120].

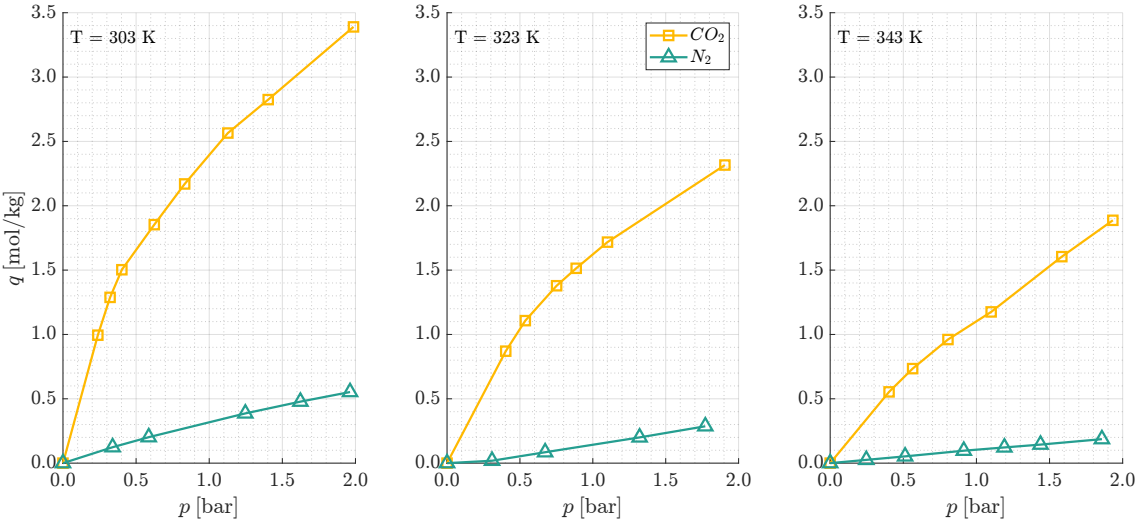

Figure 5.2: Adsorption isotherms for nitrogen and carbon dioxide on Norit R2030 activated carbon at 303 K, 323 K and 343 K.

$$(S\,l)\,\varepsilon\frac{\partial \rho_{CO_2}}{\partial t} = \dot{m}_{CO_2,\,\mathrm{in}} - \dot{m}_{CO_2} - \dot{m}_{\mathrm{ads}} \tag{5.1}$$

$$\dot{m}_{\mathrm{ads}} = (1-\varepsilon)\,(S\,l)\,\rho_{\mathrm{s}}\frac{\partial q_{CO_2}}{\partial t}M_{CO_2} \tag{5.2}$$

As can be seen, the adsorbed flow rate depended on the adsorption rate term ($\frac{\partial q_{CO_2}}{\partial t}$). This factor was calculated using the linear driving force model, expressed by Equation 5.3. The term ϱ indicates the mass diffusion resistance parameter.

$$\frac{\partial q_{CO_2}}{\partial t} = \frac{q^*_{CO_2} - q_{CO_2}}{\varrho_{CO_2}} \tag{5.3}$$

It can be seen that the adsorption rate depends on the deviation of the adsorbed phase concentration with the equilibrium value (superscript $*$), calculated using the Dubinin-Astakhov isotherm [121] as shown in the following equation.

$$\frac{q^*_{CO_2}}{q_{\mathrm{max},\,CO_2}} = e^{-\left(\frac{R\,T}{E}\ln\frac{p_{\mathrm{sat}}}{p_{CO_2}}\right)^{n_{\mathrm{D\text{-}A}}}} \tag{5.4}$$

The saturation pressure was calculated according to what is proposed in [122]. In particular, for temperatures above the critical one the calculation of the saturation pressure was replaced by the calculation of pseudo saturated vapor pressures following the method of Amankwah and Schwarz [123]. The parameters of the model referred to what is reported in [124].

5.1.2 Results

In the following, the simulation results for all the process phases will be shown and discussed. To analyze the adsorption behavior, different post-combustion sources with multiple carbon dioxide contents will be evaluated. Additionally, a complete cycle will be examined, highlighting the behavior of the chemical species as well as the trends in thermodynamic properties during both the adsorption and desorption phases. Finally, desorption will be explored in detail, with a focus on the system response at different pressure levels of the hydrogen source located upstream of the capture unit.

5.1.2.1 Adsorption behavior

Figure 5.3 illustrates the system behavior during carbon dioxide adsorption. For the carbon dioxide source, the input values consisted in various types of flue gases with different

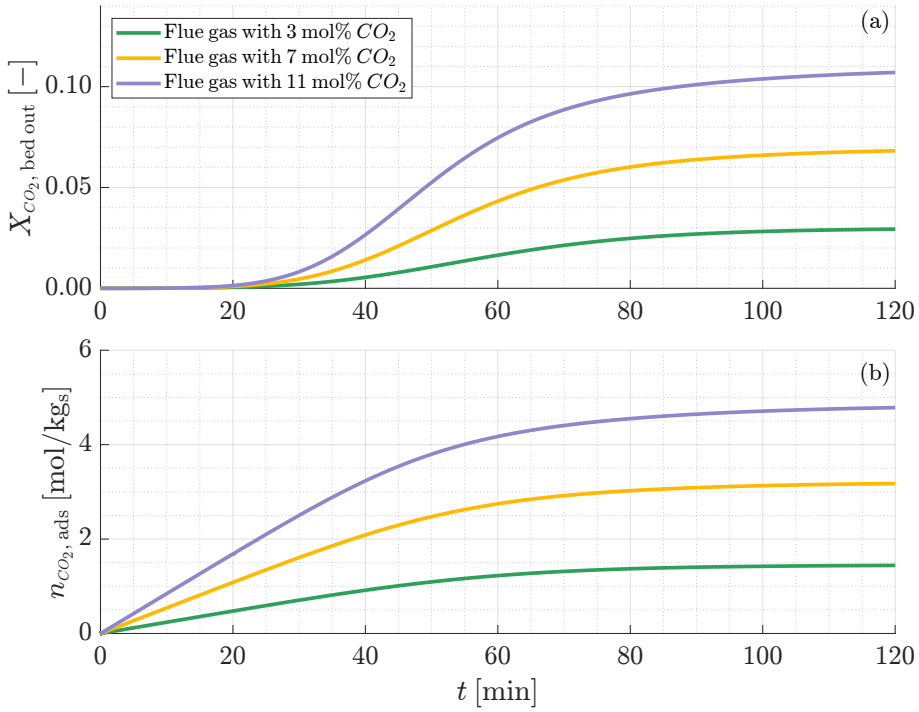

Figure 5.3: Mole fraction of carbon dioxide at the bed outlet (a) and cumulative number of moles of adsorbed carbon dioxide per unit solid mass (b) with three post-combustion carbon sources.

carbon dioxide concentrations. Specifically, a reference case (with 7 mol% CO_2) was compared to a natural gas-fired combined cycle plant (with 3 mol% CO_2), and a pulverized coal plant (with 11 mol% CO_2). The composition of the three different gas mixtures, taken as reported in [125] is presented in Table 5.1.
Figure 5.3(a) reports the evolution in time of the carbon dioxide concentration at the bed outlet, while Figure 5.3(b) presents the cumulative number of moles of carbon dioxide adsorbed, per unit mass of the solid bed, for the three cases assessed.

As shown in Figure 5.3(a), it can be observed that in all cases, during the initial period (the first 20 min), the carbon dioxide concentration in the flow exiting from the bed was zero. During this time, the carbon dioxide present in the input flue gas stream was

Table 5.1: Mole fractions of the flue gases analyzed in Figure 5.3.

	Reference case	Natural gas-fired combined cycle	Pulverized coal
N_2 [mol%]	93	77	76
O_2 [mol%]	0	14	6
H_2O [mol%]	0	6	7
CO_2 [mol%]	7	3	11

captured by adsorption within the bed and so not present in the outlet concentration. It can be seen that, a certain point, the concentration began to approach the inlet value, indicating that all incoming carbon dioxide was no longer being captured and that the bed saturation was reached.

It can be noted that the bed saturation occurred at slightly different times for the three sources under analysis. This is fue to the fact that the partial pressure of carbon dioxide differed among the sources, which in turn affected the adsorption capacity (see Equation 5.4).

At a given temperature, the higher the carbon dioxide partial pressure in the inlet stream, the bigger the adsorption capacity of the bed. As shown in Figure 5.3(b), in fact, the number of moles adsorbed in the case with 11 mol% CO_2 was higher compared to the other two cases.

5.1.2.2 Adsorption-desorption cycle features

Figure 5.4 shows a complete cycle including both the adsorption and the subsequent regeneration. The gas mixture considered for the cycle representation corresponds to the reference case (see Table 5.1), which consisted of nitrogen (93 mol%) and carbon dioxide (7 mol%). The initial condition assumed that the bed was fully charged with hydrogen. The switch time between the phases was set to 20 min. After this period, the input flow was stopped, and pure hydrogen was introduced for the bed regeneration, through which the desorption of carbon dioxide takes place.

In particular, Figures 5.4(a) and 5.4(b) display respectively the pressure and temperature of the gas flow at the bed outlet. Figure 5.4(c) shows the concentration of the gas species at the adsorption bed inlet, while Figure 5.4(d) presents the concentration at the bed outlet. Finally, Figure 5.4(e) illustrates the cumulative number of moles of carbon dioxide adsorbed.

As discussed in Figure 5.3, adsorption occurred during the initial period (the first 20 min). During this time, with nitrogen and carbon dioxide entering the bed at mole fractions of 0.93 and 0.07, only nitrogen exited the bed while the carbon dioxide was retained. Figure 5.4(d) shows that after 20 min, during the desorption phase, the previously adsorbed carbon dioxide was released. During bed regeneration, the desorption was facilitated by reducing the pressure. As shown in Figure 5.4(e), the carbon dioxide that had been adsorbed was gradually released. The pressure at the bed outlet was maintained at a constant 0.5 bar (absolute) by adjusting the compressor rotational speed. Additionally, to promote desorption, as explained in Section 5.1.1 the temperature was increased.

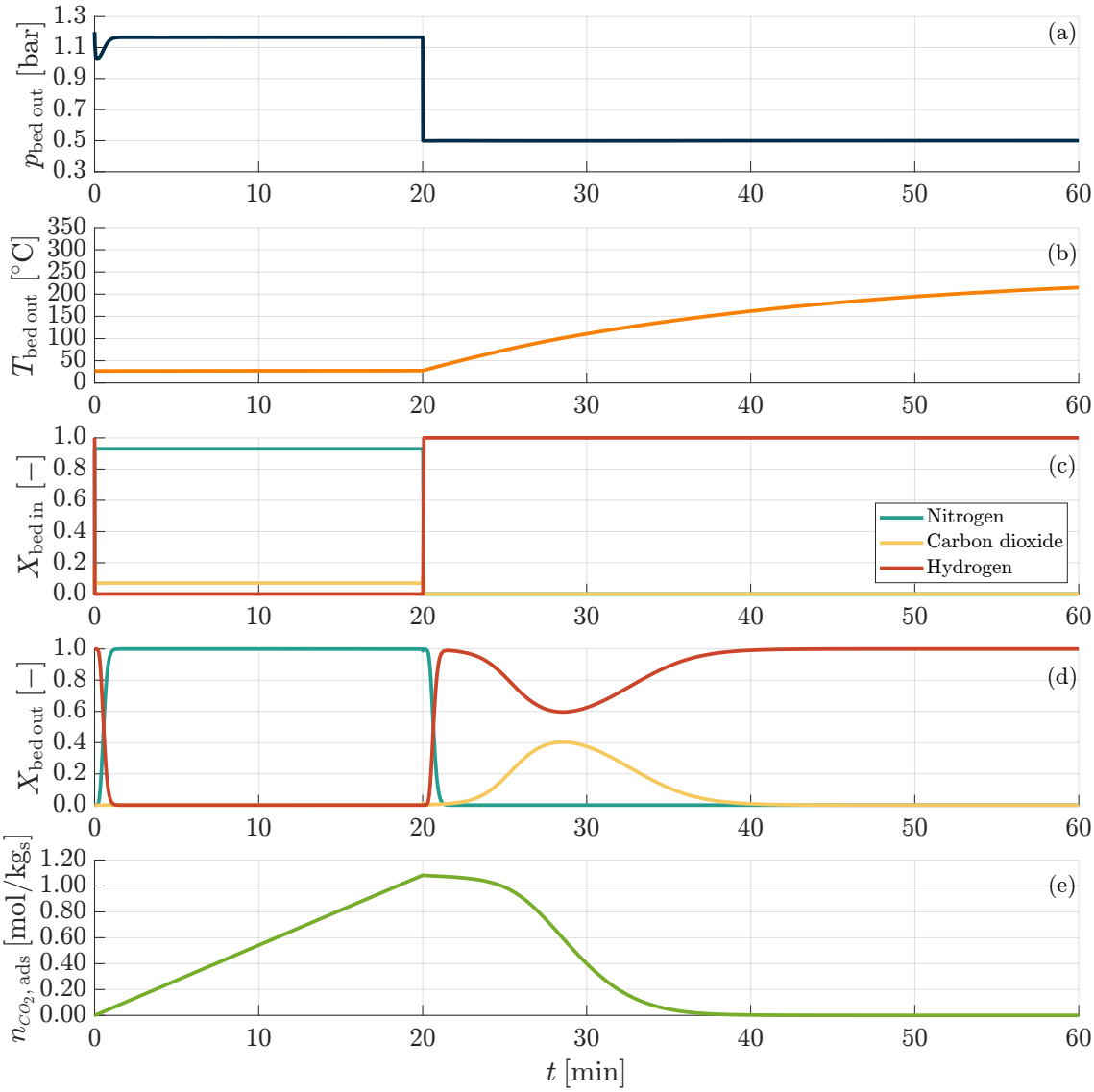

Figure 5.4: Analysis of a complete cycle with 93 mol% nitrogen and 7 mol% carbon dioxide in the inlet flow during the capture phase and 100 mol% hydrogen inlet flow during the regeneration phase. Gas pressure at the bed outlet (a); gas temperature at the bed outlet (b); mole fractions at the bed inlet (c); mole fractions at the bed outlet (d); cumulative number of moles of adsorbed carbon dioxide per unit solid mass (e).

5.1.2.3 Hydrogen bed regeneration insights

In the following, the results related specifically to the desorption phase will be presented. The conditions of the preceding adsorption phase were the same as those discussed in Section 5.1.2.2. The pressure of the hydrogen source upstream of the adsorption bed was varied to assess its effects on regeneration. The set point for the pressure at the bed outlet

was maintained constant at 0.5 bar, controlled by adjusting the compressor speed. As a result, changes in the pressure of the hydrogen source led to variations in the flow rate of hydrogen fed into the bed.

In this regard, Figure 5.5(a) presents the variation in the hydrogen flow rate entering the bed during the desorption phase (starting at 20 min), while Figure 5.5(b) shows the corresponding carbon dioxide mole fraction in the gas mixture exiting the bed.

It can be observed that the mass flow rate curves exhibit a bell-shaped trend during regeneration. This is due to the compressor control, which, in order to maintain a constant pressure in the bed during carbon dioxide release, increased the flow drawn from the bed volume. The time span of carbon dioxide release can be clearly identified in Figure 5.5(b). Once the release of desorbed carbon dioxide was complete, the mass flow rate curves stabilized at a constant value, determined by the pressure difference between the purge hydrogen source and the constant pressure maintained at the outlet of the adsorption bed.

Regarding the mole fraction of carbon dioxide exiting the adsorption bed (Figure 5.5(b)), it is noteworthy that as the pressure of the purge hydrogen source decreased, the peak concentration of carbon dioxide reached a higher value. This is attributed to a reduced dilution effect. Additionally, it is evident that the maximum concentration peaks

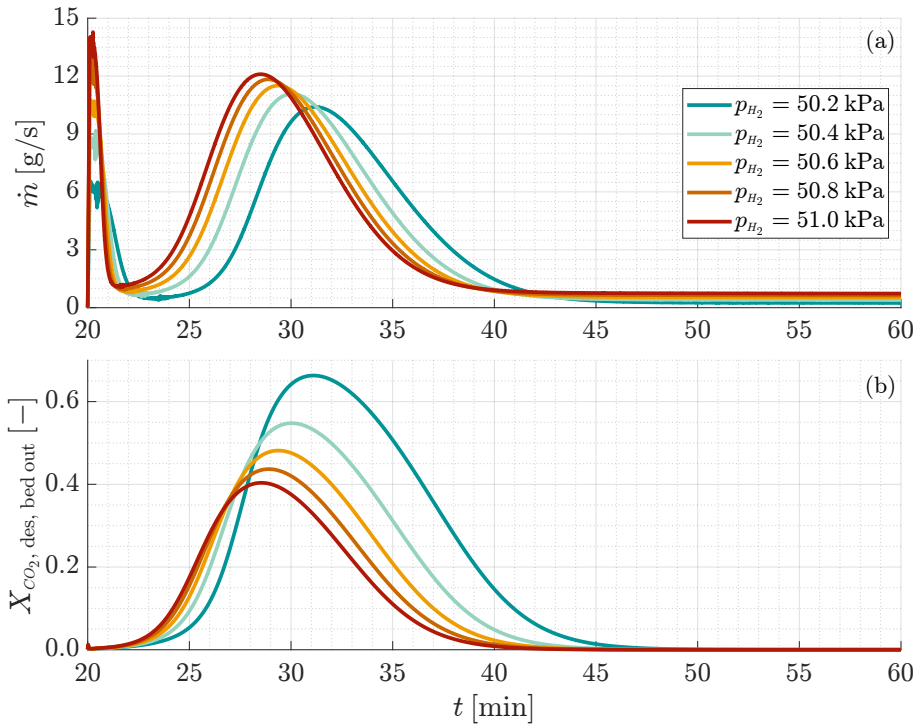

Figure 5.5: Analysis of the regeneration phase considering different hydrogen source pressures. Mass flow rate (a) and mole fraction of carbon dioxide at the bed outlet (b).

shifted to the right as the purge hydrogen source pressure decreased. This shift occurred because, as the purge gas mass flow rate decreased, the desorption strength was weakened, which in turn lengthened the duration of the regeneration phase.

In preparation for the subsequent methanation process, it is crucial to avoid excessive dilution of carbon dioxide content. As shown in Equation 2.2, the molar ratio between the hydrogen and carbon dioxide reactants should be 1:4, corresponding to 20 mol% carbon dioxide.

Building on the discussion of Figure 5.5, Table 5.2 presents the average values of the carbon dioxide mole fraction during desorption, as the purge hydrogen source pressure was varied. Specifically, the mole fraction values shown in Figure 5.4(d) were averaged over the time period during which carbon dioxide desorption occurred. Since the desorption durations varied across the different cases, it was arbitrarily decided to consider the desorption phase complete when the carbon dioxide mole fraction reached 1 mol%.

To provide a comprehensive overview, the table also includes information on the cumulative number of moles of hydrogen and carbon dioxide, as well as the desorption times. It can be seen that as the pressure of the hydrogen source increases, the cumulative moles of carbon dioxide released increases slightly while those for hydrogen increase by an order of magnitude. This leads to excessive dilution of the extracted carbon dioxide. Therefore, as can be observed, only at low flow rates it was possible to maintain a carbon dioxide concentration of 20 mol% or higher. However, from a plant management perspective, achieving the exact stoichiometric value is not strictly necessary. In fact, if the average mole fraction of carbon dioxide is slightly over-stoichiometric, additional hydrogen could be introduced before the methanation reactor to restore the system to stoichiometric conditions. The flow rate of this hydrogen would be corrected based on real-time measurements of the carbon dioxide concentration in the reactant mixture.

In contrast, an excess of hydrogen (i.e., carbon dioxide at sub-stoichiometric concentrations) can be tolerated within certain limits. This condition would result in some

Table 5.2: Comparison of desorption times, cumulative number of moles of carbon dioxide and hydrogen and average carbon dioxide mole fraction at the bed outlet during the desorption phase with increasing pressure of the hydrogen source.

p_{H_2} [kPa]	t_{des} [s]	$n_{\text{cum},\,CO_2}$ [mol]	$n_{\text{cum},\,H_2}$ [mol]	$X_{\text{out, avg},\,CO_2}$ [mol%]
50.2	1535	519.6	694.2	42.81
50.4	1376	624.2	2322.2	21.19
50.6	1288	645.3	5080.6	11.27
50.8	1228	674.9	6499.1	9.41
51.0	1183	688.2	8427.9	7.55

unreacted hydrogen remaining in addition to the methane produced. As shown in [126], based on the characteristics of the natural gas network, only a limited amount of hydrogen can be accepted. Furthermore, it is important to note that as the pressure of the hydrogen source (and consequently its flow rate) decreased, the duration of the desorption phase was longer.

5.1.3 Discussion

This section examined the adsorptive capture of carbon dioxide and the potential use of hydrogen for sorbent regeneration through a dynamic system model. Framed within the context of power-to-gas, the captured carbon dioxide is seen with a view to its subsequent conversion to methane.

The dynamic aspects of the cyclic process for adsorptive carbon dioxide capture and utilization were analyzed comprehensively, considering the interaction between all components of the system. Initially, the adsorption bed was exposed to a flow containing carbon dioxide, which was separated and retained, and then desorbed. For bed regeneration, a pressure and temperature swing adsorption technique with a hydrogen stream was employed. This approach ensured that the mixture of purge hydrogen and desorbed carbon dioxide would serve as the feedstock for the subsequent catalytic conversion into methane.

A comparison of the adsorption of different potential post-combustion carbon dioxide sources revealed the system behavior in terms of saturation time and the number of moles adsorbed. As the concentration of carbon dioxide in the exhaust gas (and, consequently, its partial pressure) decreases, less carbon dioxide can be adsorbed due to a reduced adsorption capacity. At the same time, this results in longer saturation times. This suggests that adsorption durations are more influenced by the geometry of the adsorption bed (i.e., its volume) than by the concentration of carbon dioxide in the source flow.

The feasibility of regenerating the adsorption bed using a hydrogen stream was also assessed. The effects of varying the purge hydrogen source pressure, and consequently its mass flow rate, underlined the importance of limiting the hydrogen flow to prevent excessive dilution of carbon dioxide, even though this would lead to longer desorption times. Considering all of the factors discussed, this procedure is practically viable.

The time variability of renewable energy generation, carbon dioxide source availability, and methane demand underscores the importance of using dynamic system models, like the one employed in this study, to optimize and understand the behavior of such integrated processes.

5.2 Integration of adsorptive carbon capture and catalytic methanation

This section will outline the methods adopted for the analysis by first presenting the system analyzed and then the mathematical model used for its simulation. The results will delve into system-related aspects and into the integration between adsorptive carbon dioxide capture and catalytic methanation. Remarks will be made about cyclic operation once regime conditions are met.

5.2.1 Methods

5.2.1.1 System layout

Figure 5.6 shows the system investigated. It can be seen that this system is an extension of the one studied in Section 5.1 and schematized in Figure 5.1. It can be noted the presence of a buffer tank, an element that couples the capture system with that of methanation. It is underlined that the capture system, as seen above, operates discontinuously while the catalytic methanation process is assumed to work continuously in steady state.

In addition to the adsorption and desorption phases, the capture process also involved a cooling phase, which was necessary to restore the system to its initial conditions. During the cooling phase, both inlet and outlet flows to the adsorption bed were interrupted and heat was extracted considering a constant global heat trasnfer coefficient. The flow exiting the buffer tank was determined by the pressure difference from the one of the buffer tank and the one downstream of the process. That flow contained a nonstoichiometric mixture of hydrogen and carbon dioxide, whose proportions depended on the mixture present inside the buffer tank. Therefore, a source was provided to supply hydrogen in an appropriate

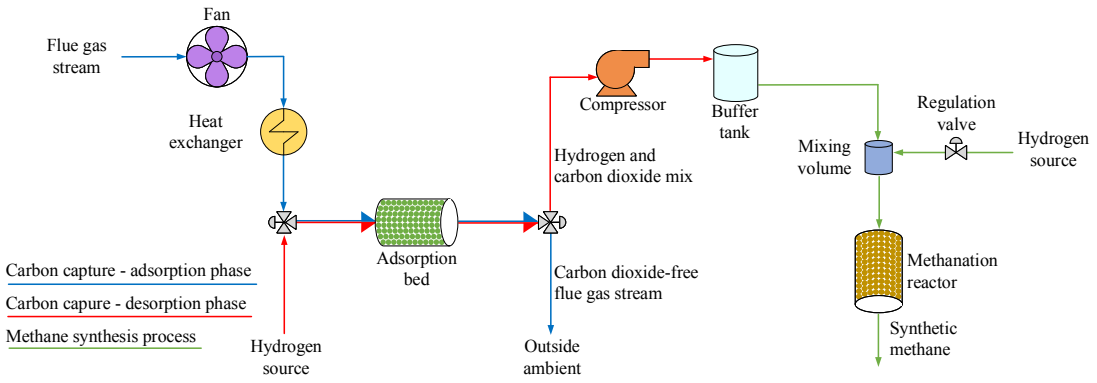

Figure 5.6: System layout schematic.

quantity. The pressure of the hydrogen source was assumed to be constant at a value of 2 bar. The appropriate amount was supplied by a regulation valve whose opening was controlled by a PID controller that estimated the deviation of the concentration of one of the two reactants from the stoichiometric level. The corrective flow rate of hydrogen was combined with that leaving the buffer tank in a mixing volume. Then, the gas mixture under stoichiometric conditions was led toward the methanation reactor, which carried out the chemical conversion. The pressure at the outlet of the reactor was assumed to be constant at a value of 1.4 bar.

5.2.1.2 Mathematical model

The investigation of the adsorptive capture of carbon dioxide and catalytic methanation was conducted by means of simulations, using a dynamic model. Specifically, the model equations were written in the MATLAB®/Simulink® environment and solved with the ordinary differential equation solver ode15s, suitable for stiff problems.

As a result of the fact that the system just described is an extension of the one already analyzed in Section 5.1, the mathematical model used to reproduce the behavior of the system is also an extension of the one already described. For this reason, to examine the mathematical models of the components already explained above it is possile to consult Section 5.1.1, while for those involving the system extension (catalytic methanation process) reference is made to Chapter 4. In particular, the methanation reactor modeled was considered to be cooled with a fluid passing in the tubular jacket. The buffer tank and the mixing volume were modeled on the basis of the tank modeling approach described in Section 4.2. The same for the regulation valve model. The methanation reactor model developed for this specific case was covered in Section 4.1.2. In the present analysis, as a boundary condition, a flue gas stream containing only carbon dioxide and nitrogen, with mole concentrations of 10 % and 90 % respectively, was considered.

5.2.2 Results

5.2.2.1 Cyclic operation

The behavior of the system was analyzed considering multiple cycles. Figure 5.7 shows the cyclic trend of some of the main variables of the whole system. Specifically, a reference is made to the mole fraction of carbon dioxide in the outflow from the adsorption bed 5.7(a), the temperature of the adsorption bed 5.7(b) and the pressure of the buffer tank 5.7(c), which, as mentioned, connects the capture process to the methane conversion process. The cycles are numbered in the figure and are alternately highlighted with gray areas in the background. Each cycle is divided into three phases, separated by dashed vertical lines.

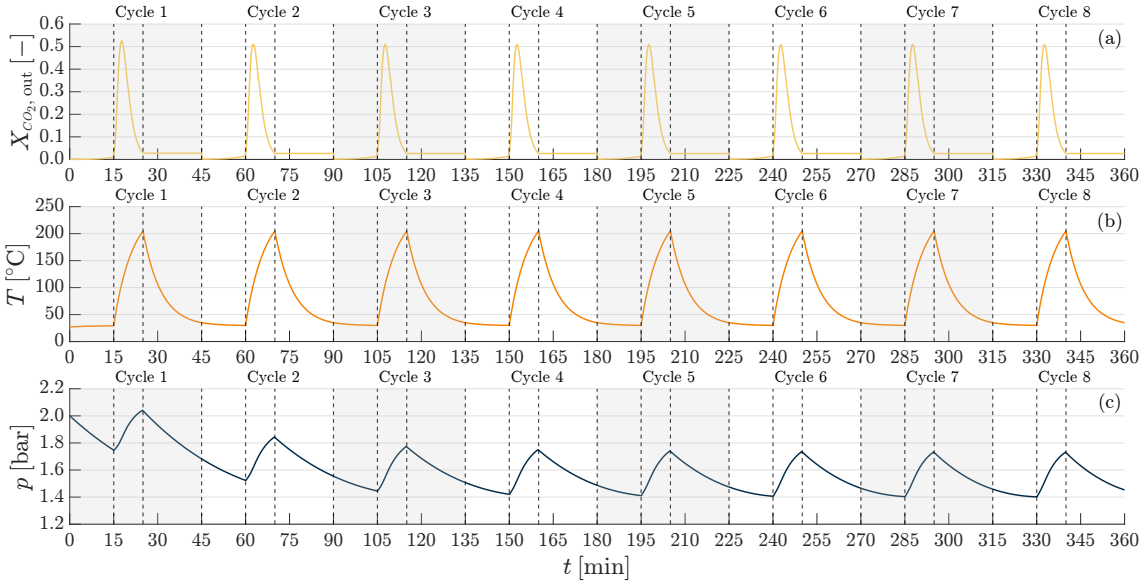

Figure 5.7: System cyclic operation. Adsorption bed outlet carbon dioxide mole fraction (a); adsorption bed temperature (b); buffer tank pressure (c).

Specifically, from the left to the right it is possible to see (i) the adsorption phase, (ii) the desorption phase and (iii) the cooling phase.

Referring to Figure 5.7(b), it can be seen that the temperature of the adsorption bed was restored to the starting value (room temperature) at the end of the cooling phase. In addition, since the inflows and outflows to the adsorption bed were stopped during that phase, it can be seen that the mole fraction of carbon dioxide (Figure 5.7(a)) does not change during those periods. During the desorption phases, the pressure of the buffer tank increases as it is replenished with a mixture of purge hydrogen and desorbed carbon dioxide. This flow rate is higher than the one exiting (that required by the methanation process) as will be seen analyzing Figure 5.9. Conversely, during the adsorption and cooling phases, the pressure tends to decrease because there is only an outflow rate and no replenishment.

Figure 5.8 overlays the last two cycles (number 7 and number 8) relative to the same trends described in Figure 5.7. As can be seen, in all three cases the curves are superimposed. This indicates that the system has reached a regime condition. In other words, the influence of the imposed initial conditions has been exhausted. Considering that the part of the system dealing with capture is discontinuous while the part dealing with the methanation process operates continuously, this regime appears to be periodic. In what follows, reference will be made to a typical cycle under regime conditions.

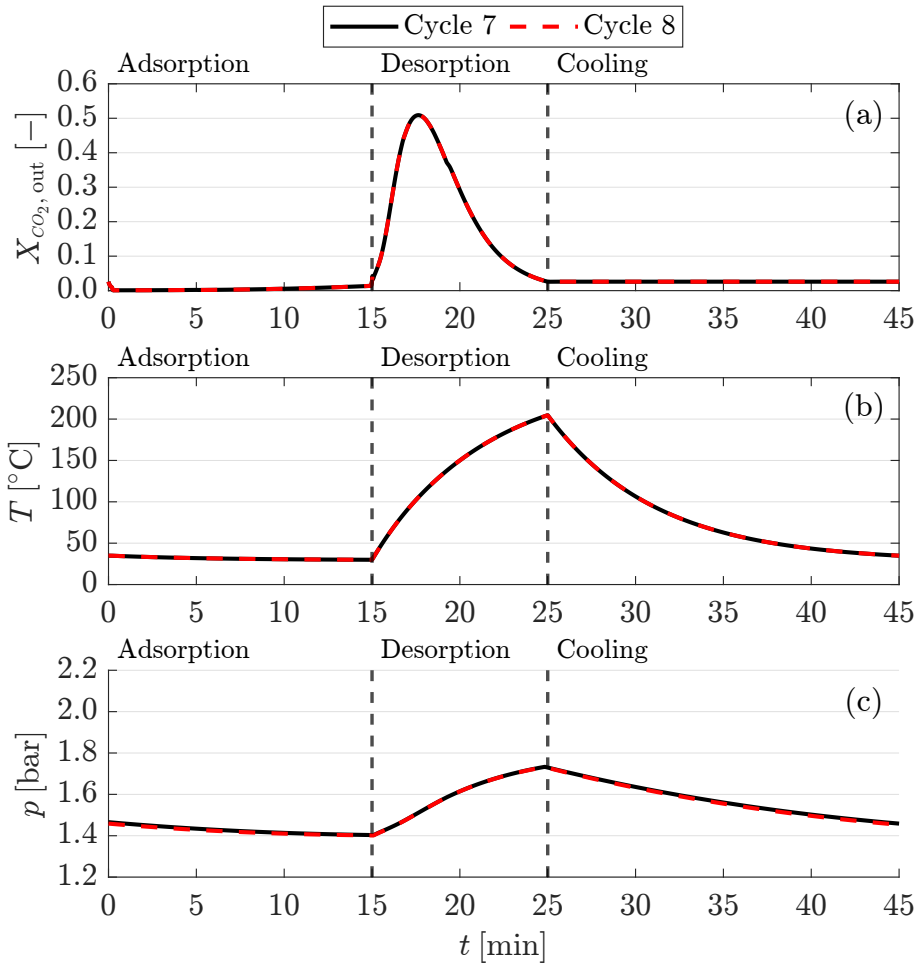

Figure 5.8: Superimposition of relevant trends in cycle 7 and cycle 8. Adsorption bed outlet carbon dioxide mole fraction (a); adsorption bed temperature (b); buffer tank pressure (c).

5.2.2.2 System behavior

As was mentioned earlier, the system under investigation is composed of two subsystems. One related to the capture of carbon dioxide and one related to its conversion to methane. The connecting element between the two systems is what has been labeled as buffer tank. Figure 5.9 describes what occurs in the buffer tank during a typical cycle under regime conditions. Figure 5.9(a) shows the inlet and outlet mass flow rates while Figure 5.9(b) shows the pressure change in the buffer tank. For ease of understanding, the adsorption, desorption and cooling phases are highlighted.

It can be seen that the inlet mass flow rate corresponds to the mass flow rate of desorbed carbon dioxide and purge hydrogen arriving from the adsorption bed during the desorption phase. In the other phases, there is no flow entering the buffer tank. The trend

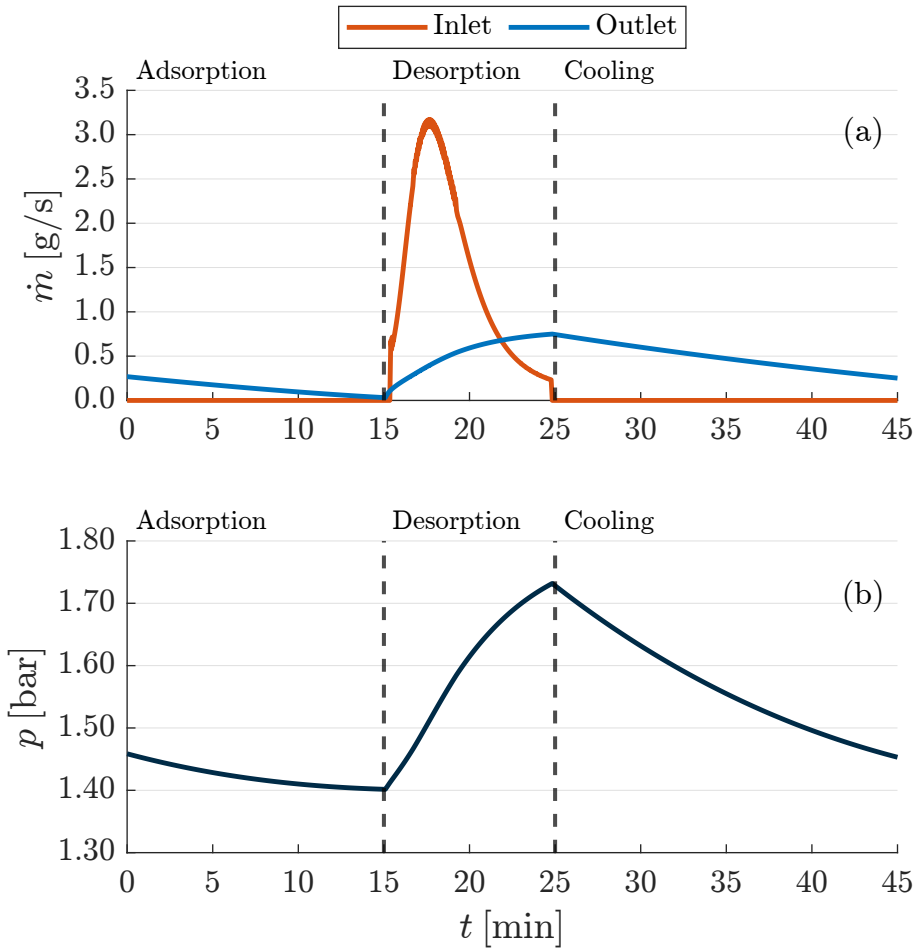

Figure 5.9: Buffer tank behavior. Inlet and outlet mass flow rates (a); pressure (b).

of this mass flow rate is similar to that described in Section 5.1 where only the capture system was examined. It is also noted that the inlet mass flow rate during desorption is greater than the outlet one; this leads to the increase in pressure. The outlet mass flow rate depends on the difference between the tank pressure and the downstream pressure. Considering that the downstream pressure has been set as constant, it can be seen that as the tank pressure increases, the mass flow rate exiting is correspondingly higher. The buffer tank outlet mass flow rate is extremely important as it determines the amount of reactants that will undergo chemical conversion in the methanation reactor. Considering that the methanation reaction is exothermic, the higher the flow rate of reactants the higher the heat that will be developed and that will have to be removed. Controlling the flow rate of the reactants is crucial in order to avoid the overheating of the catalytic bed that could lead to its eventual failure.

Figure 5.10 illustrates the behavior of the mixing volume, the element located upstream

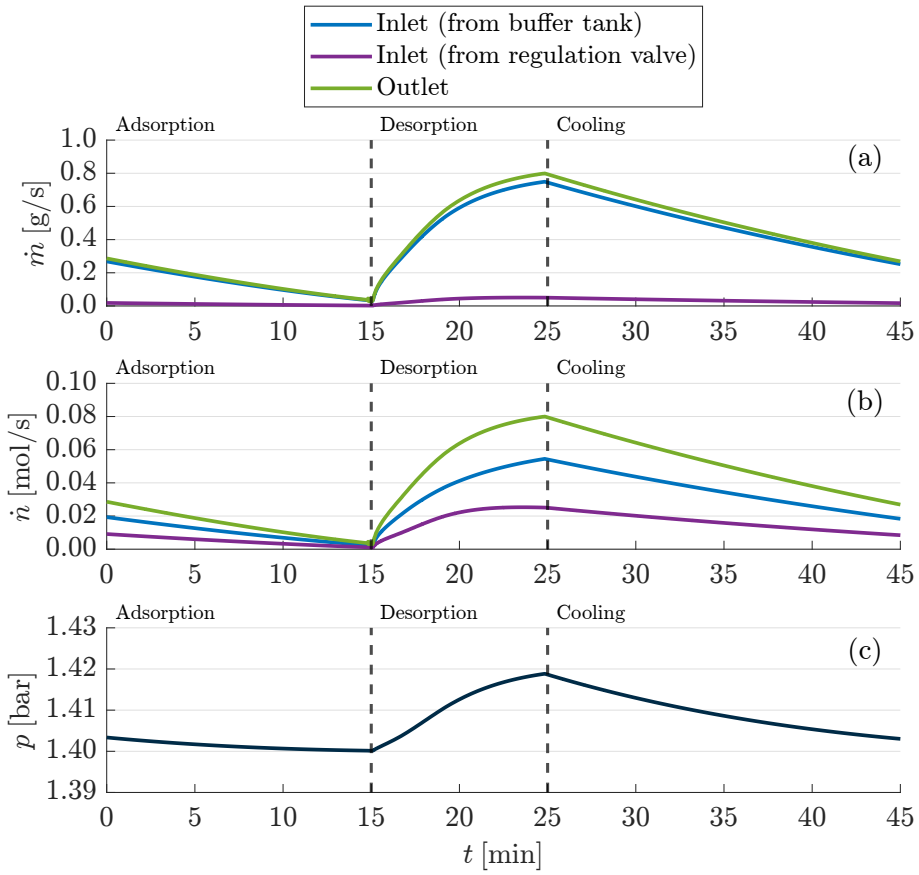

Figure 5.10: Mixing volume behavior. Inlet and outlet mass flow rates (a); inlet and outlet mole flow rates (b); pressure (c).

of the methanation reactor. As with the buffer tank, 5.10(a) shows the inlet and outlet mass flow rates and 5.10(c) shows the pressure trend. In addition, 5.10(b) shows the inlet and outlet mole flow rates.

There are two flow rates at the inlet to the mixing volume, the flow rate coming out of the buffer tank and the flow rate being added by the regulating valve. Since the composition of the mixture of carbon dioxide and hydrogen exiting the buffer tank was not in stoichiometric conditions, the regulating valve had the task of flushing enough hydrogen to make the mixture of reactants entering the methanation reactor reach the stoichiometric ratio. It can be seen that the pressure of the mixing volume is affected by the same buffer tank dynamics described in Figure 5.9. The analysis of the mixing volume, however, provides an opportunity to highlight a seemingly trivial but critically important aspect when dealing with processes of this type. At low to medium pressures such as those involved in this analysis, hydrogen has a significantly lower density than the other gaseous species considered. By comparing Figure 5.10(a) with Figure 5.10(b),

it can be seen that hydrogen (inlet flow coming from the regulation valve) in terms of mass flow rate makes a negligible contribution but this contribution becomes much more relevant when the mole (and, consequently, the volume) flow rate is considered. Dealing with gaseous mixtures, volumetric flows are more interesting since they are closely related to the pressure variations of the components involved.

Keeping in mind the considerations made above, Figure 5.12 shows the evolution of the mole fractions of the species involved in the various lines of the system. Figure 5.11 shows the schematic of the present system with the addition of the numbering of the considered lines. Based on this numbering, Figure 5.12(a) shows the mole fractions of the mixture in line (1) (exit from the adsorption bed), Figure 5.12(b) in line (2) (exit from buffer tank), Figure 5.12(c) in line (3) (exit from mixing volume) and Figure 5.12(d) in line (4) (exit from methanation reactor).

In line (1), gas passage occurred only during the desorption phase. The mixture obtained in this period perturbs the mole fractions in the buffer tank and consequently those in line (2), which can be seen during the desorption phase in 5.12(b). It can also be seen that between line (2) and line (3) there is a transition from nonstoichiometric mole fractions (Figure 5.12(b)) to mole fractions in stoichiometric ratio (Figure 5.12(c)). As an instance, it can be seen that the mole fraction of hydrogen increases from about 0.7 to exactly 0.8, reaching the stoichiometric ratio of 4 with carbon dioxide whose fraction is 0.2. Finally, in line (4), it can be seen that the flux of reactants was mostly converted into products.

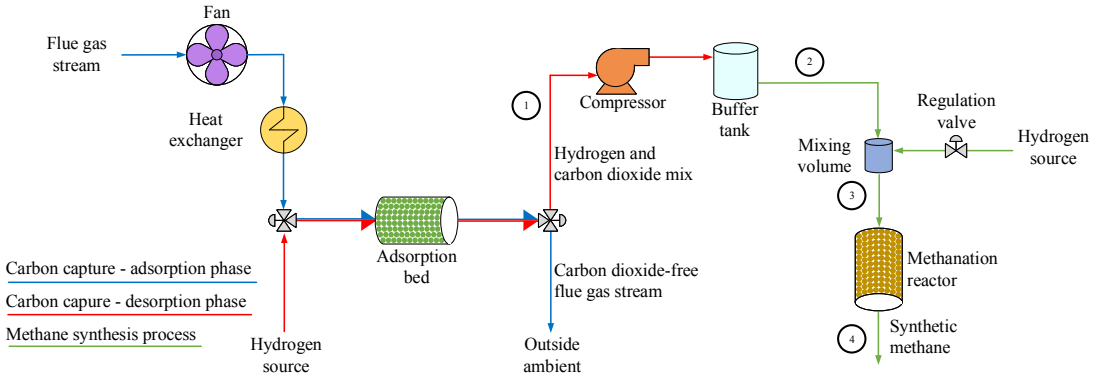

Figure 5.11: System layout schematic with the highlighting of the lines relevant for the analysis of Figure 5.12.

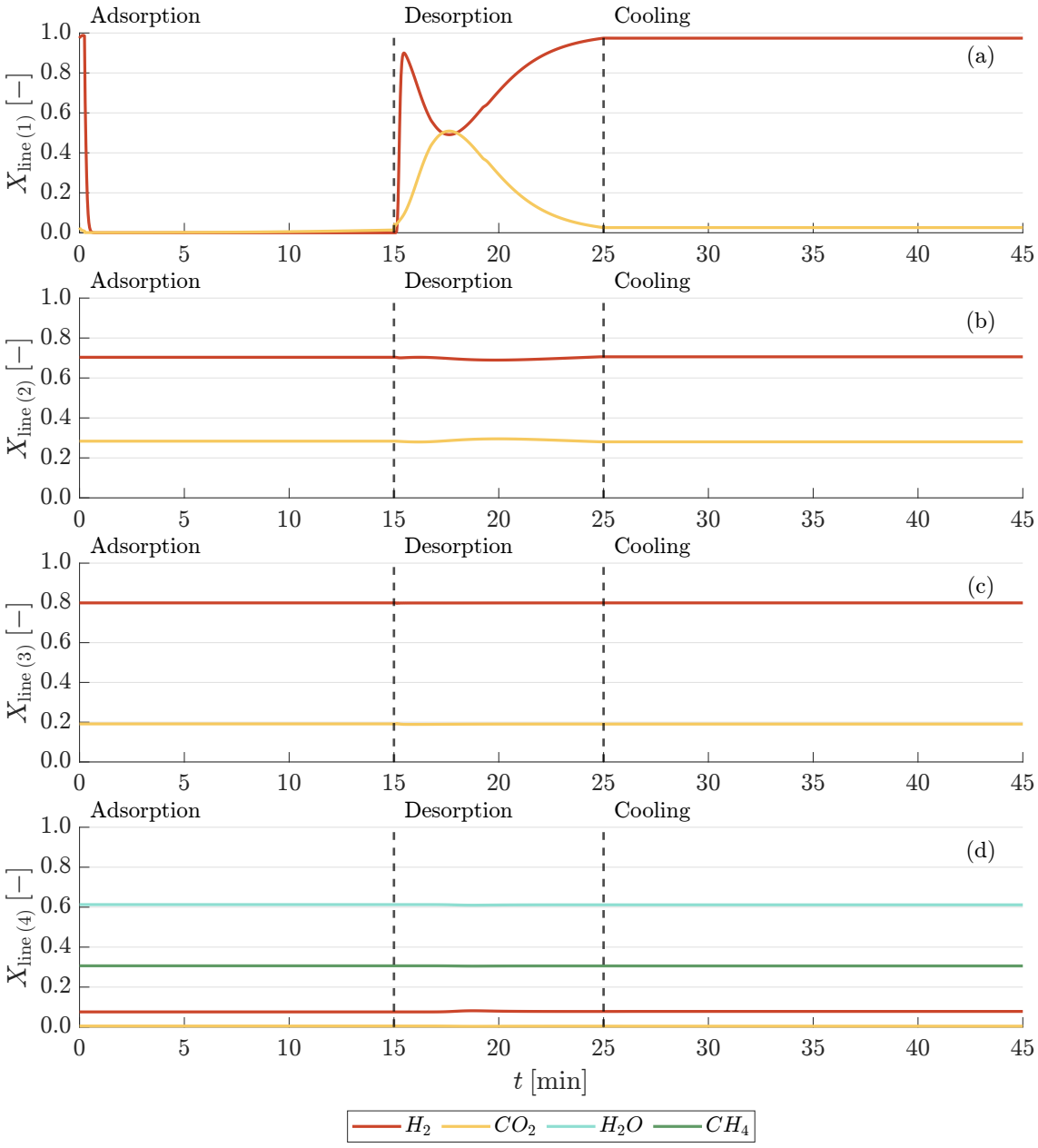

Figure 5.12: Mole fractions of the species in the lines of the system numbered in Figure 5.11.

5.2.3 Discussion

The analysis performed in this section extends the considerations made in Section 5.1 regarding the adsorptive carbon capture. In this case, in addition, the system analyzed also included the carbon dioxide conversion to methane. The study envisaged the development of a dynamic mathematical model and its use.

The analyses performed focused on considerations related to system behavior. This is considered extremely relevant since the two processes that are part of the system operate markedly differently. In the case of the adsorptive capture of carbon dioxide, as illustrated in Section 5, the process needs to work in a discontinuous manner, alternating phases of capture with phases of carbon dioxide release. In contrast, the methane synthesis process operates continuously, converting a continuous stream of carbon dioxide and hydrogen.

In order to evaluate the operation of the system in a regime condition, it was decided to simulate it for multiple operating cycles. With regard to the adsorptive capture, a cooling phase was additionally included with the adsorption and desorption phases, which was necessary to bring the adsorption bed back to the proper condition to be able to undertake a new cycle. By superimposing the trends of several important variables, a regime condition was defined in which, despite the inherent periodicity of the system, each cycle would be equal to the previous and the following one. This was necessary so that the imposed initial conditions would no longer have an influence in the system. Furthermore, this implied that the mass of carbon dioxide undertaking the methanation process would be exactly that which was adsorbed, preventing strorage accumulations from compromising the analysis.

Being the connecting element of the two subsystems, the buffer tank needs special concern at the design stage. Despite it is unavoidable to make the buffer tank pressure oscillating, it is important to consider this aspect thoroughly. In fact, on the one hand, having small pressure variations would mean making use of a very large volume tank. This, beyond the plant complications, implies that the mass of captured carbon dioxide that is fed in would be very small compared to that already present in the tank. On the other hand, it is necessary that the buffer tank pressure does not oscillate excessively since all downstream components are affected by its dynamics, especially the methanation reactor.

With the operating conditions adopted, in a typical cycle, the energy supplied to the adsorption bed during the desorption phase (calculated as the integral of the thermal power exchanged through the bed wall) per unit mass of produced methane was 22.24 kWh/kg_{CH_4}, while the energy withdrawn for cooling was 22.13 kWh/kg_{CH_4}. Conversely, the thermal energy withdrawn from the methanation reactor was 2.31 kWh/kg_{CH_4}, which was about 10 % of the energy required for desorption. These values can lead to two distinct considerations. First, in the management of the adsorption bed it would be good to employ the energy withdrawn during cooling for other purposes. This is necessary to improve the efficiency of the process as a whole. Second, in the case of intending to recover heat, the energy withdrawable from the methanation reactor would not be sufficient to guarantee desorption. Therefore, the resulting plant complication due to the heat recovery

circuit could not be viable. In any case, this aspect could be improved by optimizing the operating conditions of the methanation process (e.g., by operating at higher pressures) or by improving the layout of the reactor in order to more effectively remove heat.

The efficiency of the system needs to account also for the fact that there are combustible chemical species entering and leaving the system. In this case, with reference to a typical cycle, the energy input in the form of hydrogen for the purge of the adsorption bed was 9.17 kWh/kg_{CH_4}, while that for the hydrogen input from the control valve was 7.29 kWh/kg_{CH_4}. At the outlet, however, the methane produced had an energy of 13.90 kWh/kg_{CH_4} while the remaining unconverted hydrogen had an energy of 1.06 kWh/kg_{CH_4}. Clearly, both the carbon dioxide and the water at the output cannot be further oxidized. This means that the carbon and hydrogen contained in them cannot be exploited for energy purposes. It should be always considered that the hydrogen it is not present in nature and needs energy for its production.

Chapter 6

Sorption-enhanced catalytic methane synthesis

This chapter will deal with specific aspects related to the improvement that catalytic methanation can have from the exploitation of adsorption. In particular, Section 6.1 will present the results of tests performed on a reactor for sorption-enhanced methanation by evaluating its behavior under off-design conditions [127]. Section 6.2 will outline the development of a dynamic mathematical model of a sorption-enhanced methane synthesis system and its application for the analysis of a system with two reactors operated alternatively [128].

6.1 Experimental test of part-load and transient response of sorption-enhanced methanation systems

This section will present the experimental methodology adopted for the investigation and the mathematical model utilized. The results will cover both considerations about the partial load and the transient behavior of the system discussing also the effect that this kind of operation can have on temperature peaks.

6.1.1 Methods

6.1.1.1 Experimental setup

The experimental setup featured a fixed-bed oil-cooled catalytic reactor, consisting of four reactor ducts arranged in parallel (Figure 6.1). The bed was composed of pellets made of adsorbent material impregnated with the catalyst. Specifically, it consisted of zeolite 13X pellets with diameters ranging from 1.6 mm to 2.6 mm, which were impregnated with 5

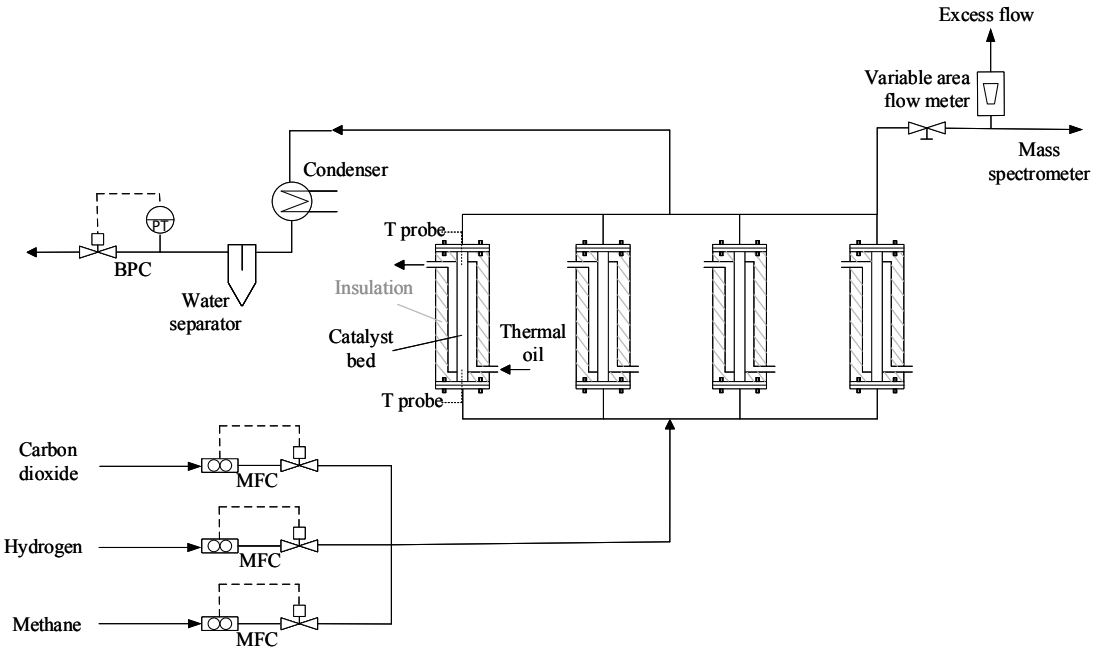

Figure 6.1: Sorption-enhanced methanation test rig schematic representation.

mass% nickel [106]. To partially absorb the heat released and to enhance heat transfer, in the inlet zones of the reactors, these pellets were mixed with aluminum beads. This strategy was employed to address the issue of continuous heat release in the inlet zone, as discussed in [106].

Each of the four reactor ducts contained a pellet bed with a length of 1 m and a diameter of 32 mm. The ducts were cooled by the circulation of thermal oil through an external jacket surrounding each reactor duct. The temperature was regulated and maintained at a constant level using a PID controller (Julabo HT60 thermostat). The temperature was measured at the inlet and outlet zones of each reactor duct using thermocouples (Type K class A, with a 1.5 mm jacket diameter), with a 0.5 Hz sampling frequency. The pressure was regulated using a back pressure controller (BPC, Bronkhorst EL-PRESS) located downstream of the reactor, while the inlet gas flow was controlled by mass flow controllers (MFC, Bronkhorst EL-FLOW Prestige).

A sample of the produced gas mixture was collected at the outlet of one of the four reactor ducts and directed to a mass spectrometer (Hiden Analytical RGA) for measuring the mole fractions of the various chemical species.

6.1.1.2 Testing procedure

Prior to each experiment, the reactor was heated, using thermal oil, to the operating temperature of 300 °C and purged with an inert gas stream (i.e., nitrogen). After reaching the desired temperature, the reactor was purged with methane, and the absolute pressure was increased to the operating point of 10 bar. Once stable conditions were established, the reaction was initiated by introducing a defined mixture of reactants. A carbon dioxide mole flux of 0.4 $\mathrm{mol\,m^{-2}s^{-1}}$ was set as the reference condition. The reactant ratio for both full and partial load tests was adjusted to closely match stoichiometric conditions, with a slight excess of hydrogen to compensate for the inaccuracies in the control instrumentation. This minor surplus of hydrogen was deemed acceptable, given that the resulting syngas was intended for injection into natural gas pipelines.

The reaction phase of each experiment was concluded when the temperature readings at the reactor outlet indicated that the reaction front had reached the outlet section of the reactor. Subsequently, the reactor entered the drying phase, during which the bed was purged with hydrogen to return to its initial state in terms of water content. The partial load behavior of the system was examined at 25 %, 50 %, and 75 % of the reference inlet mole flow of carbon dioxide.

Considering that less water production results in a longer time required to saturate the bed, the reaction time is inversely proportional to the load. In each case, the reaction time was not predetermined but was determined based on temperature and product gas measurements. Using these measurements, step variations were defined to characterize the transients considered during the time frames.

6.1.1.3 Calculation methods

In order to have a reference to reactors without sorption enhancement, a dynamic model was used. The reactor model had the same geometry as the sorption-enhanced reactor tested and was implemented in MATLAB®/Simulink®. The model was based on the chemical kinetics equations of the process, as well as mass and energy balances as already described in Section 4.1.2. In addition to the comparison to the tested system with the model of the reactor without sorption enhancement, calculations related to the chemical teoretical equilibrium were also perfomed using the software Cantera®.

6.1.2 Results

As a reference for the partial load and transient tests, a single experiment is analyzed to demonstrate the operation of a sorption-enhanced catalytic reactor. To illustrate this, Figure 6.2 shows the variations in the outlet mole fractions of the most relevant gases

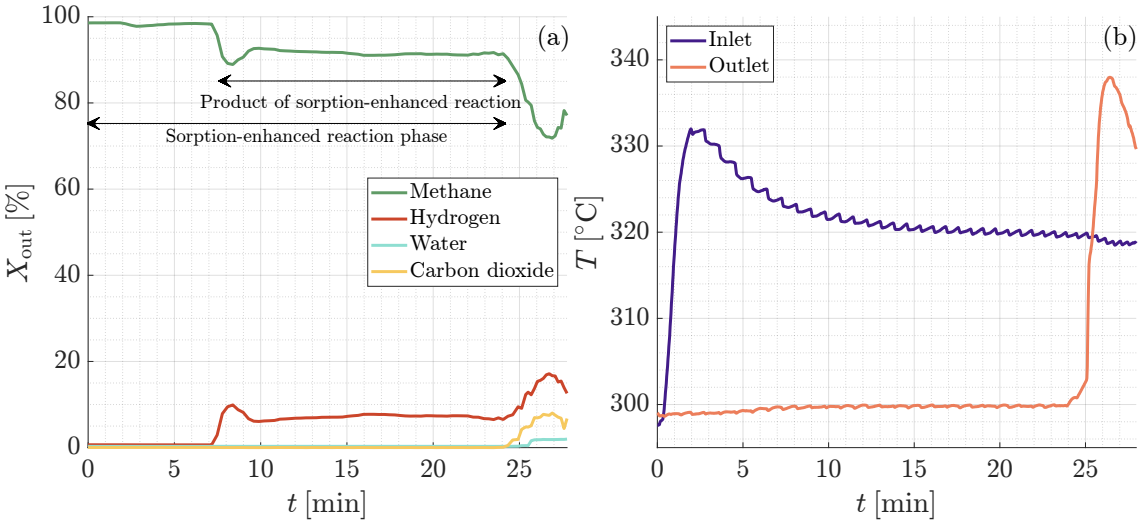

Figure 6.2: Measured mole fractions at the reactor outlet (a) and temperatures measured in the inlet and outlet zones of the reactor (b) using a constant inlet flux of carbon dioxide of 0.3 mol m^{-2} s^{-1} and reaction absolute pressure of 10 bar.

in the mixture, alongside the temperatures measured at both the inlet and outlet zones of the reactor. For this reference case, a carbon dioxide flux set at 0.3 mol m^{-2} s^{-1} was used while the hydrogen/carbon dioxide ratio was determined according to the sorption-enhanced reaction experiments (see Table 6.1). The data reported spans the entire range of the test, starting from the initial condition (when no water is adsorbed in the bed) to the final condition (when the bed is completely saturated with water).

Figure 6.2(a) presents the composition of the gas mixture at the reactor outlet. The initial methane content corresponds to the gas that was already present in the reactor after the system pressurization (as discussed in Section 6.1.1.2). The observed decline in the methane content marks the point when the methane produced during the reaction reached the reactor outlet, signaling the beginning of the conversion process. The produced methane measured at the outlet is delayed with respect to the feed of reactants that started at time $t = 0$.

It should be observed that when the first synthesized methane reached the reactor outlet, its mole fraction experienced a slight downward peak. This behavior is attributed to an overshoot in the hydrogen flow rate in the moment when the reactant flow value was set through the flow controllers. The temporary excess hydrogen in the system caused this initial fluctuation in the methane concentration, which then stabilized as the reaction proceeded and the flow rates were properly adjusted.

The methane mole fraction decrease at the end of the test corresponds to the moment when the sorption front reached the reactor outlet. This indicates that the bed became

saturated with water, and thus, the sorption-enhancement capability was exhausted. As a result, a mixture of reactants and products reached the outlet, leading to a decline in the methane concentration. In the final phase of the experiment, the behavior of the reactor clearly signaled that the synthesis phase ended. Typically, in real operations, the reaction would be stopped, and the bed drying phase would begin before this saturation point is reached to ensure efficient regeneration and continuation of the process.

The carbon dioxide content remained below 1 % during the sorption-enhanced reaction phase, while ethane and propane concentrations were measured at less than 0.5 %, and the water content stayed below 0.2 %. The temperatures shown in Figure 6.2(b) follow a pattern influenced by the movement of the coupled adsorption and reaction front and the heat removed from the catalyst bed. Comparing the reaction enthalpy to the heat of adsorption, it can be stated that the former has a stronger influence. The peak observed in the inlet zone temperature can be attributed to the reaction front passing through the temperature sensor. After this, in the inlet region of the bed, the reaction proceeds without sorption enhancement, as the bed becomes fully saturated with water. The heat released from the exothermic reaction leads to a temperature stabilization at a level higher than that of the coolant. The maximum temperature in the inlet zone is lower than at the outlet, which is due to the utilization of aluminum beads within the catalyst bed.

Additionally, a comparison between the behavior of methanation reactors with and without sorption enhancement highlights the key differences between the two systems. To illustrate this, Figure 6.3 presents the simulated steady-state temperature profile along the reactor axis of a conventional fixed-bed catalytic reactor [67].

The simulation took into account the same bed geometry and operating conditions with respect to those used for the sorption-enhanced case. Specifically, a carbon dioxide flux of

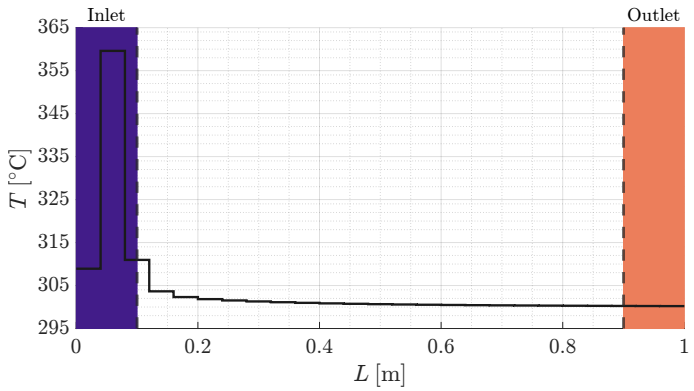

Figure 6.3: Simulated temperature profile along the length of a non-sorption-enhanced reactor using a constant inlet flux of carbon dioxide of 0.3 mol m^{-2} s^{-1} and reaction absolute pressure of 10 bar.

0.3 $\mathrm{mol\,m^{-2}\,s^{-1}}$, a H_2/CO_2 ratio as determined in the sorption-enhanced reaction experiments (see Table 6.1), an initial reactor temperature and temperature control setpoint of 300 °C, and an absolute reaction pressure of 10 bar were considered. Since a discretized lumped parameter approach was applied, the temperature profile is shown as a series of steps.

In the conventional reactor, the temperature profile stabilizes with a profile shown in Figure 6.3. The location of the maximum temperature is fixed with constant inlet reactant flow rate. In contrast, as seen in Figure 6.2(b), the temperature peak in sorption-enhanced systems is dynamic, shifting through the reactor alongside the reaction front.

The following sections will discuss the partial load operation (Section 6.1.2.1), transient behavior of the system (Section 6.1.2.2), and the thermal behavior (Section 6.1.2.3).

6.1.2.1 Partial load behavior

The system was evaluated under partial load conditions by repeating the above-shown experiment (conducted at 75 % of the reference load), using inlet flow rates of 25 %, 50 %, and 100 % of the reference load. Table 6.1 shows the carbon dioxide conversion based on the measured outlet gas composition. For comparison, results related to simulated conventional reactor, equilibrium conversion calculations at 300 °C, and measurements of the sorption-enhanced reactor are presented. Equation 6.1 was used to calculate the carbon dioxide conversion (ξ) based on the mole fraction (X) of carbon dioxide at the inlet and at the outlet of the reactor.

$$\xi_{CO_2} = 1 - \frac{X_{CO_2,\,\mathrm{out}}}{X_{CO_2,\,\mathrm{in}}} \tag{6.1}$$

The measured mole fractions were averaged over the time period marked in Figure 6.2(a) as the "product of sorption-enhanced reaction". For the simulations and equilibrium conversion calculations, the actual flux determined from the experiments was used. The simulation results for the conventional reactor show a decrease in conversion with increasing load (increasing inlet mole flux), due to the reduced residence time. Compared to the equilibrium calculations, the gap between the equilibrium conversion and the simulated reactor conversion widens as the load increases. The changes in equilibrium conversion in the table are due to variations in the inlet stoichiometry for different load conditions. In contrast, the carbon dioxide conversion in the sorption-enhanced reactor experiments remains independent of load. It is significantly higher than the equilibrium conversion in all cases, which aligns with the previously discussed shift in the chemical equilibrium due to water removal.

Along with the carbon dioxide conversion data presented in Table 6.1, Table 6.2 displays the outlet methane content for the conventional reactor simulation, the equilibrium value, and the average values measured during the sorption-enhanced reaction. This variable is the more relevant one when the feeding into the natural gas network is considered. The methane mole fraction for both the simulation and the equilibrium calculation was considered on a dry basis. Additionally, for further analysis of the sorption-enhanced reactor measurements, the standard deviation of the averaged data is also provided.

The results for the simulated conventional reactor align with the trend observed for carbon dioxide conversion. The theoretical maximum methane content from equilibrium highlights the significant impact of the non-stoichiometric reactant ratio, particularly at low partial load. The methane content in the product measured for the sorption-enhanced reactor depends on the stoichiometry, with the product quality being limited by the precision of the initial mixing rather than the conversion itself. Additionally, the low standard deviation of the measured data indicates that the production process is very stable. Another key feature of the sorption-enhanced reactor system is the duration of the production phase. To explore this further, Figure 6.4 presents the duration at different partial load conditions (Λ), measured from the start of feed supply until an increase in carbon dioxide mole fraction above 1 % is detected at the reactor outlet.

The figure includes, in addition to the measured durations, the durations that would have occurred if the adsorption capacity had remained constant and equal to that observed at the lowest load. Moreover, on the secondary vertical axis, the amount of water adsorbed under the corresponding conditions is shown. The water adsorbed (and, by extension, the adsorption capacity of the reactor) was estimated by multiplying the duration by the water production rate, which was calculated from the conversion of the inlet carbon dioxide flow rate.

In an ideal system, the water adsorption capacity would remain unchanged regardless of the load conditions. However, Figure 6.4 demonstrates a decline in this capacity as the

Table 6.1: Carbon dioxide conversion at different partial loads with corresponding inlet mole fluxes.

Φ_{in} [mol m^{-2} s^{-1}]	Reactant ratio [-]	ξ_{CO_2} [-]		
CO_2	H_2/CO_2	Conventional reactor simulation	Equilibrium at 300 °C and 10 bar	Sorption-enhanced reactor measurements
0.1	4.18	0.9622	0.9985	0.9998
0.2	4.14	0.9187	0.9960	0.9998
0.3	4.09	0.8864	0.9902	0.9997
0.4	4.09	0.8657	0.9892	0.9999

Table 6.2: Methane outlet mole fraction at different partial loads with corresponding inlet mole fluxes.

Φ_{in} [mol m^{-2} s^{-1}]	Reactant ratio [-]	$X_{CH_4,\,out}$ [%]		
CO_2	H_2/CO_2	Conventional reactor simulation	Equilibrium at 300 °C and 10 bar	Sorption-enhanced reactor measurements
0.1	4.18	82.965	84.1165	84.548 (std: 0.625)
0.2	4.14	73.682	87.053	88.063 (std: 0.454)
0.3	4.09	67.476	89.097	91.565 (std: 0.435)
0.4	4.09	63.852	89.269	92.346 (std: 0.460)

load increases. The durations of sorption-enhanced reactions are slightly shorter when the adsorption capacity decreases. This observation is consistent with what observed in [106], which attributed the behavior to higher bed temperatures and less distinct reaction fronts due to kinetic limitations. This aspect is crucial when designing similar systems.

6.1.2.2 Transient response

The response of the sorption-enhanced reactor system to load variations was assessed by examining its behavior under single and multiple steps in the feed flow rate. For the single

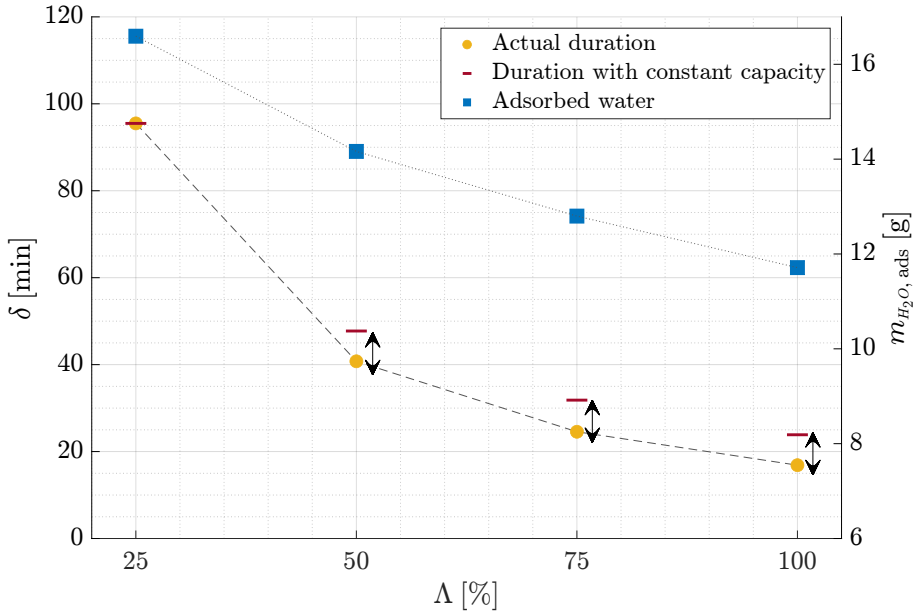

Figure 6.4: Production phase actual duration with respect to calculated durations assuming constant capacity at different partial loads. Mass of adsorbed water under the same conditions.

step test, the system operated at full load (100 %) for 6 minutes, then reduced to 25 % load for another 6 minutes, before returning to full load. Figure 6.5(a) shows the outlet mole fraction of the species in the gas mixture for this single step scenario. For the multiple step test, the procedure involved three steps of 3 minutes each, as shown in Figure 6.5(b). Figures 6.5(c) and 6.5(d) display the feed flow rates set by the mass flow controllers for these tests.

Figure 6.5(a) highlights the same methane synthesis characteristics as those evaluated in Figure 6.2 for the steady-state case. The downward spike in methane fraction corresponds to the moment when the inlet flux was decreased. A similar pattern is observed in Figure 6.5(b). During the transition between different loads, the methane content gradually adjusts to the levels seen in steady-state partial load tests. In addition, a non-negligible delay is noted in the outlet with respect to the changed conditions at the inlet. This must be taken into account in the control of the system.

Table 6.2 shows that the outlet methane mole fraction varies for different partial load tests. The spikes in hydrogen fraction are linked to changes in the reactants ratio used in these conditions. The steps appear to have no significant impact on carbon dioxide conversion, as indicated by the carbon dioxide outlet mole fraction.

6.1.2.3 Effect on temperature

Lastly, the peak temperature values recorded under various load and transient conditions are examined. These peaks, measured at the reactor inlet and outlet, show minimal

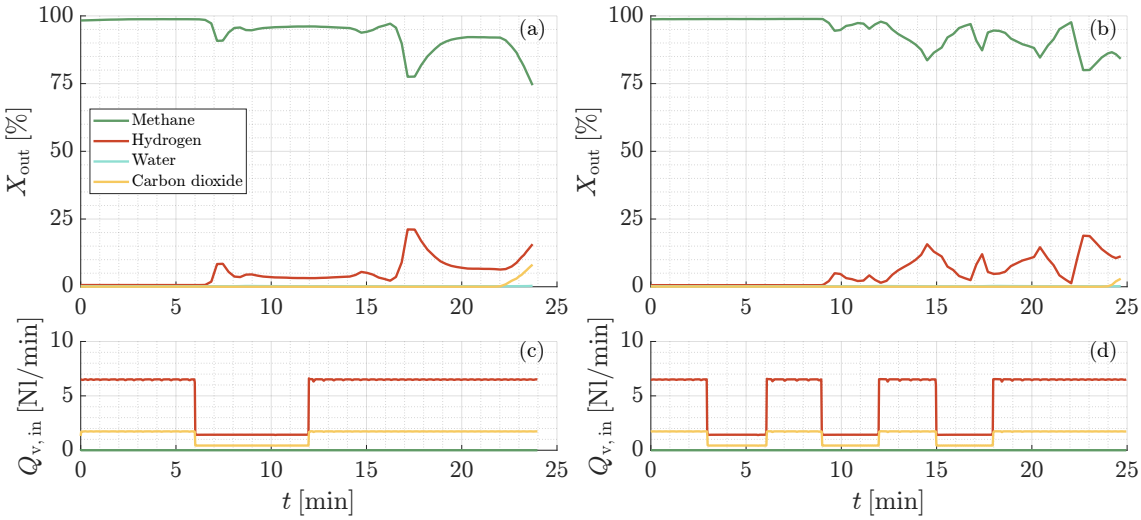

Figure 6.5: Measured outlet mole fractions in case of single-step input (a) and multiple-step input (b). Reactants inlet flow rate in case of single-step input (c) and multiple-step input (d).

variation across different load conditions, as presented in Table 6.3. The inlet temperatures are lower than those at the outlet, due to the catalyst being mixed with aluminum beads in the reactor initial zone.

At any given time, the location of the front experiences maximum conversion and the highest heat release, due to both the exothermic reaction and the adsorption process. This local temperature increase enhances the chemical kinetics, thereby boosting the conversion of reactants into products. As water is produced more rapidly, the bed becomes saturated faster, causing the front to advance along the reactor axis. Because the temperature peak is dynamic, the system effectively mitigates the issue of hot-spot formation. This contrasts with conventional fixed-bed catalytic methanation reactors, where the temperature peak at a given flow remains steady, as discussed in Figure 6.2.

6.1.3 Discussion

This section presents an investigation regarding methane production under transient and partial load conditions. In the framework of the analysis is the sustainable fuel production from renewable energy sources. The potential of sorption-enhanced catalysis for the methanation of carbon dioxide was analyzed, highlighting its capability for achieving high conversion rates under flexible operating conditions. To this end, the performance of an oil-cooled fixed-bed methanation reactor equipped with a bi-functional catalyst was experimentally tested and compared to a dynamic model of a fixed-bed reactor with no sorption enhancement.

Partial load conditions were examined by varying the reactant flow rates. Additionally, transient load changes were investigated by assessing the system response to step changes from one partial load to another. These responses were evaluated with a focus on conversion and thermal stability, which is a primary concern in the literature for conventional catalytic reactor systems. The results demonstrate that the system exhibits exceptional thermal stability in response to transients, despite the exothermic nature of both the ad-

Table 6.3: Peak temperatures measured in the cases analyzed in the inlet and outlet zones of the reactor.

Partial load/step response	$T_{\text{max, in}}$ [°C]	$T_{\text{max, out}}$ [°C]
$\Lambda = 25\%$	323.5	333.8
$\Lambda = 50\%$	328.3	338.1
$\Lambda = 75\%$	332.0	338.0
$\Lambda = 100\%$	331.7	340.8
Single step	326.2	339.4
Multiple step	323.4	339.5

sorption and the methanation reaction. The system autonomously manages temperature peaks, thereby preventing catalyst deactivation due to thermal degradation. Moreover, the sorption-enhanced catalyst ensures complete conversion without ignition issues.

From a product quality perspective, the sorption-enhanced reactor demonstrates an outstanding carbon dioxide conversion rate exceeding 99.97 %, regardless of the load. In contrast, simulation results for a conventional catalytic reactor of the same dimensions show carbon dioxide conversion rates ranging from 96.2 % to 86.7 %, which decline as the feed flow rate increases. Sorption-enhanced reactors achieve higher carbon dioxide conversions than those predicted for an equilibrium reactor, owing to the continuous removal of water. The conventional reactors simulated in this study approach the theoretical equilibrium conversion at low flow rates.

A notable feature of the sorption-enhanced reaction is the presence of a coupled reaction and adsorption front that progresses through the reactor. The duration of the sorption-enhanced reaction phase is governed by the water adsorption capacity of the catalyst bed under the given conditions. As a result, reducing the load causes the front to move more slowly through the reactor. It was observed that the adsorption capacity of the reactor slightly diminishes with increasing load, which is attributed to transport limitations within the reactor bed. Nevertheless, this characteristic enables the system to function effectively at low partial loads.

The investigation of step responses to analyze transient behavior revealed that carbon dioxide conversion remains consistently high throughout the sorption-enhanced production phase, even during abrupt load changes. This stability is advantageous for direct coupling with the fluctuating supply of reactants. The identified characteristics aid in designing power-to-gas systems and minimizing the need for electricity or hydrogen storage, as the system can operate at very low partial loads during periods of low wind speed or solar irradiation. Based on these findings, the presented results demonstrate the excellent performance of sorption-enhanced catalysis during transient operations and partial load conditions, particularly useful in the context of coupling methane synthesis with renewable energy generation.

6.2 Dynamic modeling of sorption-enhanced methane synthesis plants

This section will deal with the sorption-enhanced system model development and its utilization. Specifically, Section 6.2.1 will illustrate in detail the mathematical model equations while Section 6.2.2 will deal with its validation and with its application.

6.2.1 Methods

6.2.1.1 Reactor model development

A heterogeneous chemical reactor dynamic mathematical model for sorption-enhanced methanation was developed. In addition to mass and energy balance equations and the chemical kinetics, also the adsorption dynamics were taken into account. Therefore, the model developed for this specific study extended the one presented in Section 4.1.2 for conventional fixed-bed reactors (i.e., without sorption enhancement). Regarding the chemical kinetics, as will be explained below, it was modified to tailor the specific characteristics of the system with which the model was validated.

In the following, details will be given regarding the additional terms needed in the conservation equations to account for the adsorption phenomenon.

Chemical kinetics

Also in this case the model involved the three chemical reactions of the Sabatier process: carbon dioxide methanation (cdm, Equation 6.2), carbon monoxide methanation (cmm, Equation 6.3), and the reverse water-gas shift reaction (rwgs, Equation 6.4) [10]. These reactions are reported again her for the sake of clarity.

$$CO_{2_{(g)}} + 4H_{2_{(g)}} \leftrightarrows CH_{4_{(g)}} + 2H_2O_{(g)}, \qquad \Delta H_r^0 = -165.1 \ \text{kJ/mol} \tag{6.2}$$

$$CO_{(g)} + 3H_{2_{(g)}} \leftrightarrows CH_{4_{(g)}} + H_2O_{(g)}, \qquad \Delta H_r^0 = -206.2 \ \text{kJ/mol} \tag{6.3}$$

$$CO_{2_{(g)}} + H_{2_{(g)}} \leftrightarrows CO_{(g)} + H_2O_{(g)}, \qquad \Delta H_r^0 = +41.3 \ \text{kJ/mol} \tag{6.4}$$

Similarly to the approach shown in Section 4.1.2, the reaction rates were calculated based on temperature, on the partial pressures of the involved species, and on chemical equilibrium, following the relations proposed by Xu and Froment [115] for heterogeneous catalysis. In addition, each of these equations included two multiplicative factors: χ and ζ.

The factor χ accounts for the reactor model discretization, as will be detailed later, and ζ accounts for the use of a different catalyst compared to the one referenced in the literature.

$$r_{\text{cdm}} = \frac{\chi_{\text{cdm}}\,\zeta_{\text{cdm}}\,\frac{k_{\text{cdm}}}{p_{H_2}^{3.5}}\left(p_{CH_4}\,p_{H_2O}^2 - \frac{p_{H_2}^4\,p_{CO_2}}{K_{\text{cdm}}}\right)}{\left(1+\beta_{CO}\,p_{CO}+\beta_{H_2}\,p_{H_2}+\beta_{CH_4}\,p_{CH_4}+\frac{\beta_{H_2O}\,p_{H_2O}}{p_{H_2}}\right)^2} \tag{6.5}$$

$$r_{\text{cmm}} = \frac{\chi_{\text{cmm}}\,\zeta_{\text{cmm}}\,\frac{k_{\text{cmm}}}{p_{H_2}^{2.5}}\left(p_{CH_4}\,p_{H_2O} - \frac{p_{H_2}^3\,p_{CO}}{K_{\text{cmm}}}\right)}{\left(1+\beta_{CO}\,p_{CO}+\beta_{H_2}\,p_{H_2}+\beta_{CH_4}\,p_{CH_4}+\frac{\beta_{H_2O}\,p_{H_2O}}{p_{H_2}}\right)^2} \tag{6.6}$$

$$r_{\text{rwgs}} = \frac{\chi_{\text{rwgs}}\,\zeta_{\text{rwgs}}\,\frac{k_{\text{rwgs}}}{p_{H_2}}\left(p_{CO}\,p_{H_2O} - \frac{p_{H_2}\,p_{CO_2}}{K_{\text{rwgs}}}\right)}{\left(1+\beta_{CO}\,p_{CO}+\beta_{H_2}\,p_{H_2}+\beta_{CH_4}\,p_{CH_4}+\frac{\beta_{H_2O}\,p_{H_2O}}{p_{H_2}}\right)^2} \tag{6.7}$$

Adsorption dynamics

The adsorption dynamics was modeled using the solid linear driving force model, as proposed in [120].

$$\frac{\partial q_{H_2O}}{\partial t} = \frac{q_{H_2O}^* - q_{H_2O}}{\varrho_{H_2O}} \tag{6.8}$$

The rate of adsorption is influenced by the deviation of the adsorbed phase concentration q_{H_2O} from its equilibrium value $q_{H_2O}^*$, as determined by the coefficient ϱ_{H_2O}. The equilibrium adsorbed phase concentration was estimated using the Dubinin-Astakhov isotherm [121].

$$\frac{q_{H_2O}^*}{q_{max,H_2O}} = e^{-\left(\frac{RT}{M_{H_2O}E}\ln\frac{p_{\text{sat}}}{p_{H_2O}}\right)^{n_{\text{D-A}}}} \tag{6.9}$$

In Equation 6.9 the water partial pressure p_{H_2O}, the saturation pressure p_{sat} at temperature T, and the characteristic energy of the adsorbent E, are taken into account. The rate of adsorption was then incorporated into a sink term for the mass flow rate and estimated using the following equation, which, in the case of water, was added to the mass balance equation.

$$\dot{m}_{\text{ads}} = (1-\varepsilon)\,(Sl)\,\rho_s\frac{\partial q_{H_2O}}{\partial t}M_{H_2O} \tag{6.10}$$

In Equation 6.10, ε denotes the void fraction of the fixed bed, S represents its cross section area, l is the thickness of the control volume in which the equation is applied, and ρ is the density of the bed solid phase (subscript s). The sorbent used, zeolite 13X, adsorbs also

a small amount of carbon dioxide. However, this effect was not considered in this study because the quantity of adsorbed carbon dioxide is significantly lower compared to that of water [104].

The heat released by adsorption was calculated using Equation 6.12 and was assumed to be emitted on the solid surface (subscript surf). This heat was then transferred to the gas flow via a convective term, as described in Equation 6.13. Consequently, the temperature of the solid phase was determined using Equation 6.11 as follows.

$$\frac{\partial T_{\text{surf}}}{\partial t} = \frac{\dot{Q}_{\text{ads}} + \dot{Q}_{\text{conv}}}{Sl(1-\varepsilon)\left(\rho_s c_s\right)} \tag{6.11}$$

$$\dot{Q}_{\text{ads}} = \rho_s Sl(1-\varepsilon)\left(-\Delta H_{\text{ads},H_2O}\right)\frac{\partial q_{H_2O}}{\partial t} \tag{6.12}$$

Where the term ΔH_{ads} represents the isosteric heat of adsorption.

$$\dot{Q}_{\text{conv}} = a_p\left(1-\varepsilon\right)\left(Sl\right)\gamma_{\text{gs}}\left(T - T_{\text{surf}}\right) \tag{6.13}$$

In these equations it was assumed a constant heat of adsorption and it was negleted the contribution of the adsorbed phase in terms of heat capacity and heat transfer.

Mass and energy balances

The mass conservation equation, in the case of water, was written including the adsorbed mass flow rate as a sink term. Therefore, it was evaluated by Equation 6.14.

$$\left(Sl\right)\varepsilon\frac{\partial \rho_{H_2O}}{\partial t} = Q_{\text{v,in}}\rho_{H_2O,\text{in}} - Q_{\text{v}}\rho_{H_2O} + \dot{m}_{H_2O,\text{gen}} - \dot{m}_{\text{ads}} \tag{6.14}$$

With regard to the energy conservation, the energy contributions for the entire control volume were expressed by Equation 6.15.

$$\left(\rho c\right)_{\text{eff}}\left(Sl\right)\varepsilon\frac{\partial T}{\partial t} = \sum_{\alpha}\left(\dot{m}_{\alpha,\text{in}}h_{\alpha,\text{in}} - \dot{m}_{\alpha}h_{\alpha}\right) + \dot{Q}_{\text{gen}} - \dot{Q}_{\text{rad}} + \dot{Q}_{\text{conv}} \tag{6.15}$$

The subscript "eff" indicates the effective thermal capacity of both the solid bed and the gaseous flow, while $\dot{Q}_{\text{gen}}$ represents the heat released by exothermic reactions. For each control volume, the radial heat $\dot{Q}_{\text{rad}}$ exchanged with the external environment (the thermal oil circulating in the reactor jacket for thermal regulation) was estimated by assuming a constant global heat transfer coefficient, denoted with U in Equation 4.7.

However, a higher constant value was employed during the regeneration phase compared to the production phase. This adjustment was made because the heat transfer coefficient

of the mixture in the regeneration phase (which contains high concentrations of hydrogen and water vapor) is greater than that of the mixture present during the production phase.

The convective term $\dot{Q}_{\text{conv}}$ denotes, as previously mentioned, the heat exchanged between the gaseous flow and the solid surface, which is heated by the heat of adsorption.

Models of other components of the system

Beyond the reactor, additional system components were modeled. In particular, tanks, pipes, valves, and control signals were considered. The modeling approach adopted for these components was illustrated in Section 4.2. In particular, the valve openings were regulated using PID controllers to manage the reactor pressure and the gas mass flow rates.

6.2.1.2 Experimental setup for the model validation

To validate the model, the experimental apparatus described in the previous section was employed. A temperature and pressure swing adsorption procedure was used to handle the periodic phases of adsorption and desorption. Specifically, during the regeneration phase (desorption), compared to the thermodynamic conditions established during the reaction phase, the pressure had to be decreased, while the temperature needed to be increased.

The system is the one depicted in Figure 6.1. The reactor comprised four ducts, each containing a catalyst bed with a diameter of 32 mm and a length of 1 m. A bifunctional material with both catalytic and adsorptive properties composed the fixed bed. Specifically, zeolite 13X pellets (with diameters ranging from 1.6 mm to 2.6 mm) were used as adsorbents and were impregnated with a nickel catalyst (5 mass%). In the initial zone of the reactor, zeolite pellets were mixed with aluminum beads to prevent excessive thermal loads, as documented in [106].

Upstream of the reactor, source tanks of methane, hydrogen, and carbon dioxide were utilized. Methane was used to pressurize the system when necessary, while hydrogen and carbon dioxide were used as reactant mixture. Due to the inaccuracy of the hydrogen mass flow controller at the low flow rates tested, the hydrogen mass flow rate could not be set to the stoichiometric value. However, it was possible to calculate this rate retrospectively, and the actual amount of hydrogen that entered the reactor during the experimental campaign was incorporated into the model. Consequently, the carbon dioxide flux will be hereafter taken as reference. Lastly, a flow of pure hydrogen was used to purge the bed during the regeneration phase.

The inlet gas flow was regulated using mass flow controllers (MFC, Bronkhorst EL-FLOW Prestige). Temperatures at the inlet and outlet zones of each reactor were measured with thermocouples (Type K class A, 1.5 mm jacket diameter). A thermoregulator (Julabo

HT60 thermostat) controlled the reactor temperature by circulating thermal oil through the external jacket of each duct. The temperature was maintained at 300 °C during the reaction phase and at 340 °C during the regeneration phase. The absolute pressure was increased to 10 bar for the reaction phase and decreased to 1.5 bar for the regeneration phase. Gas analysis at the reactor exit was performed using a mass spectrometer (Hiden Analytical RGA).

To validate it, the system model was tailored to the characteristics of the experimental test rig. In fact, besides the reactor, other components such as gas source tanks, connecting pipes, valves, and control signals were also modeled.

6.2.1.3 Model implementation

The equations were implemented in a MATLAB®/Simulink® environment and solved using the variable time step solver ode15s, which is suitable for stiff problems. As explained in Section 4.1 the reactor model was axially discretized into control volumes, each with homogeneous gas properties. A sensitivity analysis was performed regarding the number of control volumes used for discretization. Specifically, 5, 10, 15, and 20 CVs were considered, with several inlet reactant mole flux values. The reactant flux was quantified based on the carbon dioxide mole flux at the reactor inlet.

Table 6.4 compares the errors and computational times for different cases. The computational time was normalized to the shortest recorded simulation time, which corresponded to a flow of 0.4 $\mathrm{mol\,m^{-2}\,s^{-1}}$ with 5 control volumes. The Root Mean Square (RMS) error of the calculated outlet methane mole fraction was evaluated, with respect to the experimental measurements, during the steady-state production period. As shown in Table 6.4, the RMS error is very small (below 0.04) for all cases and can be considered negligible. However, the relative computational time increased exponentially with finer discretization. Therefore, the analysis indicated that, for the purposes of this study and under the tested conditions, a high number of control volumes was not warranted. Consequently, based on this sensitivity analysis, the reactor model was discretized into 5 control volumes.

The rectifications at the chemical kinetics discussed during the model presentation (Section 6.2.1.1) will be examined in the following. It is important to note that, according to the model architecture, the gas concentration calculated in the final control volume was considered as the concentration exiting the reactor. The species concentration was representative of each control volume and was uniformly distributed throughout the entire volume (lumped parameter approach).

Consequently, to account for the limitations due to the spatial discretization of the reactor model, each reaction rate in Equations (6.5)–(6.7) was multiplied by the factor denoted as χ. This multiplicative factor was set inversely proportional to the control

Table 6.4: Influence of the discetization on the error committed with reaspect to the measurements and on the relative computational time.

$\Phi_{CO_2,\,\mathrm{in}}$ [mol m^{-2} s^{-1}]	Number of CVs	RMS error [-]	Relative computational time
0.1	5	0.0067	1.1691
	10	0.0069	2.4246
	15	0.0069	5.2057
	20	0.0067	8.9033
0.2	5	0.0045	1.0157
	10	0.0064	2.0917
	15	0.0055	3.6779
	20	0.0060	5.7297
0.3	5	0.0154	1.0679
	10	0.0051	2.1349
	15	0.0075	3.3476
	20	0.0149	4.6488
0.4	5	0.0391	1.0000
	10	0.0076	2.1579
	15	0.0156	3.1753
	20	0.0272	5.2205

volume number (i.e., the smaller the size, the better the approximation). In particular, in the case with the most refined discretization among those tested, χ was set to 1 . In this way, a reference per unit volume was defined to be used consistently with any level of discretization.

The term ζ is employed to adjust the chemical kinetics to align with the experimental catalytic system, as compared to the correlations used. This was done because the amount of catalyst in the correlations on kinetics found in the literature was different from that adopted experimentally in this work. This value is constant (does not change with the number of CV of the discretization) and was calibrated by minimizing the error with respect to the measurements, using the model with the most refined discretization (the one with $\chi = 1$). In similar contexts, the use of multiplicative factors has also been suggested by Kang and Lee [129], and for sorption-enhanced dimethyl ether synthesis by Guffanti et al. [130].

6.2.1.4 Model application

The model was utilized to evaluate the performance of a plant with two reactors operating alternately. This configuration is necessary to achieve continuous methane production. Due to the requirement to regenerate the water-saturated bed, in fact, a single reactor cannot sustain a continuous synthesis.

Figure 6.6 provides a schematic diagram of the setup. The two methanation reactors were configured in parallel, with each reactor preceded by a mixing volume for the inlet

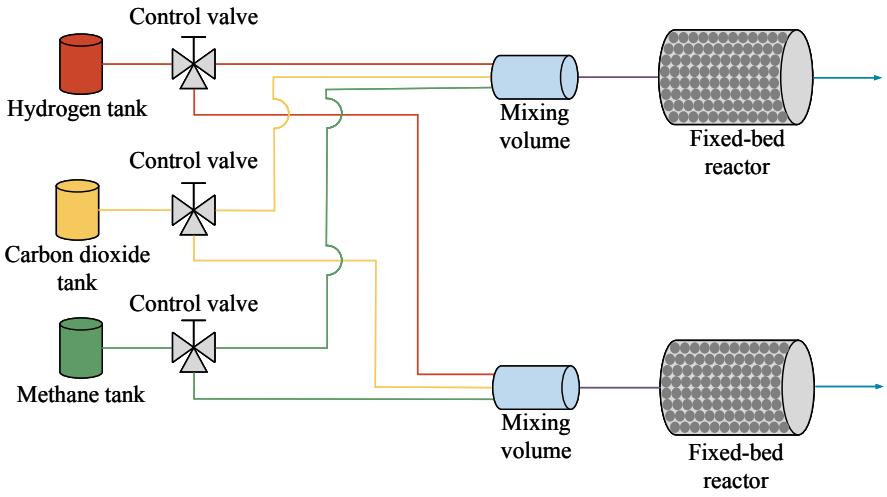

Figure 6.6: Modeled setup schematic representation in the configuration with two parallel reactors.

gaseous flows. The gases, sourced from upstream tanks, were regulated by valves and mass flow controllers before being directed into one of the two reactors according to a scheduled logic.

The production phase of the second reactor was programmed to begin immediately after the first reactor production phase ended. During the production phase of one reactor, the other reactor simultaneously underwent bed regeneration and pressurization. For the production phase, the absolute pressure was set at 10 bar and the temperature at 300 °C. Conversely, during the regeneration phase, the pressure was lowered to 1.5 bar and the temperature was increased to 340 °C.

For the reactant mixture, a carbon dioxide mole flux of 0.2 $\mathrm{molm^{-2}s^{-1}}$ and an hydrogen mole flux of 0.8 $\mathrm{molm^{-2}s^{-1}}$ were utilized in the analysis. The system underwent 24 hours of cyclic operation, encompassing 16 production phases. The system behavior was examined by varying the hydrogen flow used during bed regeneration.

6.2.2 Results

6.2.2.1 Model validation

The experimental data illustrated in Section 6.2.1.2 were used as input values to validate the model. These boundary conditions were specifically the set pressures and temperatures, and the inlet gas flow rates (reactant ratio). Figure 6.7 compares the simulated and measured outlet mole fractions of the involved gases during the phases of both production and regeneration. In this scenario, the carbon dioxide flux during the production phase

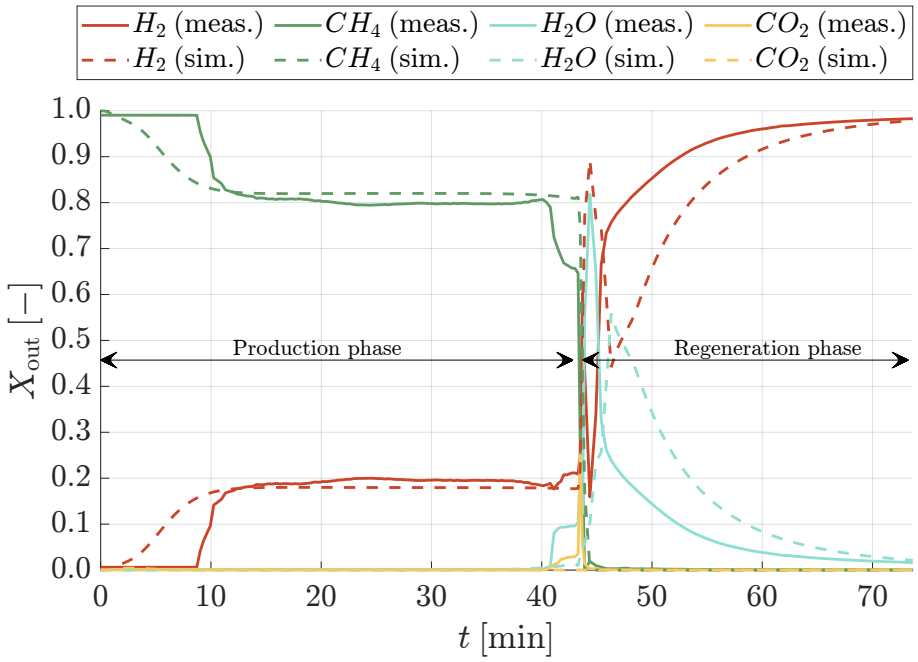

Figure 6.7: Comparison of simulated (sim.) and measured (meas.) reactor outle mole fractions with a production phase pressure of 10 bar and an inlet carbon dioxide mole flux of 0.2 mol m^{-2} s^{-1}.

was set at 0.2 mol m^{-2} s^{-1}, with the pressure increased to 10 bar. The solid lines represent the experimental data, while the dashed lines depict the model predictions.

From a qualitative point of view, the model was able to capture the principal trends of the process dynamics during both of the aforementioned phases. The discrepancies in the initial 10 min between the simulated and measured outlet methane mole fractions can be explained by the lumped parameter approach used in the model. This approach assumes homogeneity of the gas mixture properties within each control volume, which causes a broadening effect in the time trend curves. Moreover, it is important to highlight that the simulated values correspond to the final control volume, rather than a downstream element.

From 10 to 40 min, the modeled values closely match the measurements. At 43 min, the production phase concluded, and the regeneration phase commenced. Subsequently, some discrepancies between the simulation and the experimental data emerged due to similar reasons to those observed during the initial production phase. However, these discrepancies diminish as the regeneration phase progresses and stabilizes.

Although there are limitations, the model accurately estimates the species reaction trends at the outlet. The accuracy is particularly high during steady-state operation phases. Additionally, the model effectively demonstrates that reactors of this type can

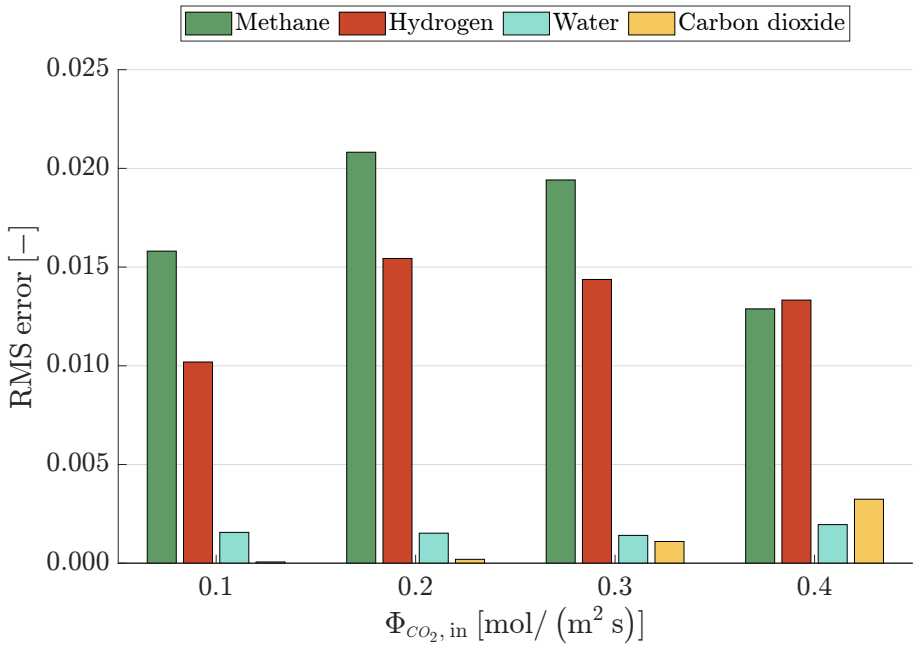

Figure 6.8: Root mean squared error committed by the model regarding the outlet mole fractions of the species involved with increasing inlet mole flux.

achieve nearly complete carbon dioxide conversion, consistent with the literature discussed in Chapter 3. The RMS between the measured and simulated outlet mole fractions was calculated for four different inlet reactant mole flux values, as shown in Figure 6.8.

The mole fraction error remains below 0.02 across all analyzed cases. Notably, the absolute errors for hydrogen and methane are greater than those for carbon dioxide and water. The simulated temperature trends in the first (CV1) and last (CV5) control volumes of the reactor model were compared with measurements from the inlet and outlet sectors, as depicted in Figure 6.9. An accurate reactor temperature estimation is crucial, as both adsorption capacity and reaction rates are temperature-dependent, decreasing as temperature rises. The average error relative to the measured data is less than 5 °C.

At 4 min, the temperature increase in CV1 to 328 °C indicates the onset of adsorption and reaction in this region, as reflected in both experimental data and simulation results. During this period, CV5 maintained a temperature of 300 °C due to thermal oil control. At 37 min, the reaction front reached CV5, where peak temperatures slightly exceeded 330 °C, surpassing those in CV1. The curve broadening in the time trends, as discussed in Figure 6.7, results from the spatial discretization used. More details about the temperature evolution within the reactor are presented in Figure 6.10.

After the production phase ended and regeneration began, some discrepancies emerged between the simulation and experimental results. These can be explained considering

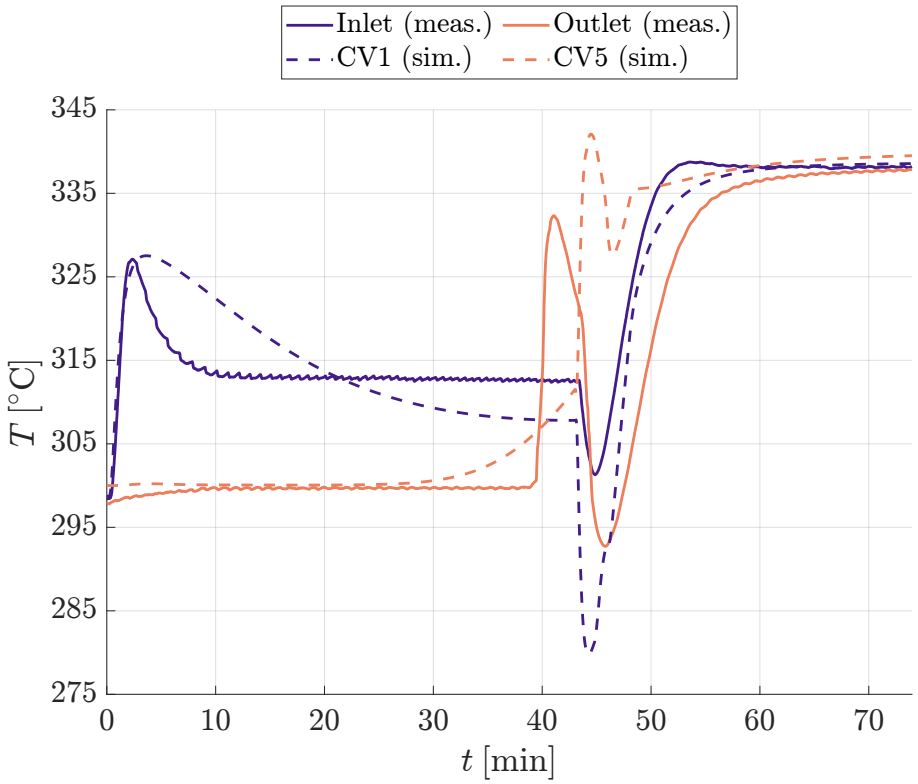

Figure 6.9: Comparison of simulated (sim.) temperatures in first and last control volumes with respect to the measured (meas.) temperatures in the inlet and outlet zones of the reactor with a production phase pressure of 10 bar and an inlet carbon dioxide mole flux of 0.2 mol m^{-2} s^{-1}.

that, in the simulation, the coolant temperature changed instantaneously, whereas the thermal oil used in the experiments exhibited significant thermal inertia. Upon reaching steady-state conditions during regeneration, the reactor temperature uniformly matched the control temperature of the thermal oil.

6.2.2.2 Process insights

The model successfully simulated the progression of the temperature front, as measured in references [100] and [106], and illustrated in Figure 6.10. The abscissa reports the control volumes sequential number along the reactor axis.

The temperature front progressed over time and along the reactor axis due to the reaction/adsorption front, as noted in [106]. The peak temperature of this front exceeded 320 °C. At 43 min, regeneration began in CV1, leading to a temperature drop, while CV5, still in the production phase, reached its peak temperature. The temperature decrease observed in the first two control volumes after 43 minutes is due to the increased global

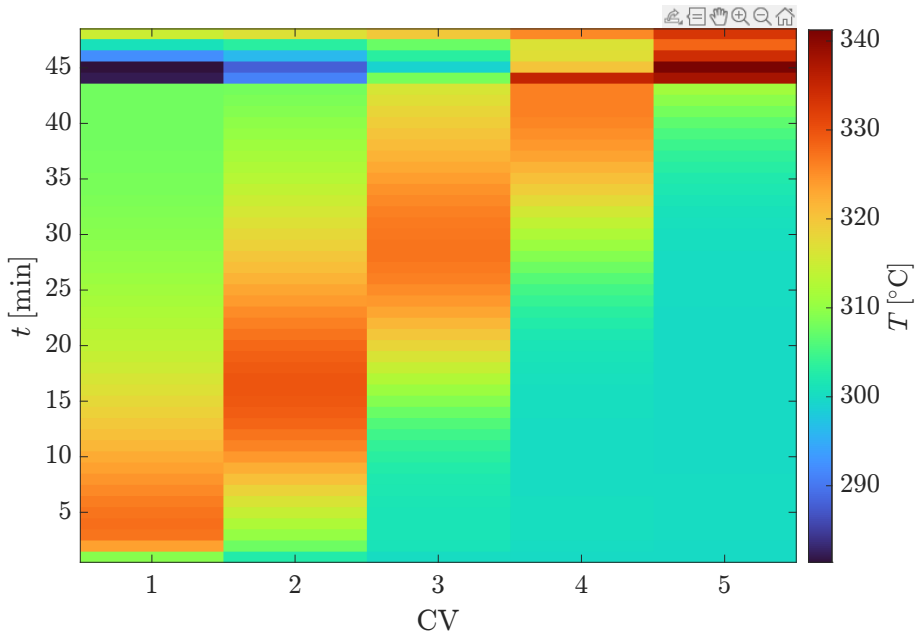

Figure 6.10: Simulated temperature trend in each control volume during the production phase with a production phase pressure of 10 bar and an inlet carbon dioxide mole flux of 0.2 mol m^{-2} s^{-1}.

heat transfer coefficient during the regeneration phase, the low enthaply of the entering purge gas and the endothermic desorption.

Figure 6.11 depicts the cumulative mass of water, the secondary reaction product alongside methane, adsorbed in each control volume bed.

During the initial 43 min (production phase), adsorption occurred, followed by desorption. Adsorption was most intense in CV1, but water quickly migrated to CV2 and CV3. This indicates that some water bypassed the reaction front, a phenomenon also noted in reference [106].

Each control volume approached its maximum sorption capacity, approximately 5.6 mg per 1 kg of catalyst bed, which was only fully achieved in CV1 and CV2. To prevent water spill-over, the production phase was terminated at 43 min, thus the sorption capacities of CV3, CV4, and CV5 were not fully utilized. Consequently, only a minor portion of CV5 was engaged in adsorption. Once CV2 reached saturation, the subsequent high water loads increased adsorption rates in the following control volumes, causing a rapid change in the slope of the curve in CV3 to CV5. This change was subtler in CV3 and more pronounced in CV4 and CV5. After 43 min, when desorption began, CV1 dried the fastest due to the continuous supply of dry hydrogen. Downstream control volumes dried more slowly because the flow entering each subsequent control volume carried increasing amounts of water.

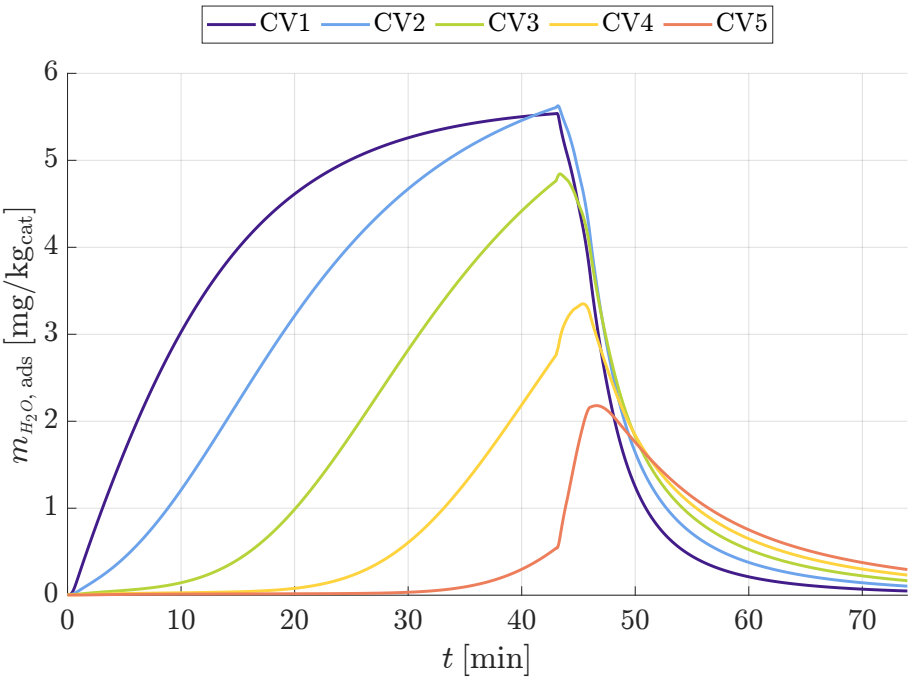

Figure 6.11: Calculated cumulative mass of adsorbed water in each control volume with a production phase pressure of 10 bar and an inlet carbon dioxide mole flux of 0.2 mol m^{-2} s^{-1}.

6.2.2.3 Application insights

The developed model was used to investigate the dynamic operation of a sorption-enhanced methanation system designed for continuous methane production. As outlined in Section 6.2.1.4, a configuration with two parallel reactors was employed. The study focused on examining various regeneration flows to determine the minimum hydrogen flow required for optimal drying. Consequently, multiple simulations were conducted, with hydrogen regeneration flow as the primary variable.

The plant, depicted in Figure 6.6, operated by alternating between production and regeneration phases, as illustrated in Figure 6.12. During the production phase in one reactor, the other reactor underwent bed regeneration (drying with a hydrogen stream) followed by pressurization (using a methane stream). The inlet reactant flow during the production phase maintained a stoichiometric ratio, with a carbon dioxide flux of 0.2 mol m^{-2} s^{-1} and an hydrogen flux of 0.8 mol m^{-2} s^{-1}. According to [127], the sorption-enhanced reaction duration for reactors with these fluxes and geometry was 43 min for the production phase and 31 min for the regeneration phase.

According to this schedule, each reactor completed 16 production cycles within a 24-hour period. The simulations revealed that the system could generate approximately

250.48 kg of methane per unit reactor volume per day. For regeneration, 13.42 kg of hydrogen per unit reactor volume per day were utilized and recirculated each cycle, while 13.36 kg of methane per unit reactor volume per day were used for pressurization and subsequently reused in each cycle.

Figure 6.13 presents the water mole fraction in the last control volume (CV5) of one reactor for various hydrogen flows used during regeneration at three critical points in the cycle: the end of the production phase, the end of the regeneration phase, and the end of the pressurization phase, which marks the start of the next production phase.

Regarding the end of regeneration (red curve) and the end of pressurization (yellow curve), an increase in regeneration flow resulted in a lower mole fraction of water exiting the reactor due to enhanced drying efficiency. The different values observed at the end of regeneration and pressurization indicate that, under the investigated conditions, the pressurization phase significantly contributes to bed drying, leading to the presence of wet methane during this phase.

At the end of the production phase (blue curve), the amount of water that was generated during production and arrived at the outlet can be observed. These values are highly dependent on the initial production conditions, which correspond to the end of the pressurization phase (yellow curve). For hydrogen flows exceeding 0.5 $\mathrm{mol\,m^{-2}\,s^{-1}}$, the water content at the end of pressurization was nearly zero, while the water content at the end of the production phase stabilized around 0.4. Conversely, at lower hydrogen regeneration flows, the slightly higher water content at the end of pressurization corresponded, at the end of production, to higher values.

Figure 6.14 displays the amount of water remaining in the bed of each control volume at the start of a new production cycle, following regeneration and pressurization according to the specified schedule. The corresponding degree of saturation, denoted as σ, is also shown.

As can be seen, the residual water adsorbed in the bed varied according to the axial

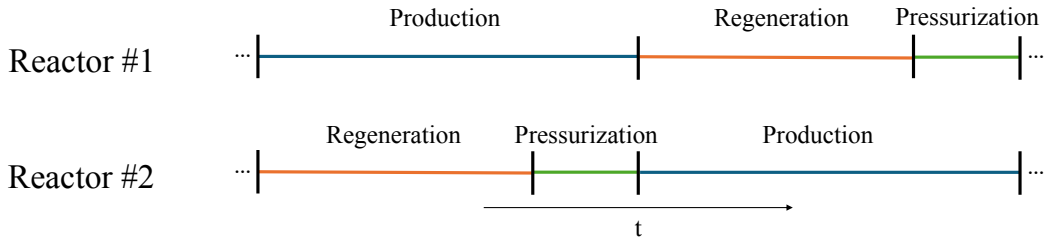

Figure 6.12: Schematic of the operation phases in case of the configuration depicted in Figure 6.6 with two alternating reactors.

position within the reactor. The first control volume (CV1), which always encountered a completely dry flow, retained the least amount of water after regeneration and pressurization. Moving towards the reactor exit, each subsequent control volume faced a drying hydrogen stream with progressively higher water content. This increased humidity reduced the efficiency of water removal and was counterproductive, as some water was adsorbed by bed portions that were not fully saturated. Consequently, each downstream control volume was less effectively dried and retained more water than the preceding one at the start of a new adsorption cycle.

At low regeneration flows, it is evident that the bed could not be thoroughly dried, resulting in a significant amount of residual water remaining adsorbed. This residual water reduced the adsorption enhancement effect, as illustrated in Figure 6.15. The figure presents a parametric analysis of the outlet mole fractions of methane, hydrogen, carbon dioxide, and water with varying degrees of saturation. The abscissa shows the degree of saturation of CV1 at the start of the production phase, while the ordinate displays the outlet mole fraction values averaged over the production phase.

As the degree of saturation of CV1 increases, the production of methane decreases, while the levels of hydrogen and carbon dioxide rise. This trend suggests a diminished conversion efficiency in the reactors. The presence of a humid bed reduces the adsorption

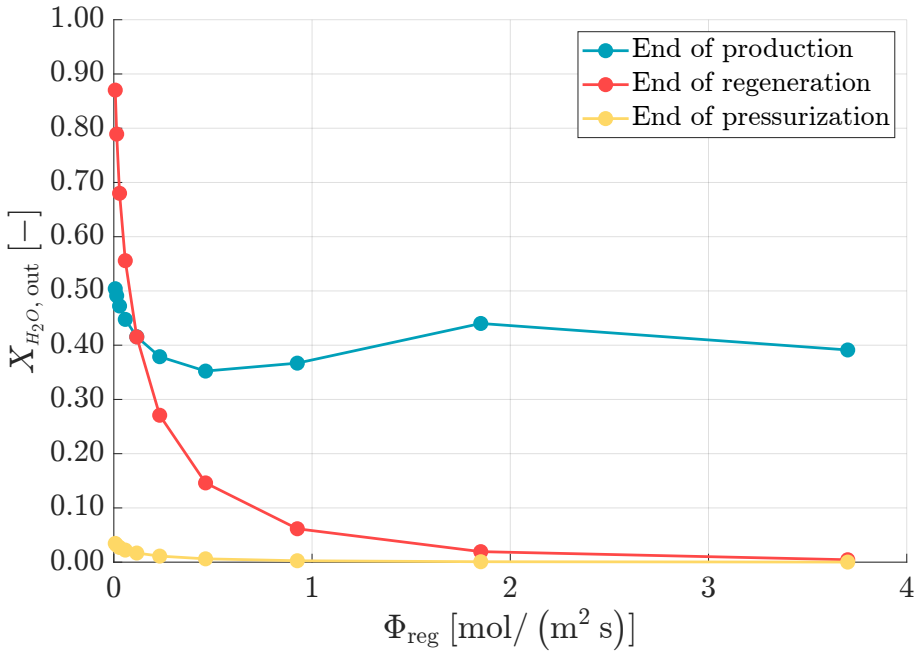

Figure 6.13: Simulated water mole fraction at the reactor outlet for different hydrogen regeneration flow values at the moments of: end of production, end of regeneration and end of pressurization.

rate (see Equation 6.8) and consequently lowers the total amount of water adsorbed.

Consequently, a humid bed cannot enhance the reaction as a completely dried bed at the moment of the production phase start. If the concentrations of hydrogen and carbon dioxide in the outlet exceed the permissible limits for grid injection, it becomes necessary to incorporate a downstream gas cleaning unit into the system. This underscores the critical role of bed drying in enhancing the purity of the synthesized gas.

6.2.3 Discussion

Methane synthesized from hydrogen and captured carbon dioxide holds significant potential to replace natural gas within various existing infrastructures and technologies. High-purity synthetic methane can be obtained through sorption-enhanced processes. The development of advanced technologies like sorption-enhanced methanation necessitates the creation of effective control and management strategies, which can be efficiently implemented using real-time simulation tools.

This chapter section presents the development of a dynamic model for the process simulation in real-time of sorption-enhanced methane synthesis plants. The model specifically

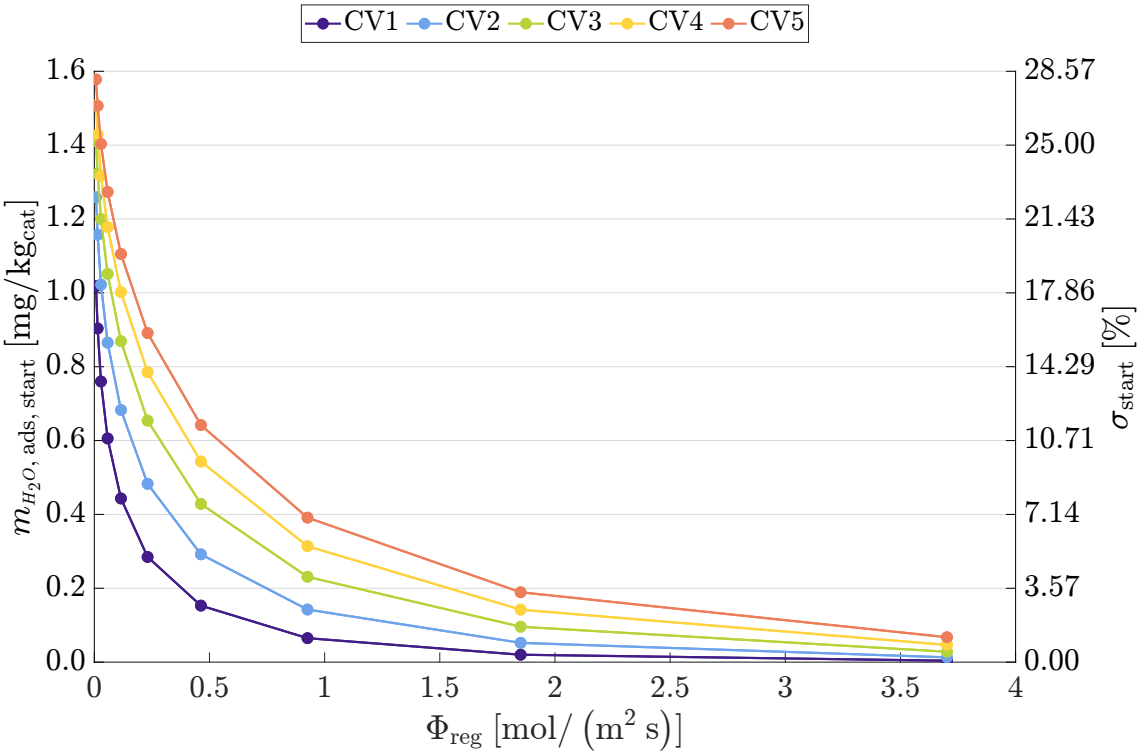

Figure 6.14: Amount of water remained adsorbed inside the bed and the corresponding degree of saturation at the beginning of a production cycle with respect to different hydrogen flux values used for the previous regeneration phase.

addresses the intermittent nature of this technology by mathematically simulating both the methane production and bed regeneration phases.

The methanation reactor model was integrated into a system with multiple components, enabling the simulation of their interactions. By modeling the entire system, the overall model could be customized to match an experimental setup and validated using experimental data. During the key phases of the process (production and regeneration), the developed model accurately predicted the concentrations of all relevant species, the temperature front progression within the reactor, and the dynamics of bed regeneration.

Consistent with findings from existing literature, the model results indicate that these systems can achieve nearly complete carbon dioxide conversion. However, calculations of the cumulative mass of water retained in the adsorption bed reveal that the full water storage capacity cannot be fully utilized. Due to water spill-over at the outlet, while the initial part of the reactor bed can become fully saturated, the final part is only partially utilized.

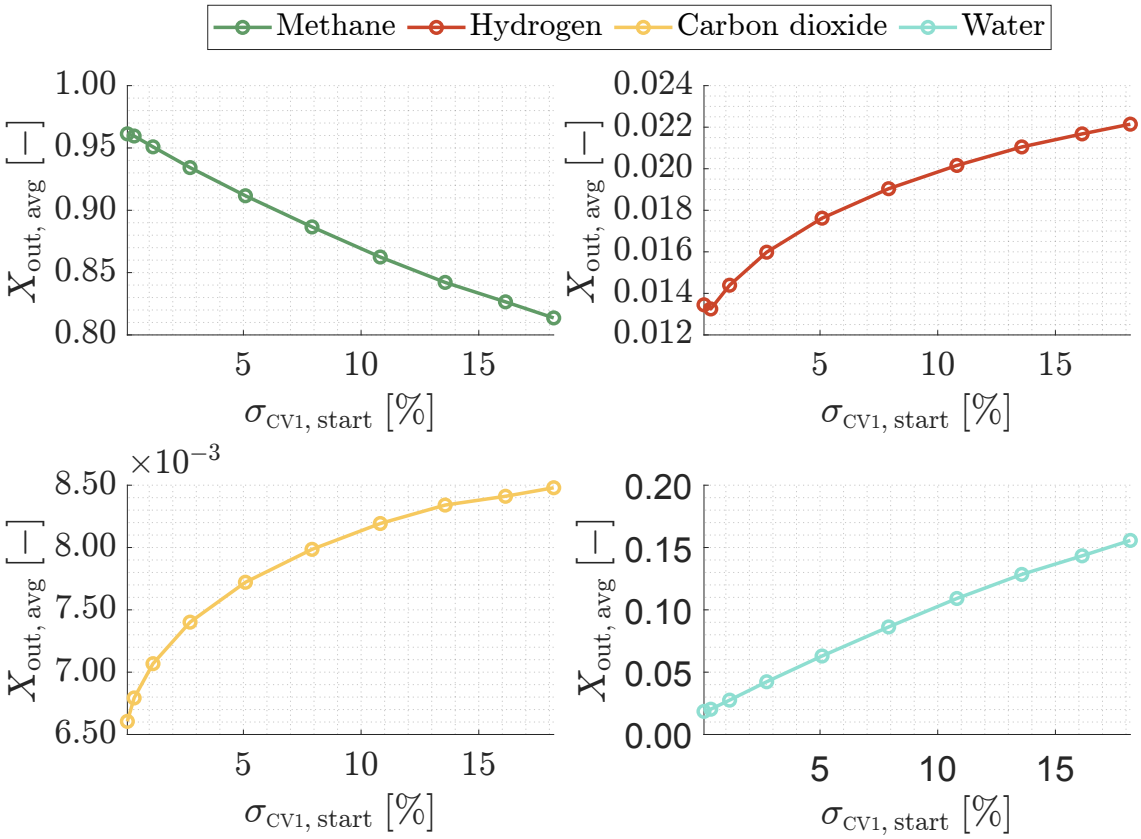

Figure 6.15: Outlet mole fractions of the species involved in the process with increasing degree of saturation of the first control volume at the beginning of the production phase, averaged over the timespan of the production phase.

The model was also applied to simulate a continuous methane production system using two parallel reactors operating alternately. This highlighted the necessity of thoroughly drying the bed before the production phase. The degree of saturation, defined as the ratio of water retained in the bed to the saturation value under the given thermodynamic conditions, was identified as the most critical parameter.

As the degree of saturation rises, the beneficial effect of water removal on the reaction (sorption enhancement) diminishes, resulting in lower system conversion. This reduction in conversion leads to unconverted reactants in the synthesized gas, which degrades its purity and may fail to meet the quality standards for direct injection into the natural gas network. Nonetheless, with optimal operation, these systems can produce methane of exceptionally high purity.

Chapter 7

Conclusions

7.1 Concluding remarks

In order to effectively achieve the energy transition in the immediate term, the use of technologies that can provide access to sustainable energy carriers is essential. Among these, power-to-gas systems are extremely attractive because they allow the long-term storage of renewable electricity by producing synthetic methane that can be used as a sustainable substitute of the fossil natural gas. For the effective implementation of these systems, however, the technologies they consist of need to be improved in order to make them competitive in the current scenario.

Within this framework, the objective of this dissertation is to contribute to the improvement of carbon dioxide capture and methane synthesis, which are key processes in power-to-gas contexts. To this end, it was chosen to investigate the possible contribution that adsorption technologies could make in these two fields. Given that the processes described above deal in multiple ways with gas mixtures, this choice was made considering the ability of adsorbent materials to separate single gases from mixtures.

The problems were investigated from a systems perspective in order to examine the behavior of individual components in their interaction with each other. The methods adopted involve both the development of dynamic mathematical models and experimental tests. The analysis of the dynamic behavior of these systems is a leitmotiv that accompanies all the investigations carried out. This was necessary for two reasons. On the one hand, because the processes studied are placed downstream of electrical generation from renewable sources, which are often nonprogrammable and of fluctuating availability. On the other hand, the use of adsorbent materials requires the implementation of a swing between adsorption and desorption phases resulting in the establishment of a cyclic regime that never reaches stationarity.

Considering the carbon capture in adsorption beds, what mostly emerges from the

analyses done is the demonstration that hydrogen can be a valuable purge agent to assist in the desorption of the captured carbon dioxide. In the course of the analyses performed, it was shown how the mixture obtained during desorption can be used, after adjustment, as a mixture of reactants for methane synthesis. It is necessary to have caution in the operation of the plant to make sure that hydrogen is in sub-stoichiometric condition, in order to make sure to be able to adjust its amount by appropriately adding more. It was observed, in the conditions analyzed in Section 5.1.2.3, that only with small purge rates (generated by a pressure difference of 400 Pa or lower) is it possible to obtain a mixture with sub-stechiometric hydrogen. This, however, gives rise to longer desorption times and consequently a possible need to use multiple beds in parallel to have continuous operation.

In addition, the cyclic behavior of a carbon dioxide capture system with adsorption and subsequent methanation was analyzed. Among the intents of the study was to evaluate the possibility of heat recovery from methanation of the captured carbon dioxide. With reference to cyclic steady state conditions and in the coditions tested, it has been calculated that the heat recoverable from methanation is about 10 % of that required during desorption. This leads to the conclusion that, at the design stage, there is a need to optimize both the operating conditions of the methanation reactor and to improve the layout of the reactor itself (for instance by considering a shell and tube configuration) to allow efficient heat removal. Otherwise, the system complication that would allow heat recovery may not be justified. It is pointed out, however, that the heat removed during the cooling of the adsorption bed could greatly contribute to the efficiency of the system if recovered and valorized by a heat pump which can increase the temperature of the coolant.

With regard to sorption-enhanced methanation, on the basis of the cosiderations carried out in the course of the thesis, it is possible to draw two main results. First, the sorption-enhanced conversion of carbon dioxide to methane turns out to be excellent during moments of non-rated operation, even working at medium-low pressures. When analyzing the partial-load response, it was found that the conversion rates of the sorption-enhanced methanation reactor exceeded 99.97 % in each case, when for reactors that do not exploit the enhancement of adsorption the conversion rates went from 96.2 % to 86.7 % as the feed flow rate increased for the same range of variability in loading conditions.

Second, it turns out that, again, the desorption step, which in this case involves the regeneration of the catalytic bed by the removal of water, is extremely delicate. In the cyclic operation, regeneration must be carried out with extreme care to ensure that the catalytic bed is sufficiently dry. This benefits both the duration of the adsorption phase, during which methane production takes place, and the purity of the synthesized gas. In particular, it was calculated as the regeneration flux decreases, especially under 2 mol m^{-2} s^{-1} for the case analyzed, the uptake of water remaining in the bed increases

exponentially, leading to a reduced enhancement effect.

As a result of the conclusions drawn, it is deduced that these systems need a significant attention during plant operation since it is necessary to implement the swing between adsorption and desorption. In general, however, it is believed that adsorption technologies can be effectively implemented for the improvement of power-to-gas systems. The potential of these technologies is evident by considering that, as seen throughout the dissertation, they can be employed in multiple modalities.

7.2 Future developments

On the basis of what has been concluded, it is believed that it is necessary to continue the work begun with this thesis in order to demonstrate comprehensively the concepts investigated.

First, for the purpose of obtaining more accurate results, it would be advisable to reinforce the methods adopted for the analyses. In developing the models used, in fact, several assumptions were made. The packed beds modeling approach, for instance, can be refined by employing finer discretizations or can be improved at the base by making use of more advanced models and algorithms. The mathematical model adopted for reproducing adsorption phenomena could be more complex than the linear driving force model that was adopted. The assumption of the adsorption of a single component could be overcome by also considering the adsorption of other components, both as pure and in the interaction with the others. Optimization algorithms could be appealed to in terms of +both the sizing of the system components and their operation.

Future work could dwell on the materials adopted for solid sorbents. Being central in the systems investigated, the development of more perfoment sorbents could benefit the entire chain. Sorbents with different characteristics than those investigated could, however, lead to considerable variations in the operation of the system as they might need different levels of pressure and temperature. This could lead to different considerations in relation to those made in this work about thermal requirements and productivity. In this regard, the models here adopted could be extended to be able to consider material degradation and its implications. Other highly relevant developmental activities could be techno-economic evaluations. Through these, in fact, the actual applicability on an industrial scale of adsorption technologies in Power-to-Gas plants could be quantified.

Future developments, moreover, may concern the application of the developed models in different situations that may show limitations and development possibilities not highlighted in this work. These models may, in addition, be extended and applied in broader contexts, such as in systems including green hydrogen generation and synthesized

gas users. The integration with multiple energy carriers may be evaluated. In particular, thermal integration with other processes is expected to be of paramount importance. Once sufficient know-how has been achieved with simulations, to prove the advantages of these systems, it will be essential to carry out experimental tests and practical demonstrations.

7.3 Scientific production

The scientific publications produced during the doctoral program are listed in the following.

- A. Barbaresi, M. Morini, and A. Gambarotta, "Review on the status of the research on power-to-gas experimental activities", *Energies*, vol. 15, no. 16, p. 5942, 2022.
- A. Barbaresi, F. Kiefer, M. Morini, P. Dimopoulos Eggenschwiler, and A. Gambarotta, "Partial-load and dynamic operation of methane synthesis reactors using sorptionenhanced catalysis", in *36th International Conference on Efficiency, Cost, Optimization, Simulation and Environmental Impact of Energy Systems (ECOS 2023)*, pp. 955–964, ECOS 2023, 2023.
- A. Barbaresi, A. Gambarotta, E. Marzi, M. Morini, and C. Saletti, "The role of methanation modeling in the simulation of power-to-gas systems", in *37th International Conference on Efficiency, Cost, Optimization, Simulation and Environmental Impact of Energy Systems (ECOS 2024)*, pp. 2195–2206, ECOS 2024, 2024.
- A. Barbaresi, M. Morini, A. Gambarotta, F. Kiefer, and P. Dimopoulos Eggenschwiler, "Modeling sorption-enhanced methane synthesis for system control and operation", *Renewable Energy*, vol. 232, p. 121020, 2024.
- A. Barbaresi, A. Gambarotta, M. Morini, and C. Saletti, "Dynamic adsorptive carbon capture in power-to-gas plants", *Journal of Physics: Conference Series*, vol. 2893, p. 012002, nov 2024.

Bibliography

[1] J. Davenport and N. Wayth, *Statistical Review of World Energy*. Energy Institute, 2024.

[2] Intergovernmental Panel on Climate Change (IPCC), "Climate change report," 2023. `https://www.ipcc.ch/report/ar6/syr/downloads/report/IPCC_AR6_SYR_SPM.pdf` - Accessed: 15 October 2024.

[3] International Energy Agency (IEA), "World energy outlook," 2023. `https://www.iea.org/reports/world-energy-outlook-2023` - Accessed: 15 October 2024.

[4] P. Sabatier, *La catalyse en chimie organique*. Librairie polytechnique, Ch. Béranger, 1920.

[5] International Energy Agency (IEA), "Natural gas information," 2024. `https://www.iea.org/data-and-statistics/data-product/natural-gas-information` - Accessed: 15 October 2024.

[6] H. Ritchie and P. Rosado, "Our world in data, fossil fuels," 2017. `https://ourworldindata.org/fossil-fuels` - Accessed: 15 October 2024.

[7] Trading Economics, "European natural gas title transfer facility," 2024. `https://tradingeconomics.com/commodity/eu-natural-gas` - Accessed: 17 October 2024.

[8] K. Hashimoto, N. Kumagai, K. Izumiya, H. Takano, and Z. Kato, "The production of renewable energy in the form of methane using electrolytic hydrogen generation," *Energy, Sustainability and Society*, vol. 4, pp. 1–9, 2014.

[9] A. Barbaresi, M. Morini, and A. Gambarotta, "Review on the status of the research on power-to-gas experimental activities," *Energies*, vol. 15, no. 16, p. 5942, 2022.

[10] M. Götz, J. Lefebvre, F. Mörs, A. M. Koch, F. Graf, S. Bajohr, R. Reimert, and T. Kolb, "Renewable power-to-gas: A technological and economic review," *Renewable energy*, vol. 85, pp. 1371–1390, 2016.

[11] M. Gruber, P. Weinbrecht, L. Biffar, S. Harth, D. Trimis, J. Brabandt, O. Posdziech, and R. Blumentritt, "Power-to-gas through thermal integration of high-temperature steam electrolysis and carbon dioxide methanation-experimental results," *Fuel Processing Technology*, vol. 181, pp. 61–74, 2018.

[12] H. Lange, A. Klose, W. Lippmann, and L. Urbas, "Technical evaluation of the flexibility of water electrolysis systems to increase energy flexibility: A review," *International Journal of Hydrogen Energy*, vol. 48, no. 42, pp. 15771–15783, 2023.

[13] E. S. Rubin, H. Mantripragada, A. Marks, P. Versteeg, and J. Kitchin, "The outlook for improved carbon capture technology," *Progress in energy and combustion science*, vol. 38, no. 5, pp. 630–671, 2012.

[14] D. Krekel, R. C. Samsun, R. Peters, and D. Stolten, "The separation of CO2 from ambient air–a techno-economic assessment," *Applied energy*, vol. 218, pp. 361–381, 2018.

[15] P. Webley and D. Danaci, "CO2 capture by adsorption processes," in *Carbon Capture and Storage*, pp. 106–167, Royal Society of Chemistry, 2019.

[16] A. Al-Mamoori, A. Krishnamurthy, A. A. Rownaghi, and F. Rezaei, "Carbon capture and utilization update," *Energy Technology*, vol. 5, no. 6, pp. 834–849, 2017.

[17] P. Markewitz, W. Kuckshinrichs, W. Leitner, J. Linssen, P. Zapp, R. Bongartz, A. Schreiber, and T. E. Müller, "Worldwide innovations in the development of carbon capture technologies and the utilization of co 2," *Energy & environmental science*, vol. 5, no. 6, pp. 7281–7305, 2012.

[18] P. Madejski, K. Chmiel, N. Subramanian, and T. Kuś, "Methods and techniques for co2 capture: Review of potential solutions and applications in modern energy technologies," *Energies*, vol. 15, no. 3, p. 887, 2022.

[19] F. Raganati, F. Miccio, and P. Ammendola, "Adsorption of carbon dioxide for post-combustion capture: a review," *Energy & Fuels*, vol. 35, no. 16, pp. 12845–12868, 2021.

[20] B. Sreenivasulu, D. Gayatri, I. Sreedhar, and K. Raghavan, "A journey into the process and engineering aspects of carbon capture technologies," *Renewable and Sustainable Energy Reviews*, vol. 41, pp. 1324–1350, 2015.

[21] W. J. Lee, C. Li, H. Prajitno, J. Yoo, J. Patel, Y. Yang, and S. Lim, "Recent trend in thermal catalytic low temperature CO2 methanation: A critical review," *Catalysis today*, vol. 368, pp. 2–19, 2021.

[22] M. Götz, A. M. Koch, and F. Graf, "State of the art and perspectives of CO2 methanation process concepts for power-to-gas applications," in *International gas union research conference*, vol. 13, International Gas Union Fornebu, Norway, 2014.

[23] I. Langmuir, "The adsorption of gases on plane surfaces of glass, mica and platinum," *Journal of the American Chemical society*, vol. 40, no. 9, pp. 1361–1403, 1918.

[24] J. Seader, E. J. Henley, and D. K. Roper, *Separation process principles: With applications using process simulators*. John Wiley & Sons, 2016.

[25] D. D. Do, *Adsorption analysis: Equilibria and kinetics (with cd containing computer MATLAB programs)*, vol. 2. World Scientific, 1998.

[26] M. A. Al-Ghouti and D. A. Da'ana, "Guidelines for the use and interpretation of adsorption isotherm models: A review," *Journal of hazardous materials*, vol. 393, p. 122383, 2020.

[27] S. O. Akpasi and Y. M. Isa, "Review of carbon capture and methane production from carbon dioxide," *Atmosphere*, vol. 13, no. 12, p. 1958, 2022.

[28] P. Melo Bravo and D. P. Debecker, "Combining CO2 capture and catalytic conversion to methane," *Waste Disposal & Sustainable Energy*, vol. 1, no. 1, pp. 53–65, 2019.

[29] B. Carvill, J. Hufton, M. Anand, and S. Sircar, "Sorption-enhanced reaction process," *AIChE Journal*, vol. 42, no. 10, pp. 2765–2772, 1996.

[30] D. Schollenberger, S. Bajohr, M. Gruber, R. Reimert, and T. Kolb, "Scale-up of innovative honeycomb reactors for power-to-gas applications–the project store&go," *Chemie Ingenieur Technik*, vol. 90, no. 5, pp. 696–702, 2018.

[31] DVGW, "Power-to-gas: The key enabler for a CO2-neutral energy system," 2019. `https://www.storeandgo.info/fileadmin/downloads/publications/2018-10-05_STORE_GO_E-Book-Oct-2018.pdf` - Accessed: 17 October 2024.

[32] M. Friedl, B. Meier, E. Frank, V. Crameri, C. Cianelli, L. Schmidlin, *et al.*, "Pilot and demonstration plant power-to-methane, HSR," in *Heat and Electricity Storage 2nd Symposium-Book of Abstracts, Paul Scherrer Institute*, 2015.

[33] B. Castellani, S. Rinaldi, E. Morini, B. Nastasi, and F. Rossi, "Flue gas treatment by power-to-gas integration for methane and ammonia synthesis–energy and environmental analysis," *Energy conversion and management*, vol. 171, pp. 626–634, 2018.

[34] Lübesse, "Energie vor ort erzeugen und nutzen," 2019. `https://luebesse-energie.de/projekt-luebesse/` - Accessed: 17 October 2024.

[35] Jupiter1000, "Convert renewable power surplus into green hydrogen and syngas for storage," 2014. `https://www.jupiter1000.eu/english` - Accessed: 17 October 2024.

[36] F. Brissaud, A. Chaise, V. Delphin, L. Palluotto, K. Gault, J. Cren, V. Seguin, C. Lopez, M. Bertin, G. Ferrand, *et al.*, "R&D activities on Jupiter 1000, a power-to-gas industrial demonstrator with electrolysis, methanation and gas injection to the gas transmission network," in *28th World Gas Conference, Daegu, Korea*, pp. 23–27, 2022.

[37] F. Brissaud, A. Chaise, K. Gault, and S. Soual, "Lessons learned from jupiter 1000, an industrial demonstrator of power-to-gas," *International Journal of Hydrogen Energy*, vol. 49, pp. 925–932, 2024.

[38] K. Schirmer, "Project exytron demonstrationsanlage," 2024. `https://demoplants21.best-research.eu/projects/info/3956/VEcQZJ` - Accessed: 17 October 2024.

[39] T. Kruse, "Kit-ebi ceb forschung-katalytisch-chemische verfahren-methquest." Online, 2023. `https://www.methquest.de/en/about-methquest/methfuel/` - Accessed: 15 October 2024.

[40] T. Chwoła, T. Spietz, L. Więcław-Solny, A. Tatarczuk, A. Krótki, S. Dobras, A. Wilk, J. Tchórz, M. Stec, and J. Zdeb, "Pilot plant initial results for the methanation process using CO2 from amine scrubbing at the łaziska power plant in poland," *Fuel*, vol. 263, p. 116804, 2020.

[41] M. Bailera, B. Peña, P. Lisbona, J. Marín, and L. M. Romeo, "Lab-scale experimental tests of power to gas-oxycombustion hybridization: System design and preliminary results," *Energy*, vol. 226, p. 120375, 2021.

[42] D. C. Miller, M. Syamlal, D. S. Mebane, C. Storlie, D. Bhattacharyya, N. V. Sahinidis, D. Agarwal, C. Tong, S. E. Zitney, A. Sarkar, *et al.*, "Carbon capture simulation

initiative: a case study in multiscale modeling and new challenges," *Annual review of chemical and biomolecular engineering*, vol. 5, no. 1, pp. 301–323, 2014.

[43] H. Li, H. D. Jiang, B. Yang, and H. Liao, "An analysis of research hotspots and modeling techniques on carbon capture and storage," *Science of the total environment*, vol. 687, pp. 687–701, 2019.

[44] H. Asgharian, F. Iov, S. S. Araya, T. H. Pedersen, M. P. Nielsen, E. Baniasadi, and V. Liso, "A review on process modeling and simulation of cryogenic carbon capture for post-combustion treatment," *Energies*, vol. 16, no. 4, p. 1855, 2023.

[45] E. M. Ryan, D. DeCroix, R. Breault, W. Xu, E. D. Huckaby, K. Saha, S. Dartevelle, and X. Sun, "Multi-phase CFD modeling of solid sorbent carbon capture system," *Powder technology*, vol. 242, pp. 117–134, 2013.

[46] D. Im, H. Jung, and J. H. Lee, "Modeling, simulation and optimization of the rotating packed bed (RPB) absorber and stripper for MEA-based carbon capture," *Computers & Chemical Engineering*, vol. 143, p. 107102, 2020.

[47] M. Yuan, K. Narakornpijit, R. Haghpanah, and J. Wilcox, "Consideration of a nitrogen-selective membrane for postcombustion carbon capture through process modeling and optimization," *Journal of membrane science*, vol. 465, pp. 177–184, 2014.

[48] K. Seo, Z. Chen, T. F. Edgar, J. F. Brennecke, M. A. Stadtherr, and M. Baldea, "Modeling and optimization of ionic liquid-based carbon capture process using a thin-film unit," *Computers & Chemical Engineering*, vol. 155, p. 107522, 2021.

[49] P. Mahapatra, J. Ma, B. Ng, D. Bhattacharyya, S. E. Zitney, and D. C. Miller, "Integrated dynamic modeling and advanced process control of carbon capture systems," *Energy Procedia*, vol. 63, pp. 1354–1367, 2014.

[50] K. Ramasubramanian, H. Verweij, and W. W. Ho, "Membrane processes for carbon capture from coal-fired power plant flue gas: A modeling and cost study," *Journal of membrane science*, vol. 421, pp. 299–310, 2012.

[51] R. Khalilpour, A. Abbas, Z. Lai, and I. Pinnau, "Modeling and parametric analysis of hollow fiber membrane system for carbon capture from multicomponent flue gas," *AIChE journal*, vol. 58, no. 5, pp. 1550–1561, 2012.

[52] C. Li, H. Shi, Y. Cao, Y. Kuang, Y. Zhang, D. Gao, and L. Sun, "Modeling and optimal operation of carbon capture from the air driven by intermittent and volatile wind power," *Energy*, vol. 87, pp. 201–211, 2015.

[53] O. Furst, L. Wehrle, D. Schmider, J. Dailly, and O. Deutschmann, "Modeling, optimization and comparative assessment of power-to-methane and carbon capture technologies for renewable fuel production," *Applied Energy*, vol. 375, p. 123972, 2024.

[54] C. Bassano, P. Deiana, L. Pacetti, and N. Verdone, "Integration of SNG plants with carbon capture and storage technologies modeling," *Fuel*, vol. 161, pp. 355–363, 2015.

[55] Y. Ma, H. Wang, F. Hong, J. Yang, Z. Chen, H. Cui, and J. Feng, "Modeling and optimization of combined heat and power with power-to-gas and carbon capture system in integrated energy system," *Energy*, vol. 236, p. 121392, 2021.

[56] E. Güler and S. Ergin, "An investigation on the solvent based carbon capture and storage system by process modeling and comparisons with another carbon control methods for different ships," *International Journal of Greenhouse Gas Control*, vol. 110, p. 103438, 2021.

[57] C. Drechsler and D. W. Agar, "Intensified integrated direct air capture-power-to-gas process based on H2O and CO2 from ambient air," *Applied Energy*, vol. 273, p. 115076, 2020.

[58] S. García-Luna and C. Ortiz, "Partial oxycombustion and amines-driven waste-to-methane for improved carbon capture and utilization (CCU)," *Energy Conversion and Management*, vol. 302, p. 118125, 2024.

[59] Q. Wu and C. Li, "Modeling and operation optimization of hydrogen-based integrated energy system with refined power-to-gas and carbon-capture-storage technologies under carbon trading," *Energy*, vol. 270, p. 126832, 2023.

[60] L. He, Z. Lu, J. Zhang, L. Geng, H. Zhao, and X. Li, "Low-carbon economic dispatch for electricity and natural gas systems considering carbon capture systems and power-to-gas," *Applied energy*, vol. 224, pp. 357–370, 2018.

[61] Z. Zhang, M. Zhu, S. Liu, and X. Wu, "Dynamic modeling and coupling characteristics analysis of biomass power plant integrated with carbon capture process," *Energy Conversion and Management*, vol. 273, p. 116431, 2022.

[62] F. V. Lima, P. Daoutidis, and M. Tsapatsis, "Modeling, optimization, and cost analysis of an IGCC plant with a membrane reactor for carbon capture," *AIChE Journal*, vol. 62, no. 5, pp. 1568–1580, 2016.

[63] M. Mostafa, C. Varela, M. B. Franke, and E. Zondervan, "Dynamic modeling and control of a simulated carbon capture process for sustainable power-to-x," *Applied Sciences*, vol. 11, no. 20, p. 9574, 2021.

[64] S. Rönsch, J. Schneider, S. Matthischke, M. Schlüter, M. Götz, J. Lefebvre, P. Prabhakaran, and S. Bajohr, "Review on methanation–from fundamentals to current projects," *Fuel*, vol. 166, pp. 276–296, 2016.

[65] P. J. Lunde, "Modeling, simulation, and operation of a Sabatier reactor," *Industrial & Engineering Chemistry Process Design and Development*, vol. 13, no. 3, pp. 226–233, 1974.

[66] K. L. Fischer, M. R. Langer, and H. Freund, "Dynamic carbon dioxide methanation in a wall-cooled fixed bed reactor: comparative evaluation of reactor models," *Industrial & Engineering Chemistry Research*, vol. 58, no. 42, pp. 19406–19420, 2019.

[67] A. Barbaresi, A. Gambarotta, E. Marzi, M. Morini, and C. Saletti, "The role of methanation modeling in the simulation of power-to-gas systems," in *37th International Conference on Efficiency, Cost, Optimization, Simulation and Environmental Impact of Energy Systems (ECOS 2024)*, pp. 2195–2206, ECOS 2024, 2024.

[68] L. Sun, K. Luo, and J. Fan, "Three-dimensional simulation of the methanation process in a circulating fluidized-bed reactor," *Industrial & Engineering Chemistry Research*, vol. 60, no. 45, pp. 16417–16429, 2021.

[69] D. Schlereth and O. Hinrichsen, "A fixed-bed reactor modeling study on the methanation of CO2," *Chemical Engineering Research and Design*, vol. 92, no. 4, pp. 702–712, 2014.

[70] M. Gruber, D. Wiedmann, M. Haas, S. Harth, A. Loukou, and D. Trimis, "Insights into the catalytic CO2 methanation of a boiling water cooled fixed-bed reactor: Simulation-based analysis," *Chemical Engineering Journal*, vol. 406, p. 126788, 2021.

[71] E. Moioli, N. Gallandat, and A. Züttel, "Model based determination of the optimal reactor concept for sabatier reaction in small-scale applications over Ru/Al2O3," *Chemical Engineering Journal*, vol. 375, p. 121954, 2019.

[72] E. Moioli and A. Züttel, "A model-based comparison of Ru and Ni catalysts for the Sabatier reaction," *Sustainable Energy & Fuels*, vol. 4, no. 3, pp. 1396–1408, 2020.

[73] J. Bremer, K. H. Rätze, and K. Sundmacher, "CO2 methanation: Optimal start-up control of a fixed-bed reactor for power-to-gas applications," *AIChE Journal*, vol. 63, no. 1, pp. 23–31, 2017.

[74] R. Güttel, "Study of unsteady-state operation of methanation by modeling and simulation," *Chemical Engineering & Technology*, vol. 36, no. 10, pp. 1675–1682, 2013.

[75] E. I. Koytsoumpa and S. Karellas, "Equilibrium and kinetic aspects for catalytic methanation focusing on CO2 derived substitute natural gas (SNG)," *Renewable and Sustainable Energy Reviews*, vol. 94, pp. 536–550, 2018.

[76] G. Fambri, C. Diaz-Londono, A. Mazza, M. Badami, and R. Weiss, "Power-to-gas in gas and electricity distribution systems: A comparison of different modeling approaches," *Journal of Energy Storage*, vol. 55, p. 105454, 2022.

[77] N. Kezibri and C. Bouallou, "Conceptual design and modelling of an industrial scale power to gas-oxy-combustion power plant," *International Journal of Hydrogen Energy*, vol. 42, no. 30, pp. 19411–19419, 2017.

[78] F. Salomone, E. Giglio, D. Ferrero, M. Santarelli, R. Pirone, and S. Bensaid, "Techno-economic modelling of a power-to-gas system based on soec electrolysis and CO2 methanation in a RES-based electric grid," *Chemical Engineering Journal*, vol. 377, p. 120233, 2019.

[79] G. Iaquaniello, S. Setini, A. Salladini, and M. De Falco, "CO2 valorization through direct methanation of flue gas and renewable hydrogen: a technical and economic assessment," *International Journal of Hydrogen Energy*, vol. 43, no. 36, pp. 17069–17081, 2018.

[80] D. Sun and D. S. Simakov, "Thermal management of a sabatier reactor for CO2 conversion into CH4: simulation-based analysis," *Journal of CO2 Utilization*, vol. 21, pp. 368–382, 2017.

[81] Y.-L. Kao, P.-H. Lee, Y.-T. Tseng, I.-L. Chien, and J. D. Ward, "Design, control and comparison of fixed-bed methanation reactor systems for the production of substitute natural gas," *Journal of the Taiwan Institute of Chemical Engineers*, vol. 45, no. 5, pp. 2346–2357, 2014.

[82] E. Giglio, R. Pirone, and S. Bensaid, "Dynamic modelling of methanation reactors during start-up and regulation in intermittent power-to-gas applications," *Renewable Energy*, vol. 170, pp. 1040–1051, 2021.

[83] C. Dhoke, A. Zaabout, S. Cloete, and S. Amini, "Review on reactor configurations for adsorption-based CO2 capture," *Industrial & Engineering Chemistry Research*, vol. 60, no. 10, pp. 3779–3798, 2021.

[84] R. Ben-Mansour, M. Habib, O. Bamidele, M. Basha, N. Qasem, A. Peedikakkal, T. Laoui, and M. Ali, "Carbon capture by physical adsorption: materials, experimental investigations and numerical modeling and simulations–a review," *Applied Energy*, vol. 161, pp. 225–255, 2016.

[85] J. V. Veselovskaya, P. D. Parunin, O. V. Netskina, L. S. Kibis, A. I. Lysikov, and A. G. Okunev, "Catalytic methanation of carbon dioxide captured from ambient air," *Energy*, vol. 159, pp. 766–773, 2018.

[86] F. Rezaei and M. Grahn, "Thermal management of structured adsorbents in CO2 capture processes," *Industrial & engineering chemistry research*, vol. 51, no. 10, pp. 4025–4034, 2012.

[87] M. S. Duyar, M. A. A. Treviño, and R. J. Farrauto, "Dual function materials for CO2 capture and conversion using renewable H2," *Applied Catalysis B: Environmental*, vol. 168, pp. 370–376, 2015.

[88] C. Jeong-Potter and R. Farrauto, "Feasibility study of combining direct air capture of CO2 and methanation at isothermal conditions with dual function materials," *Applied Catalysis B: Environmental*, vol. 282, p. 119416, 2021.

[89] K. H. Chai, L. K. Leong, D. S.-H. Wong, D.-H. Tsai, and S. Sethupathi, "Effect of CO2 adsorbents on the ni-based dual-function materials for CO2 capturing and in situ methanation," *Journal of the Chinese Chemical Society*, vol. 67, no. 6, pp. 998–1008, 2020.

[90] J. A. Martins, V. F. Martins, C. V. Miguel, A. E. Rodrigues, and L. M. Madeira, "A cyclic sorption-reaction process for continuous synthetic methane production from flue gas and green hydrogen," *Chemical Engineering Journal*, vol. 476, p. 146375, 2023.

[91] J. V. Veselovskaya, P. D. Parunin, and A. G. Okunev, "Catalytic process for methane production from atmospheric carbon dioxide utilizing renewable energy," *Catalysis Today*, vol. 298, pp. 117–123, 2017.

[92] J. V. Veselovskaya, P. D. Parunin, O. V. Netskina, and A. G. Okunev, "A novel process for renewable methane production: combining direct air capture by K2CO3/alumina sorbent with CO2 methanation over Ru/alumina catalyst," *Topics in Catalysis*, vol. 61, pp. 1528–1536, 2018.

[93] S. Yamamoto, S. Sayama, S. Kunitomi, K. Ogasawara, and N. Baba, "Demonstration of a high-efficiency carbon dioxide capture and methanation system with

heat/material integration for power-to-gas and zero carbon dioxide emissions in flue gasses," *International Journal of Greenhouse Gas Control*, vol. 114, p. 103584, 2022.

[94] I. Iliuta, M. C. Iliuta, and F. Larachi, "Sorption-enhanced dimethyl ether synthesis—multiscale reactor modeling," *Chemical engineering science*, vol. 66, no. 10, pp. 2241–2251, 2011.

[95] Z. Dehghani, M. Bayat, and M. Rahimpour, "Sorption-enhanced methanol synthesis: Dynamic modeling and optimization," *Journal of the Taiwan Institute of Chemical Engineers*, vol. 45, no. 4, pp. 1490–1500, 2014.

[96] E. Moioli and T. Schildhauer, "Tailoring the reactor properties in the small-scale sorption-enhanced methanol synthesis," *Chemie Ingenieur Technik*, vol. 95, no. 5, pp. 631–641, 2023.

[97] A. Borgschulte, N. Gallandat, B. Probst, R. Suter, E. Callini, D. Ferri, Y. Arroyo, R. Erni, H. Geerlings, and A. Züttel, "Sorption enhanced CO2 methanation," *Physical Chemistry Chemical Physics*, vol. 15, no. 24, pp. 9620–9625, 2013.

[98] A. Borgschulte, E. Callini, N. Stadie, Y. Arroyo, M. Rossell, R. Erni, H. Geerlings, A. Züttel, and D. Ferri, "Manipulating the reaction path of the CO2 hydrogenation reaction in molecular sieves," *Catalysis Science & Technology*, vol. 5, no. 9, pp. 4613–4621, 2015.

[99] R. Delmelle, J. Terreni, A. Remhof, A. Heel, J. Proost, and A. Borgschulte, "Evolution of water diffusion in a sorption-enhanced methanation catalyst," *Catalysts*, vol. 8, no. 9, p. 341, 2018.

[100] A. Borgschulte, R. Delmelle, R. B. Duarte, A. Heel, P. Boillat, and E. Lehmann, "Water distribution in a sorption enhanced methanation reactor by time resolved neutron imaging," *Physical Chemistry Chemical Physics*, vol. 18, no. 26, pp. 17217–17223, 2016.

[101] S. Walspurger, G. D. Elzinga, J. W. Dijkstra, M. Sarić, and W. G. Haije, "Sorption enhanced methanation for substitute natural gas production: Experimental results and thermodynamic considerations," *Chemical Engineering Journal*, vol. 242, pp. 379–386, 2014.

[102] L. Wei, H. Azad, W. Haije, H. Grenman, and W. de Jong, "Pure methane from CO2 hydrogenation using a sorption enhanced process with catalyst/zeolite bifunctional materials," *Applied Catalysis B: Environmental*, vol. 297, p. 120399, 2021.

[103] I. Agirre, E. Acha, J. Cambra, and V. Barrio, "Water sorption enhanced CO2 methanation process: Optimization of reaction conditions and study of various sorbents," *Chemical Engineering Science*, vol. 237, p. 116546, 2021.

[104] A. Coppola, F. Massa, P. Salatino, and F. Scala, "Evaluation of two sorbents for the sorption-enhanced methanation in a dual fluidized bed system," *Biomass Conversion and Biorefinery*, vol. 11, pp. 111–119, 2021.

[105] L. Gómez, I. Martínez, M. V. Navarro, T. García, and R. Murillo, "Sorption-enhanced CO and CO2 methanation (SEM) for the production of high purity methane," *Chemical Engineering Journal*, vol. 440, p. 135842, 2022.

[106] F. Kiefer, M. Nikolic, A. Borgschulte, and P. Dimopoulos Eggenschwiler, "Sorption-enhanced methane synthesis in fixed-bed reactors," *Chemical Engineering Journal*, vol. 449, p. 137872, 2022.

[107] F. Massa, A. Coppola, and F. Scala, "A thermodynamic study of sorption-enhanced CO2 methanation at low pressure," *Journal of CO2 Utilization*, vol. 35, pp. 176–184, 2020.

[108] P. Bareschino, G. Piso, F. Pepe, C. Tregambi, and E. Mancusi, "Numerical modelling of a sorption-enhanced methanation system," *Chemical Engineering Science*, vol. 277, p. 118876, 2023.

[109] R. Haghpanah, A. Majumder, R. Nilam, A. Rajendran, S. Farooq, I. A. Karimi, and M. Amanullah, "Multiobjective optimization of a four-step adsorption process for postcombustion co2 capture via finite volume simulation," *Industrial & Engineering Chemistry Research*, vol. 52, no. 11, pp. 4249–4265, 2013.

[110] F. L. Dryer, F. M. Haas, J. Santner, T. I. Farouk, and M. Chaos, "Interpreting chemical kinetics from complex reaction–advection–diffusion systems: Modeling of flow reactors and related experiments," *Progress in energy and combustion science*, vol. 44, pp. 19–39, 2014.

[111] S. Ergun and A. A. Orning, "Fluid flow through randomly packed columns and fluidized beds," *Industrial & Engineering Chemistry*, vol. 41, no. 6, pp. 1179–1184, 1949.

[112] A. Gambarotta, M. Manganelli, and M. Morini, "A model for the simulation of the gas cleaning system in a syngas-fed CHP plant," in *AIP Conference Proceedings*, vol. 2191, AIP Publishing, 2019.

[113] E. Tsotsas, "M7 heat and mass transfer in packed beds with fluid flow," in *VDI Heat Atlas*, 2010.

[114] B. E. Poling, J. M. Prausnitz, J. P. O'connell, *et al.*, *The properties of gases and liquids*. Mcgraw-hill New York, 5 ed., 2001.

[115] J. Xu and G. F. Froment, "Methane steam reforming, methanation and water-gas shift: I. intrinsic kinetics," *AIChE journal*, vol. 35, no. 1, pp. 88–96, 1989.

[116] E. Marzi, M. Morini, C. Saletti, and A. Gambarotta, "Coordinating multiple power-to-gas plants for optimal management of e-fuel seasonal storage," *Smart Energy*, vol. 14, p. 100143, 2024.

[117] B. J. Mcbride, S. Gordon, and M. Reno, "Nasa technical memorandum 4513," *Coefficients for Calculating Thermodynamic and Transport Properties of Individual Species (Hampton, VA: NASA STI)*, 1993.

[118] A. Barbaresi, A. Gambarotta, M. Morini, and C. Saletti, "Dynamic adsorptive carbon capture in power-to-gas plants," *Journal of Physics: Conference Series*, vol. 2893, p. 012002, nov 2024.

[119] C. A. Grande, F. V. Lopes, A. M. Ribeiro, J. M. Loureiro, and A. E. Rodrigues, "Adsorption of off-gases from steam methane reforming (h2, co2, ch4, co and n2) on activated carbon," *Separation Science and Technology*, vol. 43, no. 6, pp. 1338–1364, 2008.

[120] O. T. Qazvini and S. Fatemi, "Modeling and simulation pressure–temperature swing adsorption process to remove mercaptan from humid natural gas; a commercial case study," *Separation and Purification Technology*, vol. 139, pp. 88–103, 2015.

[121] M. Dubinin and V. Astakhov, "Description of adsorption equilibria of vapors on zeolites over wide ranges of temperature and pressure," *Advances in Chemistry*, vol. 102, pp. 69–85, 1971.

[122] S. Jribi, T. Miyazaki, B. B. Saha, A. Pal, M. M. Younes, S. Koyama, and A. Maalej, "Equilibrium and kinetics of CO2 adsorption onto activated carbon," *International Journal of Heat and Mass Transfer*, vol. 108, pp. 1941–1946, 2017.

[123] K. Amankwah and J. Schwarz, "A modified approach for estimating pseudo-vapor pressures in the application of the dubinin-astakhov equation," *Carbon*, vol. 33, no. 9, pp. 1313–1319, 1995.

[124] T. L. Dantas, F. M. T. Luna, I. J. Silva Jr, D. C. de Azevedo, C. A. Grande, A. E. Rodrigues, and R. F. Moreira, "Carbon dioxide–nitrogen separation through adsorption on activated carbon in a fixed bed," *Chemical Engineering Journal*, vol. 169, no. 1-3, pp. 11–19, 2011.

[125] M. J. Lashaki, S. Khiavi, and A. Sayari, "Stability of amine-functionalized CO2 adsorbents: a multifaceted puzzle," *Chemical Society Reviews*, vol. 48, no. 12, pp. 3320–3405, 2019.

[126] G. Guzzo, L. Cheli, and C. Carcasci, "Hydrogen blending in the italian scenario: Effects on a real distribution network considering natural gas origin," *Journal of Cleaner Production*, vol. 379, p. 134682, 2022.

[127] A. Barbaresi, F. Kiefer, M. Morini, P. Dimopoulos Eggenschwiler, and A. Gambarotta, "Partial-load and dynamic operation of methane synthesis reactors using sorption-enhanced catalysis," in *36th International Conference on Efficiency, Cost, Optimization, Simulation and Environmental Impact of Energy Systems (ECOS 2023)*, pp. 955–964, ECOS 2023, 2023.

[128] A. Barbaresi, M. Morini, A. Gambarotta, F. Kiefer, and P. Dimopoulos Eggenschwiler, "Modeling sorption-enhanced methane synthesis for system control and operation," *Renewable Energy*, vol. 232, p. 121020, 2024.

[129] W. R. Kang and K. B. Lee, "Effect of operating parameters on methanation reaction for the production of synthetic natural gas," *Korean Journal of Chemical Engineering*, vol. 30, pp. 1386–1394, 2013.

[130] S. Guffanti, C. G. Visconti, J. van Kampen, J. Boon, and G. Groppi, "Reactor modelling and design for sorption enhanced dimethyl ether synthesis," *Chemical Engineering Journal*, vol. 404, p. 126573, 2021.

La borsa di dottorato è stata cofinanziata con risorse del Programma Operativo Nazionale Ricerca e Innovazione 2014-2020, risorse FSE REACT-EU Azione IV.4 “Dottorati e contratti di ricerca su tematiche dell’innovazione” e Azione IV.5 “Dottorati su tematiche Green”.